UiT The Arctic University of Norway

Faculty of Science and Technology

Department of Geosciences

Geomorphological study of unstable rock slope deformation on Ståluvárri, Kåfjorden, Troms

Iver Magnarson Nypan

Master's thesis in Geology,GEO-3900, May 2024

Cover Photo by Sindre Norheim 2018

Abstract

Unstable rock slope failures are catastrophic hazards with a long history in Norway. A large portion of these have been detected within Troms County, with a high percentage of them the Lyngenfjorden fault zone. Stáluvárri, a mountain in Kåfjord commune, is such a slope with detected bodies undergoing slow displacement rates. Bedrock compositions on the slope has abundant mica schists, with a thrust faults emplacing more gneissic compositions on top.

As part of a nationwide task by NGU, this study will focus on identifying some of the geomorphological signs on the slope, assess potential controlling mechanisms and address the hazard it poses. The field is complex with generally different scenes happening, and four scenarios has been identified on the slope related to deformational processes where one of them stand out as the bigger hazard.

Stáluvárri can be seen influenced by normal faulting from post-Caledonian extension and rifting. Two larger fault systems can be seen in NW-SE and NE-SW fashion and is directly controlling the related rear rupture surfaces of the displaced material.

Because of the sheer size of the slope, with inherited large fault systems controlling larger sections of the slope, it has been classified as being controlled deep-seated gravitational slope deformation, a landslide case which has slow displacement rates associated with it.

Acknowledgements

I would like to thank both my supervisors Louise Mary Vick (UiT) and Martina Böhme (NGU) for helpful insights during the writing of this thesis. Vanja Haugsnes (NGU) and Maria Bredal (NGU), I would like to thank for a good field trip to both Stáluvárri and Seidi in September, although the weather conditions weren't always with us. And of course, thanks Sindre Norheim for beginning your study here and establishing good source of data I would not have been able to access otherwise during field season.

Thank you, Fabrice Kaltenrieder, for amazing field trips to our sites together. I will never forget driving to the site and eating good food with amazing northern lights over us.
Also, thanks to the rest of my co-students for ski trips and overall good times during our two years together. And a special thanks to my co-student and roommate Teitur, glad we didn't get sick of each other.

And, finally, thanks to my family for being so supportive during all my years in Tromsø. Mom, thanks for all the good lunches together and Sunday dinners which I so desperately needed!

Iver Magnarson Nypan

Contents

Abstract II

Acknowledgements III

1 Introduction 1

1.1 Abbreviations 1

1.2 Background for the thesis 1

1.2.1 Aim and motivation of the study 2

1.3 Location and study area 3

1.3.1 Climate and weather 5

1.4 Available data from the study area 5

1.5 Geological setting 6

1.5.1 Regional geology 6

1.5.2 Post-Caledonian extension and rifting 8

1.6 Quaternary geology and periglacial processes 9

1.6.1 Quaternary history 9

1.6.2 Periglacial processes 11

2 Rock Slope deformation theory 12

2.1 Structurally controlled instability 12

3 Foliation 12

3.1.1 Joints and faults 12

3.2 Geomorphological features 13

4 Methods 14

4.1 Movement data 14

4.1.1 dGNSS Data 14
4.1.2 Extensometer data 14
4.1.3 InSAR data 15
4.2 Structural and geomorphological mapping 16
4.3 Available desktop data 16
4.4 Fieldwork 17
4.4.1 Structural data gathering 17
4.5 Samples and thin sections 18
4.6 Kinematic analysis 19
4.7 Risk assessment 19
5 Results 21
5.1 Structural data 21
5.1.1 Lower domain 22
5.1.2 The Upper Domain 25
5.1.3 Deformed Domain 26
5.2 Kinematic analysis 28
5.2.1 Lower domain Kinematics 29
5.2.2 Upper Domain Kinematic analysis 30
5.3 Morphological mapping 31
5.3.1 Surficial cover 31
5.3.2 Morphostructural Mapping 35
5.4 Movement data 43
5.4.1 dGNSS 43
5.4.2 Extensometers lower domain 46
5.4.3 InSAR Movement 48
5.5 Lithology 51

6 Discussion 57
6.1 Lithology 57
6.2 Displacement data 58
6.3 Defining scenarios 60
6.3.1 Scenario 1 64
6.3.2 Scenario 2 65
6.3.3 Scenario 4 66
6.4 Conceptual model 68
6.5 Hazard assessment 71
7 Conclusion 73
References 1
Appendix Material 4
Appendix A 6

Table of Tables

Table 1: Displacement rates along the extensometer tape 47
Table 2: Mineral compositions and descriptions of the samples. 56
Table 3: Scenario 1 through 3 with their hazard classification 72

Tables of Figures

Figure 1: Overview map of the location of the study area 3
Figure 2: Topographic map of Stáluvárri, ... 4
Figure 3: Schematic cross section of the thrust nappes in Troms 7
Figure 4: Bedrock map of Stáluvárri and surrounding areas 8
Figure 5: Quaternary map over Stáluvárri and Ytre-Nordmannvik 10
Figure 6: Example over the observed movement of Stáluvárri 16
Figure 7: Structural domains on Stáluvárri 22

Figure 8: Example of the observations and structural elements 23
Figure 9: Averaged structural elements within the lower domain 24
Figure 10: Example structural features in upper domain. 25
Figure 11: Structural measurements from the upper domain. 26
Figure 12: Structural measurements and elements within the deformed domain 27
Figure 13: Overview map of slope aspect on Stáluvárri. 28
Figure 14: Kinematics analysis for the lower domain 29
Figure 15: Kinematics analysis for the upper domain 30
Figure 16: Classifications of the different surficial ground cover observed. 32
Figure 17: Morphological map of the surface cover on Stáluvárri 34
Figure 18: Scarp observed on the top of the mountain. 35
Figure 19: Morpho structural map of Stáluvárri 36
Figure 20: Structures which can be seen along the top ridge 37
Figure 21: Large horst and graben system within the lower domain. 38
Figure 22: Large faults following the NW-SE (orange) and NE-SW (red). 39
Figure 23: Fault plane evidence from lower domain soutwest facing section 40
Figure 24: Morphstructural observations along a few more sections. 41
Figure 25: Map of Stáluvárri showing how the slope inclination 42
Figure 26: Points of dGNSS positions on Stáluvárri, ... 43
Figure 27: Displacement graphs 45
Figure 28: Locations of extensometer tape 46
Figure 29: Extensometer data from fractured system within the lower domain 47
Figure 30: InSAR data with averaged movement 48
Figure 31: InSAR movement along the slope 49
Figure 32: Localities of the various samples collected on Stáluvárri. 51
Figure 33: Approximated mineral assemblages 52
Figure 34: Mica schist thin sections 54
Figure 35: Overview pictures gneissic and amphibole-rich samples. 55
Figure 36: Proposed adjustment to the bedrock map. 58
Figure 37: Conceptual model of the block movements within the lower domain, ... 59
Figure 38: Cross sections and scenarios on Stáluvárri 61
Figure 39: Cross section 1 from scenario 1 62

Figure 40: Cross section 2 from scenario 1 62
Figure 41: Cross section 3 along the upper domain of the slope. 63
Figure 42: Cross section 4 of deformational structures on the peak. 63
Figure 43: Cross section 5 on scenario 4 67
Figure 44: Simplified conceptual model of the development of the Stáluvárri 70
Figure 45: Risk matrix of the hazard assessment 72

1 Introduction

1.1 Abbreviations

InSAR = Interferometric Synthetic Aperture Radar

GIS = Geographical Information System

DEM = Digital Elevation Model

RSD = Rock Slope Deformation

DGSD = Deep Seated Gravitational slope deformation

M.a.s.l. = Meters above sea level

GPS = Global Positioning System

RNC = Reisa Nappe Complex

NGU = Norges Geologiske Undersøkelse

NVE = Norges Vassdrags- og Energidirektorat

1.2 Background for the thesis

The mountainous regions in Norway give rise for threats and natural hazards such as snow avalanches, rock fall and rock avalanches. Steep terrain found in valleys and fjords tends to promote gravitational mass movement downslope. One of the more devastating natural hazards generated in these sorts of terrain is catastrophic rock slope failure, where large bodies of rock are released from the mountain-side. Such disastrous events happen quite rarely, but throughout history in Norway they have destroyed and devastated communities when they happen close by.

There are a few known incidents of these catastrophic rock slope failures, such as the Tafjord incident in 1934 which took 40 lives, the Loen incidents in 1905 and 1936 which took in total 135 lives and the 1810 Pollfjellet incident taking 14 lives (Furseth, 2006). Due to the topography and the resources found along the coasts of Norway, a lot of settlements are in fjords where the hazard of the rock slope failure would be increased due to the risk of it generating displacement waves. All the above-mentioned incidents are examples of where catastrophic rock slope failures happened and initiated massive displacement waves. Since the 14th century there has been approximated around 13 000 events of rock failures registered in Norway, which has resulted in 932 fatalities (Hermanns et al., 2012a).

With newer technology and remote sensing, Norwegian governmental institutions can identify which slopes that have movement suggesting instability and have the potential to release. To mitigate the risk for these events affecting further local populations, a major project initiated by NGU in 2005 has been to map out these risk-objects around Norway (Hermanns et al., 2014). Together with the NVE the project has been able to detect 674 unstable slopes across Norway, where 113 of them have been given a risk and probability assessment as of 2024 (NVE, 2023b). The aim is to assess the risk of the object, install the necessary measures and adhere to the building code TEK17 when assessing future projects. Protective measures which can be used includes installing GPS trackers which measure the deformation of the slope continuously and for some of the lower risk objects measuring the deformation periodically (NVE, 2021). In Kåfjord three such installations of continuous surveillance have been placed on Gámanjunni-3, Jettan and Indre Nordnes (NVE, 2023a).

This thesis is focused on Stáluvárri, one of the over 100 identified slopes showing signs of deformational processes in Troms County (Bunkholt et al., 2012). It is a rather large slope with complex topography with a main west-southwest aspect. The site is located close to Kåfjorden, where surrounding slopes can be identified with similar deformational processes. This study is meant to establish and document the deformational processes on Stáluvárri.

1.2.1 Aim and motivation of the study

The aim of this study is to by using mapping tools, fieldwork investigations, movement data and thin section work, to identify controlling aspects rock slope deformation on Stáluvárri. The motivation of the thesis is to continue the work on assessing hazardous rock slope failures in Norway and identify potential mechanisms controlling it. Lastly a risk assessment based on these observations will be given for scenarios identified on the slope.

The following objectives are relevant for this study:

- Creating a geomorphological map of the slope, assessing the surficial cover and linear expressions.
- Interpreting the bedrock geology and relate it to the slope gravitational processes.
- Define potential extents and scenarios of the rock slope deformational processes.
- Using movement data to establish an interpreted direction of slope movement.
- Assess the risk for the various scenarios, using NGUs risk and consequence matrix.

1.3 Location and study area

This study of Ståluvárri (1251 m.a.s.l) is part of a nationwide task of NGU to map and assess unstable rock slopes in Norway. It is located within Kåfjord Commune in Troms County, where the largest and nearest settlement to the slope, Olderdalen, has 286 inhabitants (SSB, 2023).

To the south of the slope the Nordmannvik valley runs in an east-west direction ending in Lyngenfjorden and the small farmland community of Ytre-Nordmannvik at the foot of the mountain. Other important infrastructure in proximity of the slope is the main highway E6.

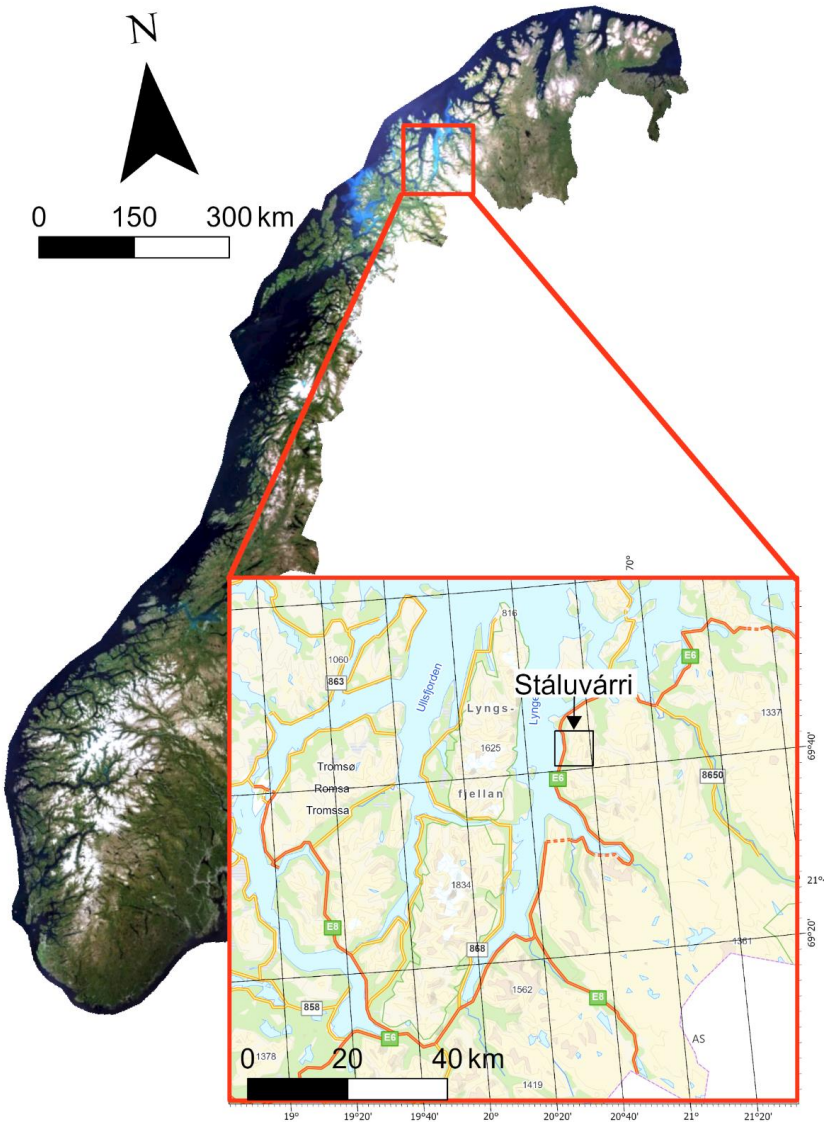

Figure 1: Overview map of the location of the study area. Black box marks the area around Ståluvárri, which is shown closer on figure 2 below.

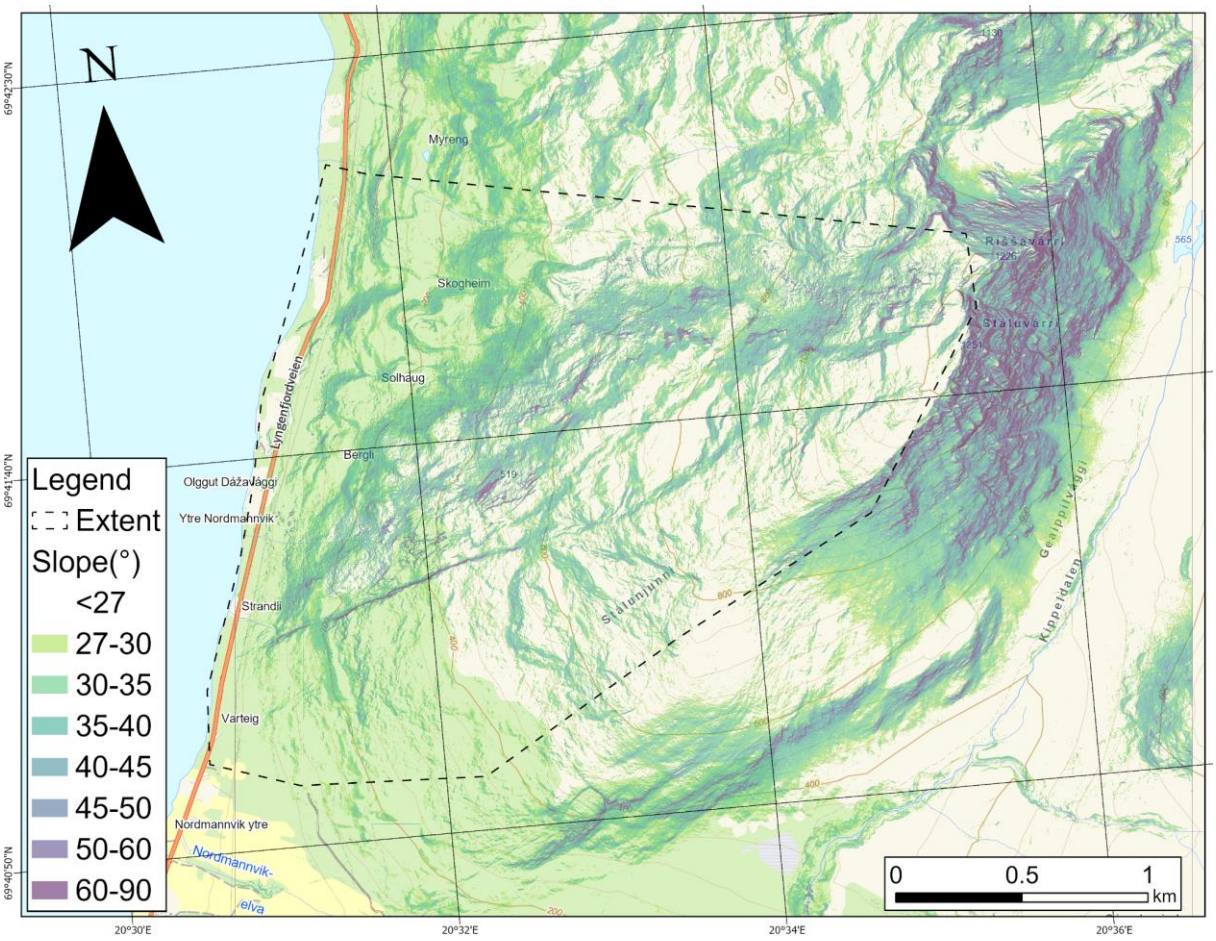

Figure 2: Topographic map of Stáluvárri, where the dotted line is the area of interest for this project.

Stáluvárri follows an 5km elongated ridge, but the area of focus is half that size. From the peak to the mountain's foot at the fjordside the distance is somewhere around 2.5-3km and has a very mixed topographic section. Towards the east to southeast of ridge, an 800m almost vertical drop defines the relief. The slopes fjord-dipping side is towards the southwest to west has a very roughed terrain. Western aspects have initially a very roughed terrain with cliff formations around the top, large segments of talus formations and a step-like moving topography. On average the western side is initially close to 20-25° dipping but increase rapidly to 30-40° below 600m.a.s.l. The southwestern-facing side begins around 800m.a.s.l and is initially defined by large blockfields and disintegrated rock on a generally gentle dipping slope of 20-25° but with some steeply dipping surfaces. Vegetation cover on the southwestern side is present up to 600m.a.s.l and thins out considerably to 200m.a.s.l on the west-facing side.

1.3.1 Climate and weather

The climate of Troms County has major variations due to the topography and geographic size of the region. The county is 25 167 km^2, and sprawls from coastal islands and Alps at the west coast, to inner fjords and gentle continental mountains inland in the east (Thorsnes, 2024). From warm moist coastal climates to the dryer inland climates, the variations in temperature and amount of precipitation changes a lot from east to west. The Lyngen Alps are responsible for creating a barrier when weather patterns coming in from the open ocean in the west hits the coast, especially during the winter months. Tall peaks and varying topography results in most of the precipitation being released before and within this zone. Beyond this barrier to the east in the municipalities of Kåfjord and Storfjord the amount of yearly precipitation is therefore greatly reduced. Only around 300-500 mm a year is released here compared to the 700-1000 mm yearly precipitation observed in Lyngen (Mamen, 2023; MET, 2023a).

The temperature in Kåfjord varies between 10-15 degrees Celsius in the summer months and down to an average of -5 to -10 degrees Celsius in the winter months. Minium values can go down to around -20 degrees Celsius in the winter months (MET, 2023b). Temperatures are relatively low in the region which leads to some of the high plateaus and mountainous areas can experience below zero degrees for most of the year. An effect of this is that these places experience permafrost, and in Kåfjorden this can be observed as happening sporadically or discontinuous in the higher altitudes (Gisnås et al., 2016)

1.4 Available data from the study area

As Stáluvárri is one of the work-in-progress sites for NGU, the slope has had observations gathered during various previous field seasons. As part of a larger risk and vulnerability study (ROS) published in 2009 covering Troms County, the mountain side were mapped using orthophotos (Osmundsen et al., 2009). In 2010 some initial fieldwork on the slope were conducted (Bunkholt et al., 2012).

In 2013 NGU executed fieldwork on Stáluvárri gathering observations and structural measurements. The same year points for measuring movement using extensometer tape were installed in the lower part of the slope, where an interval of every year to every two years the tensile movement across cracks or crevasses are measured. In the field season of 2014 GPS

points were installed around the same area as the extensometers. The GNSS method measures the movement of rock exposure over a small-time frame using GPS.

As of 2015 there were yearly measurements recorded from the Sentinel-1 satellites on the slope, which gets reprocessed to measure movement on the surface during the summer months as InSAR. This results in quite dense points clouds. The point coverage on the slope has relatively good extent, but some of the top parts of the mountain has fewer data points due to the steeper slope angle.

In 2018 a UiT master student, Sindre Norheim, started but did not complete his thesis project on Stáluvárri. He finished the field season after having collected a large database of structural measurements of the foliation and joints. As a result, quite a good coverage of data points has already been established.

1.5 Geological setting

The geological history of the Troms region, and for similar reasons the rest of Norway, is an important factor for the understanding of slope movement seen today. Lithological variations along the slope influence the brittle properties which can lead to failures, while structural properties like foliation, joints and fractures work to create weakness zones within the rock.

1.5.1 Regional geology

The regional geology of Troms is comprised of a series of allochthonous thrust-nappes which originates from the Caledonian orogenic event. Between the Ordovician to Silurian ages the Iapetus Ocean closed, resulting in the continent-continent collision of the Laurentian and Baltic plate. This produced a highly metamorphic and deformed mountain range emplaced on the Precambrian Baltic shield (Augland et al., 2014). Looking at Troms in a transect from northwest to southeast, there is a highly variable grade of metamorphic conditions, lithologies and tectonic features.

The lithologies focused on in this study are within some of the lower units of the Caledonian nappes. Units found on Stáluvárri and locations close by are dominated by the Nordmannvik Nappe and the underlying Kåfjord Nappe, both part of the major tectonic unit the Reisa Nappe Complex (RNC) (Faber et al., 2019). Figure 3 illustrates these relations between the nappe complexes in Troms.

The lithologies in Kåfjord are high grade metasedimentary rocks and lenses of metaigneous rocks. Figure 4 below shows the bedrock relations in the area, highlighting the different lithologies and structural boundaries between them. On Ståluvárri itself there is a shear zone marking the border between the overlying Nordmannvik Nappe and underlying Kåfjord Nappe (*Figure 4*). Along the slope there are also outcroppings of intrusive activities as lenses of amphibolite, pegmatite and gabbro with thicknesses from 5-50m (Zwaan et al., 2006).

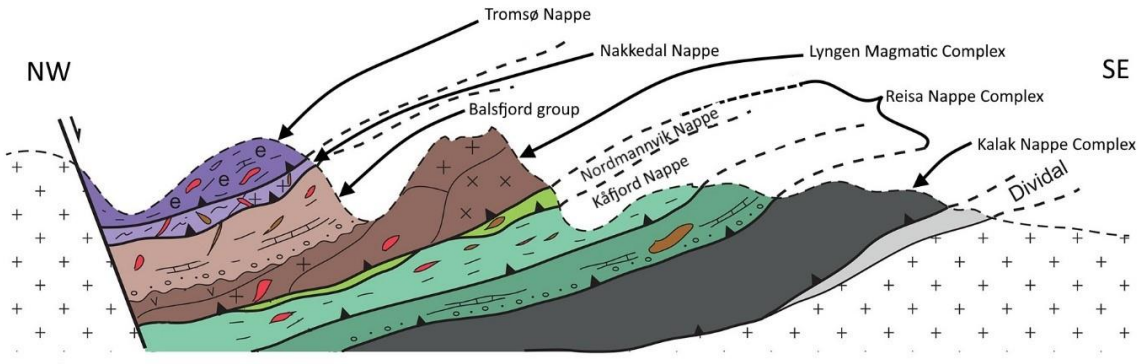

Figure 3: Schematic cross section of the thrust nappes in Troms drawn from northwest to southeast. The Reisa Nappe complex is in the lower parts of the nappe stack, with Nordmannvik- and Kåfjord nappes in the upper part of this again. Figure modified from Augland et al. (2014).

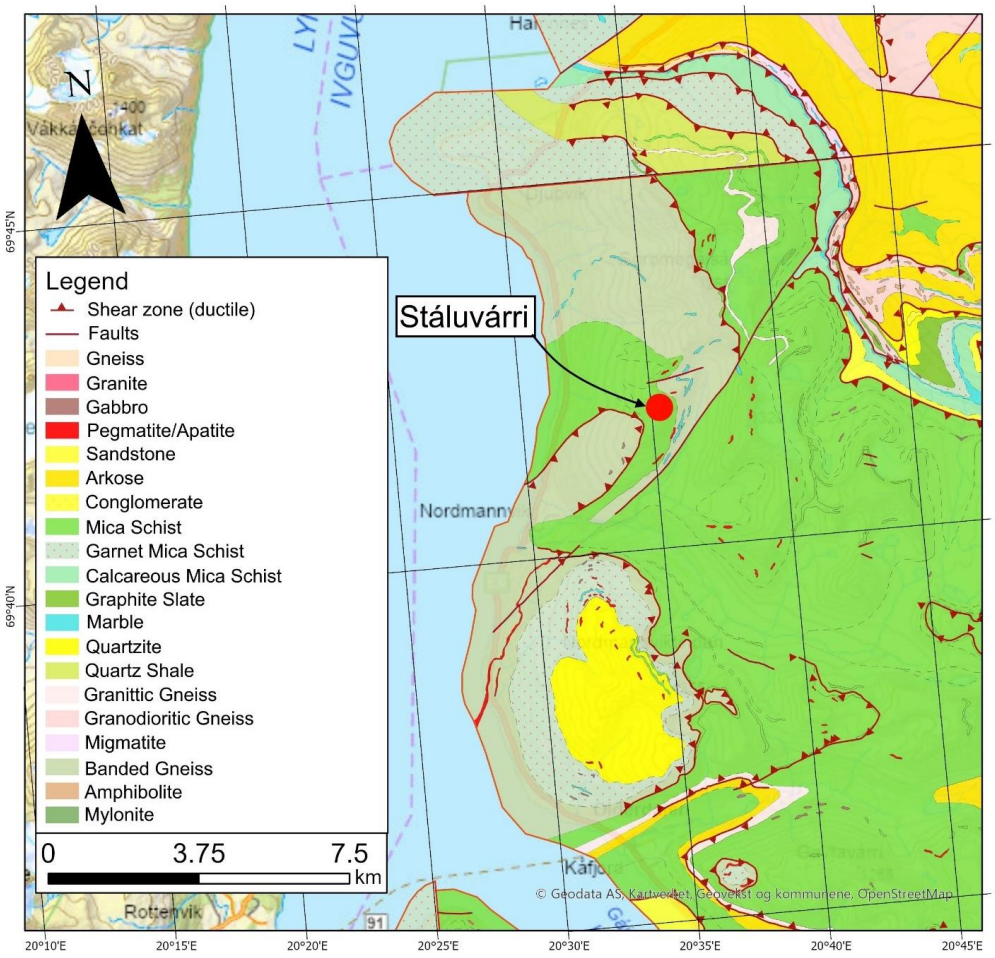

Figure 4: Bedrock map of Ståluvárri and surrounding areas Red dot marks the top of Ståluvárri. The bedrock map is based on Zwaan et al. (2006), projected with a scale of 1:50 000.

1.5.2 Post-Caledonian extension and rifting

After the Caledonian orogeny, the other major event which affected a lot of the geology is the onset of rifting and extension due to the collapse of the mountain chain and opening of the Iapetus Ocean (Ramberg et al., 2013). The presence of these extensional forces is observable in a lot of the structural geology which overprint the orogenic foliation and folding. Fault structures of this origin can be seen as major lineaments on the terrain and a lot of fjords and valleys follow this pattern as a result of the brittle properties. The tectonic lineaments in Northern Norway are heavily dominated by two faulting directions, trending NW-SE and the conjugate set going ENE-WSW (Gabrielsen et al., 2002). This fault pattern can be traced from Nordland to eastern parts of Finnmark. On the Vesterålen-Lofoten Margins, these faults developed as a stagewise clockwise rotation of the extensional forces from WNW-ESE into

NNW-SSE between the Permian and late Cretaceous (Bergh et al., 2007). S1 faulting from Permian-early Cretaceous strike NNE-SSW, developing into S2 faults striking WSW-ENE sin the early-late Cretaceous. The youngest fault system is the S3 NW-SE from late Cretaceous-Paleogene (Bergh et al., 2007).

1.6 Quaternary geology and periglacial processes

1.6.1 Quaternary history

A factor when considering rock slope deformation and stability is the influence quaternary geological history has had in an area. The last glacial maximum (LGM) during the late Weichselian ended around 18 ka BP, when thick ice sheets covered most of the northern hemisphere (Mangerud et al., 2011). From that point on the ice coverage has been receding and readvancing in shorter glacial and interglacial periods, pumping and shaping the topography. Evidence of these glacial and interglacial periods is well pronounced in the terrain in Troms. The main lateral moraine ridges seen across the valleys often stem from the younger dryas around 11-10ka BP, which are evidence of a major glacial readvancement (Mangerud, 2004). In Kåfjord valley there is evidence within the moraine material and marine limits of a few glacial retreat and readvancement events between 9800-9400 BP, before complete deglaciation began of associated fjords and valleys in the area (Corner, 1980). Most likely this happened sometime between the Ørnes event (9800 BP) and the Skibotn event (9500 BP), leading to the exposure of the valley.

Glacial erosion and the eventual debuttressing leads to overstepped valleys and fjords, creating the relief necessary for gravitational forces working the deformation of the rock slope (Crosta et al., 2013). During glacial events the ice cover work as a stabilizing factor when considering the rock slopes, but the eventual deglaciation causes reversal of these forces increasing the extensional stress along the valley flanks and compressional stress along the valley bottom. This increases the brittle properties within the rock, due to the differential stresses this causes (Crosta et al., 2013).

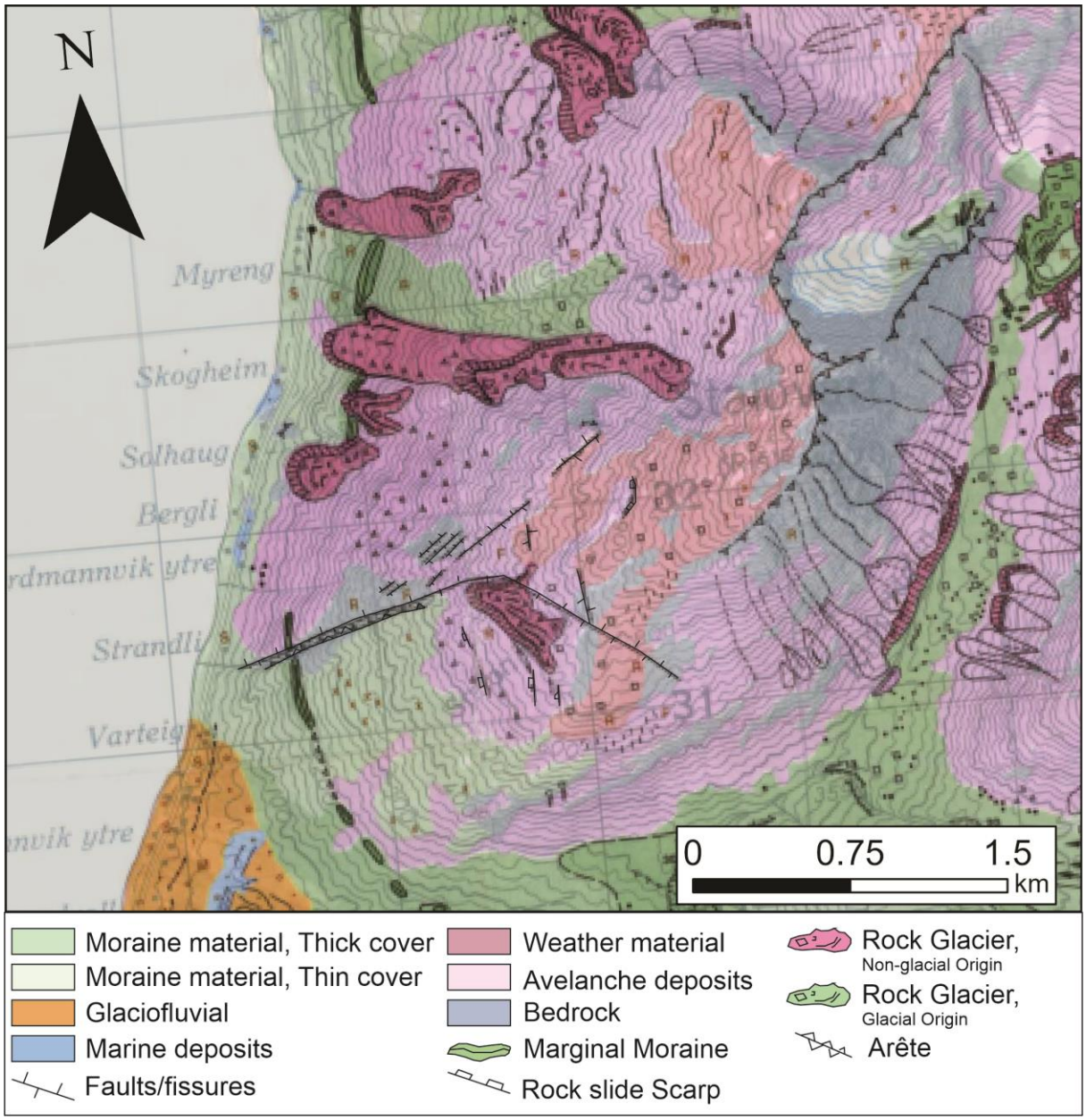

Figure 5: Quaternary map over Stáluvárri and Ytre-Nordmannvik Map modified from Tolgensbak and Sollid (1988). Map scale is projected to 1:50 000

The influence of quaternary geology around Stáluvárri can be observed as post-glacial remnants, slope deformation and periglacial processes. *Figure 5* above illustrates the quaternary geology around Stáluvárri. The lower areas of the slopes are mostly covered in moraine material, marine deposits or fluvial deposits. Further up along the mountain, the material is either a result of deformation activity, weathering of the bedrock or untouched bedrock. There is some collection of colluvial material along the eastern side of Stáluvárri as rockfall topples from the steep cliffs.

Another aspect of the post-glacial period has been the isostatic uplift which still can be observed in large parts of Scandinavia, especially further inland where the ice cover was at its thickest. After removal of the ice cover and its mass, the continental crust undergoes a rebounding phase because of the massive weight difference (Mangerud et al., 2011). The rise of the crust is an impacting factor which can decrease the stability in the newly formed alpine terrain. Crustal rebound after a glacial period can cause tectonic activity and seismicity, being an initiator for rock slope deformation or a reactivator of extinct ones (Crosta et al., 2013; Vick et al., 2020b). In the immediate aftermath of deglaciation, there is evidence of a lot of landslides which could be attributed to tectonic activity because of this (Bøe et al., 2004).

1.6.2 Periglacial processes

Periglacial processes can be defined as movement which is influenced by ground ice within the soil and is very common in high latitude and high-altitude areas (Leigh et al., 2021). Ground movement created by this affect observed movement along the mountainsides when using remote sensing. Two of the more common periglacial processes in the area considered is permafrost and rock glaciers.

A lot of the mountain sides in Kåfjord have distinguishable lobe shaped features of rock material classified as *rock glaciers*. Most of them are likely to be extinct as there is very little movement able to be observed on them, especially in the lower ones. Rock glaciers can either originate as remnant ice after deglaciation, or as in the case for Stáluvárri be of periglacial origin through permafrost processes (Tolgensbak & Sollid, 1988)

In the arctic regions a relatively common phenomenon is the permafrost. This ground process is present here for most of the year due to the cold conditions in the higher latitudes. Permafrost happens sporadically in the higher altitudes in northern Norway but can also be found further inland in the southern parts (Leigh et al., 2021). Gradual climate change in the northern regions can influence the presence of ground ice, which previously could have worked as a stabilizing factor within rock slope deformation. Melting permafrost within rock bodies increase the rock slope deformation as scarps loses a binding factor and potentially new water channels open up and increase the water pressure within fractures (Kuhn et al., 2021).

2 Rock Slope deformation theory

2.1 Structurally controlled instability

Rock slope stability is influenced a lot by the structural geology in an area (Bunkholt et al., 2012; Vick et al., 2020b). Structural features can often be traced to visible and observable fabrics found on the surface geology, where foliation, joints, fractures and folds are prime examples of this. They can form persistent planes of weakness, or discontinuities, which in turn can cause rock slope deformation to occur (Wylie & Mah, 2005).

3 Foliation

Foliation can commonly be found in metamorphic rocks, where it originates because of ductile deformational processes, or it can be observed as a primary fabric within magmatic rocks. In Metamorphic rocks it originates as either a primary fabric as a result of bedding in the sediments or as secondary fabric as a result of tectonic stress, where they form a planar to curviplanar fabric (Fossen, 2016). Due to the tectonic history of Norway this is a common observation in most of the lithology, where they in the Troms region often can be seen dipping between NW-W (Augland et al., 2014). The dip angle of the foliation relative to the downslope direction can greatly influence the stability of the slope. With the right direction and right critical angle, the foliation can become discontinuity causing instability(Vick et al., 2020b). On Stáluvárri the foliation is dipping around 20-30 degrees towards the west.

3.1.1 Joints and faults

Tectonic processes in the uppermost part of crust generate brittle deformation within rocks, which causes joints and faults to form. Faults can influence rock slope deformation either as an oversteepening factor or as a plane of weakness (Vick et al., 2020b). Faults typically contain breccia or gauge which lowers the effective strength of the rock mass (Fossen, 2016).

Joints similarly are caused by brittle deformation which accommodate for the strain but occur as smaller structures. These can appear as fracturing within the rock and can form sets hosting regular patterns, irregular patterns or as a combination of the two (Fossen, 2016). If these are persistent enough within the rock mass, they can form backscarps, scarps or rock bridges between the foliations to form a through-going sliding plane in the slope (Vick et al., 2020b).

For the case of Ståluvárri the joint sets appear most often in an orthogonal pattern towards the north and are dipping relatively vertical on the surface.

3.2 Geomorphological features

During mapping of the slope, some different types of geomorphological features will be identified and used to discuss the slope development later.

Backscarps are a prominent feature within rock slope deformation and are the detachment point of the unstable domain and the stable domain. This detachment could be because of a daylighting foliation plane, joint plane, fault or lithological boundaries (Vick et al., 2020b). Similarly, as the rock body is moved downslope, multiple *scarps* or *counterscarps* can develop intermediately as more weakness zones open due to differential movement within the displaced block (Wylie & Mah, 2005).

The intermediate scarps within the moving body may cause *ridges, trenches* or *terraces* to form to accommodate the space (Agliardi et al., 2001; Crosta et al., 2013). Ridges are accommodation of space through loose rock which is compacted to an elevated profile. Trenches or fractures form in between these ridges and scarps and are a result of extensional fracturing of the dislocated block, which can either appear as open or infilled (Agliardi et al., 2012). When intact to semi-intact rock develops scarps in the back, terraces may form as horizontal to sub-horizontal areas. This could take the form of a step-like topography.

When discussing the surface material observed some classifications are made. The mostly intact rock mass which is undeformed is the *bedrock. Disaggregated rock* describes areas of intact to semi-intact rock where the rock slope deformation has displaced it. *Disintegrated rock* refers to displaced material which has usually been transported further and is significantly broken up.

4 Methods

During this study a few different tools for gathering data and observations has been used, which includes movement data (dGNSS, InSAR and Extensometer), fieldwork, desktop data and thin sections, all of which will be elaborated below.

4.1 Movement data

4.1.1 dGNSS Data

One tool used quite frequently to gather movement data on unstable slopes is the Differential global navigation satellite system (dGNSS). Using fixed GPS points on the ground, the deformation of a slope can be observed down to millimetres per year. Points are placed in multiple locations on the assumed deforming block where a signal emitted from satellites is received for each of the giving them longitudinal, latitudinal and vertical position every 5 seconds. The positions are then calculated into horizontal and vertical vectors relative to a GPS point placed in an assumed position with zero movement (NVE, 2019; Oppikofer et al., 2013). Combining this data over multiple years can give a good indication of how much movement and in which directions both vertically and horizontally.

4.1.2 Extensometer data

Extensometers tape are useful tools for gathering displacement between crack and fractures and repeated use over years can be used for measuring millimetre displacement between two points. Because it is based off a wire connected between two hook points it is prone to uncertainties such as temperature changes and wind (Soil INSTRUMENTS, 2014).

The positional data for each location has three linear regression models applied to it: least squares, least squares with variance and robust regression. Regression models using least squares is unweighted and begins at zero, while the robust regression adjust for outliers. For most of the GPS points, the models amount to very similar numbers. The exception is GPS 1 where the outliers influence the vertical component so much that the plunge varies from almost horizontal to 18° plunge. As the robust regression give vertical displacement going out of the slope, this seems to not be the most accurate representation for this position, especially since other models give results more similar to related GPS positions. To keep the results consistent only the least squares regression model will be considered further.

Extensometer measurements has been gathered between cracks located in lower domain horst and graben system. Three locations have been documented with the respective name STAL31, STAL32 and STAL33. Distance between the hook points are relatively far apart with 16,7m for STAL31, 13,8m for sTAL32 and 13,0m for STAL33. During 2016 field season a new extensometer equipment were used, and previous data has been adjusted by the length difference because of this.

4.1.3 InSAR data

Interferometric Synthetic Aperture Radar (InSAR) is a remote sensing tool, greatly used for assessing slope deformation. Before the release of InSAR Norway, a public domain tool published by NGU and the Norwegian space agancy, around 250 unstable rock slopes were known to the public (Oppikofer et al., 2015). Since its release a lot of new ones has been detected and either been assessed or will be in the future.

The data used in InSAR Norway is gathered by the European Space Agency (ESA) satellites *Sentinel-1A* and *Sentinel-1B*, launched 2014 and 2016 respectively, orbiting earth in a near polar path (ESA, n.d.). Data collection is done by the Synthetic Aperture Radar (SAR) systems on board, which emits an electromagnetic signal that is reflected by the earth, before being received by the satellite again. The SAR technology give access to image the earth by night and day regardless of what weather might interfere (Copernicus, n.d.). Instrumentation carried by the satellites is directed right side of the orbit path and gives a swath image of up to around 250km wide. This give a line of sight (LOS) between 30º to 45º depending on how far away from the satellite it's gathered from (NGU, n.d.). Because of the polar orbit of the satellites and the fixed angle of the SAR equipment, each pass over an area gives imagining along an ascending and descending track making it possible to measure movement towards the LOS and away from the LOS. The frequency of each pass varies between every 12th to 6th day depending on how many of the satellites are operational. Since 2022 only Sentinel-1A has been operational due malfunctions on Sentinel-1B (Copernicus, n.d.). As there is frequent imaging of the earth with these satellites, deformational processes can be observed down to millimetre scale by comparing the relative speed between two points on the image.

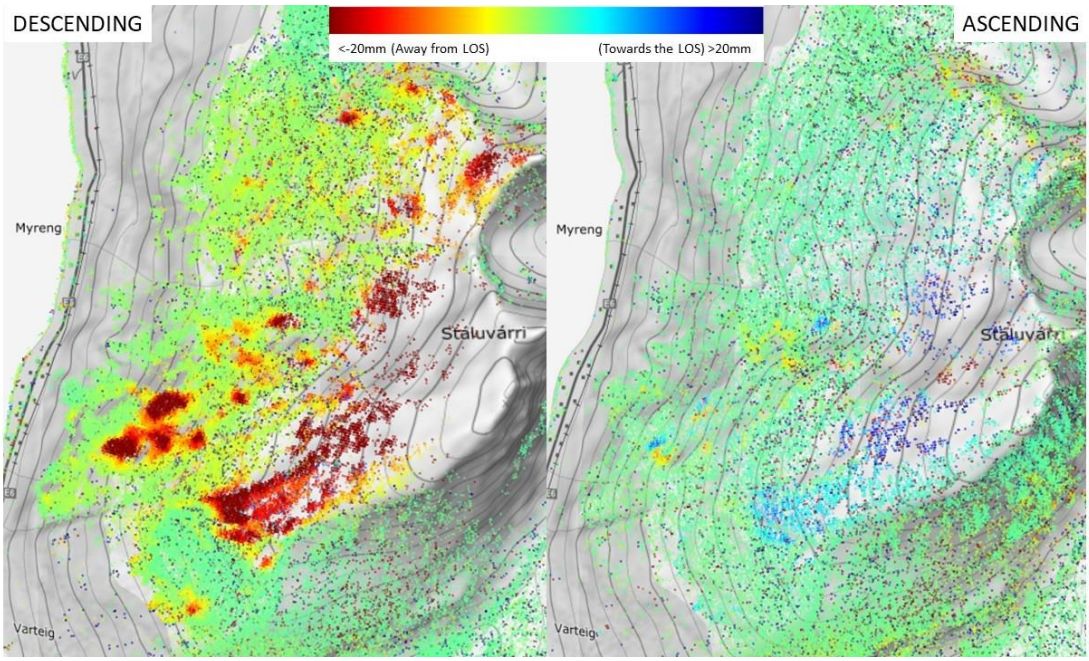

Figure 6: Example over the observed movement of Ståluvárri *The descending is movement here is observed away from the satellites, while ascending here is movement towards the satellites. The scale is between -20 and 20, but movement can also be Descending and ascending datasets are from the 2019-2023 datasets from insar.ngu.no.*

Constraints to this technique involves the polar orbit and angle of the equipment since this means the optimal slopes to observe is either facing west or east. Because of the steep terrain as well there is areas where the LOS of the equipment will observe as shadow areas, where it's too steep for it to observe the ground movement or its blocked due to its LOS. To much movement on a slope as well pose a problem as movement above a 100mm per year is not possible to properly detect. Another constraint in Norway is its arctic latitude, as there are quite long winters where the mountains are covered in snow. This greatly reduces the accuracy of the data gathered in between November to May. InSAR Norway therefor only accounts for the months June to September/October.

4.2 Structural and geomorphological mapping

4.3 Available desktop data

Kåfjord has an available 1:50 000 bedrock map produced by Zwaan et al. (2006) and a 1:50 000 quaternary map produced by Tolgensbak and Sollid (1988). There has been processed a couple of digital elevation models (DEM) for the area which can be mosaiced together. The available datasets are the following: *NDH Reisadalen 2pkt 2020, NDH Nordreisa 2pkt 2021, Kåfjord 5pkt 2019, Troms 5pkt 2015* and *Troms 2pkt 2014.* Finished DEM will be used to

help map out the geomorphology. All data available from hoydedata.no. Orthophotos available for Stáluvárri is Troms 2016 produced by Norges Kartverk. These can also be used for identifying surface visible structures and surface morphology.

4.4 Fieldwork

The fieldwork was conducted during two separate field seasons. Sindre Norheim started in 2018 and conducted fieldwork the 2nd of September, between the 11-14. September and 16-19. September. In 2023 fieldwork was conducted on the 16th of august, 15th of September and between 23-25. September.

4.4.1 Structural data gathering

As mentioned in previous chapters, an important step in assessing the stability of the slopes is gathering an understanding of the predisposed and inherited weaknesses in bedrock. In Troms County these weaknesses often follow the foliation and joints originating from earlier tectonic events.

Gathering this type of data is manual labour involving using some type of compass and clinometer tool. Traditionally this means using an analogue compass, but with the increased reliability of digital tools for measurements this is also an option. This project has relied mostly on the digital tools for measurements, where the most efficient and reliable technique for using digital tools is to take multiple measurements on the same surface and to optimize the sensors before starting to measure. This is especially important for older androids as the sensors often are not as accurate.

In 2018 the measurements for foliation and joints were gathered with a digital compass and clinometer. Unfortunately, what software and phone type which was used is an unknown factor, but since the photos taken by the student uses the format "*.heic"*, it's most likely an apple product. Most software automatically translates these measurements to true north, adding on the declination relevant for the GPS position. When comparing the dip direction gathered during this field and the dip direction gathered in similar positions during field in 2023, this seem to be the true.

During the 2023 field season the measurements were done using traditional and digital compasses. For the 2023 field season all measurements have been translated into true north. The software used were the app *FieldMove Clino* Pro v2.5.19 developed by *Petroleum*

Experts Limited. Settings for the magnetic sample size were *High (default)*, and the added declination was 10.5°. The phone used while gathering were *Samsung Galaxy A53 5G*.

In total 2765 measurements have been collected, but a large amount of this is due to the rule of collecting multiple data points per surface. Collected joints, foliation and structural elements are all shown as dip and azimuth in the datasets. These data points have then been processed into averages in the software *Rocscience Dips 8.022* developed by Rocscience. The same software can be used to do kinematic analysis of collected data.

4.5 Samples and thin sections

During the 2023 field season a couple of samples were collected for later use and examination. Eight samples were collected from various sections of the slope. Most of the collected samples were in-situ positions of stable and disaggregated rock, except for two of them which were loose rock material found within the unstable parts.

To get a better look and understanding of the microstructures and composition of the rocks, some of the gathered samples were turned into thin sections. Using a rock saw, *MK Diamond 101XL,* with a diamond edge the samples were cut into thin rectangular prisms of around 1x2x3cm in size before being handed off to the lab. The lab applies the sample to a glass plate with epoxy glue, cuts away excess material, grinds it down to around 100-200µm and polish the sample into thin sheets of around 30 µm.

Thin sections are a good tool for getting a rough understanding of the mineral assemblages and microstructures within the samples. At 30 µm the emitted light from the microscope can give insight into the specific optical properties of the minerals observed. This can be the colour seen under plain polarized light (PPL), relief, extinction angles, cleavages, pleochroic properties and birefringence. Other properties of the thin sections which can be determined is microstructures and deformational processes on the grains.

4.6 Kinematic analysis

The software Dips by Rocscience can be used to assess various theoretical failure types through constructing plots based of kinematic properties such as slope dip, slope aspect, friction angle and lateral limits. This is done to later be used in the hazard assessment, but in general these types of failure assessments is not meant for more complex failure scenarios such as large landslides as it was optimally designed for use in smaller engineered slopes (Stead & Wolter, 2015).

Slope dip and slop aspect properties define the daylight envelope, meaning the necessary relief needed for the sliding plane to develop out of the slope (Rocscience, n.d). Friction angle is constricting factor where planes above this can initiate sliding and is recommended in Norway to be set to a conservative value of 20° (Hermanns et al., 2012b). Lateral limits constrict the angular extent of failure zone as there is a tendency for planar sliding and toppling to be confined within a set range away from the slope direction (Goodman, 1980).

Since there is some deviation in the slope dip, this is adjusted to the upper value to gather a maximum criticality for each failure type. All values will therefore be given in the ranges from mean to maximum.

Three different kinematic failure plots are considered, planar sliding, wedge sliding and flexural toppling. Planar sliding considers one plane and if it can initiate sliding. Wedge sliding is the ability for two intersecting planes sliding to initiate. This is based on the intersection of data points, instead of the pole vectors when planar sliding. toppling considered. Wedge sliding can either happen along both planes or one of them and is denoted as *crit. 1* and *crit. 2* respectively. Direct toppling considers situations where a near horizontally dipping plane intersects with a plane dipping near vertically into the slope, and could as a result topple overnear vertical into the slope, which in turn can initiate failure (Wylie & Mah, 2005).

4.7 Risk assessment

NGU has over the years produced their own standardized spreadsheet for evaluating risk and consequence of potential rock slope failures. This accounts for the standardized nominal

yearly likelihood categories 1/100, 1/1000 and 1/5000 used in other hazardous events which has to be considered for public safety (Hermanns et al., 2012b).

This thesis will only account for the risk assessment as no extensive consequence analysis has been done for Stáluvárri as this would require also assessing the potential for displacement wave initiation and how devastating this would be in the surrounding area. The risk test take into account the following criterions as per Hermanns et al. (2012b): Backscarp development, potential penetrative failure surface, lateral release surfaces, kinematic feasibility, morphological expression of the basal rupture, displacement rates, acceleration, rockfall increase and presence of post-glacial events in the slopes vicinity. Each criterion is divided into several conditions, each given an individual score. These are available for review in appendix x.

5 Results

The results section below is divided into four major parts based of descriptions of the structural data and kinematics, morphological mapping and field observations, movement data (e.g. GNSS observation, InSAR and extensometers) and lithological descriptions.

5.1 Structural data

Structural data gathered during the 2018 and 2023 field seasons has been analysed. The joints can be seen as having three main orientations, where two directions are often more represented in the data. Free hand selection is used of the poles along their most clustered section. In later chapters the structural data will be used in kinematic analysis of the area and for assessing the cross sections along the slope. All stereonets use the projection setting lower hemisphere with equal angle. The poles for the averaged structural elements include variation of 1 standard deviation (1σ).

The observations have been divided into three separate domains for easier representation and to account for possible changes and are defined after the variation in the observed foliation, this includes a lower domain, an upper domain and deformed domain (Figure 7).

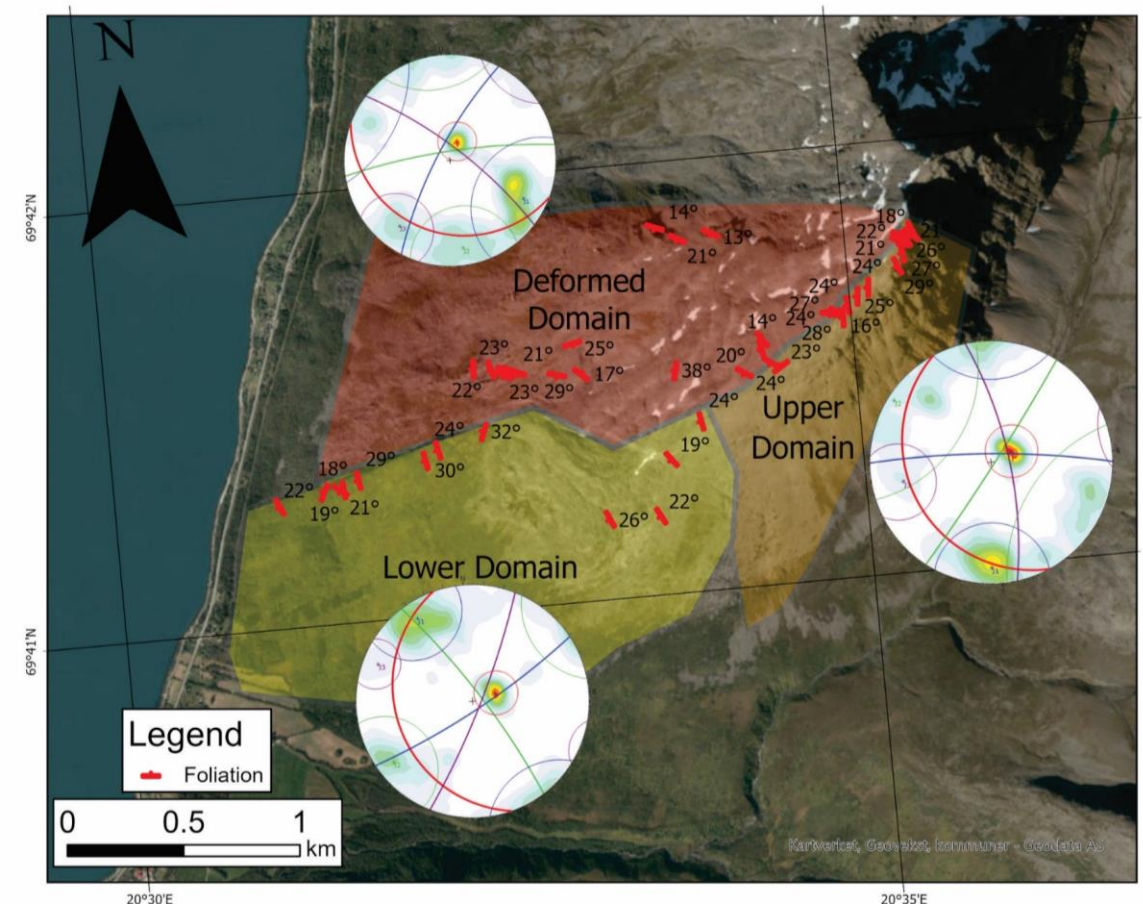

Figure 7: Structural domains on Stáluvárri Each of the data gathering points are added as foliation. The averaged measurements are shown in each stereonet, corrected towards the north.

5.1.1 Lower domain

Structural observations within the lower domain have been gathered along the outcrops around the major fault which stretches from sea level to around 600 m.a.s.l (Figure 8). Around 546 structural measurements were gathered around the fault ridge, and some points further to the east.

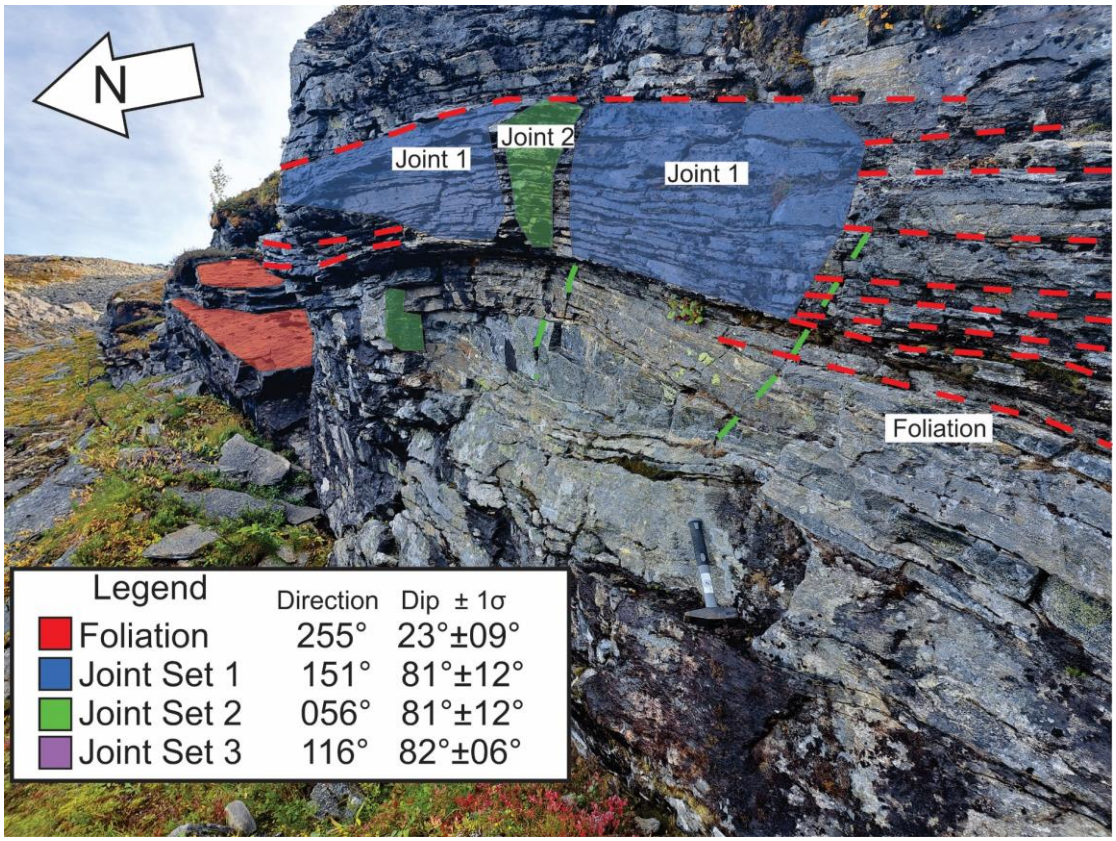

Figure 8: Example of the observations and structural elements from the lower areas of the slope, here from the major fault. Foliation marked by red lines and polygons on the horizontal surface, joint set 1 marked by blue lines and polygons along the walls and joint set 2 marked by green lines and polygons going into the walls.

Foliation in the lower area has an average dip direction and dip of 255°/23°, with a pole deviation of 9°. The pole entries show a concentrated cluster (Figure 9). In general, the foliation appears as relatively smooth to semi roughed surfaces which are very persistent throughout. Though they are often influenced by localised lenses of more competent rock.

Joints in the lower domain can be divided into three different sets, but two of these mainly stand out with higher point concentrations. Joint set 1 is a relatively vertical NE-SW striking element but has an averaged dip direction and dip of 151°/81°. The cluster is concentrated giving a deviation of 12° (Figure 9). Joint set 2 has a less concentrated cluster. It is NNW-SSE striking with averaged dip direction and dip of 059°/81° with deviation of 12° (Figure 9). Joint set 3 is the least dominant one and has a small, concentrated cluster. The averaged plane strikes SSW-NNE with averaged dip direction and dip of 116°/82° with deviation of 6° (Figure 9).

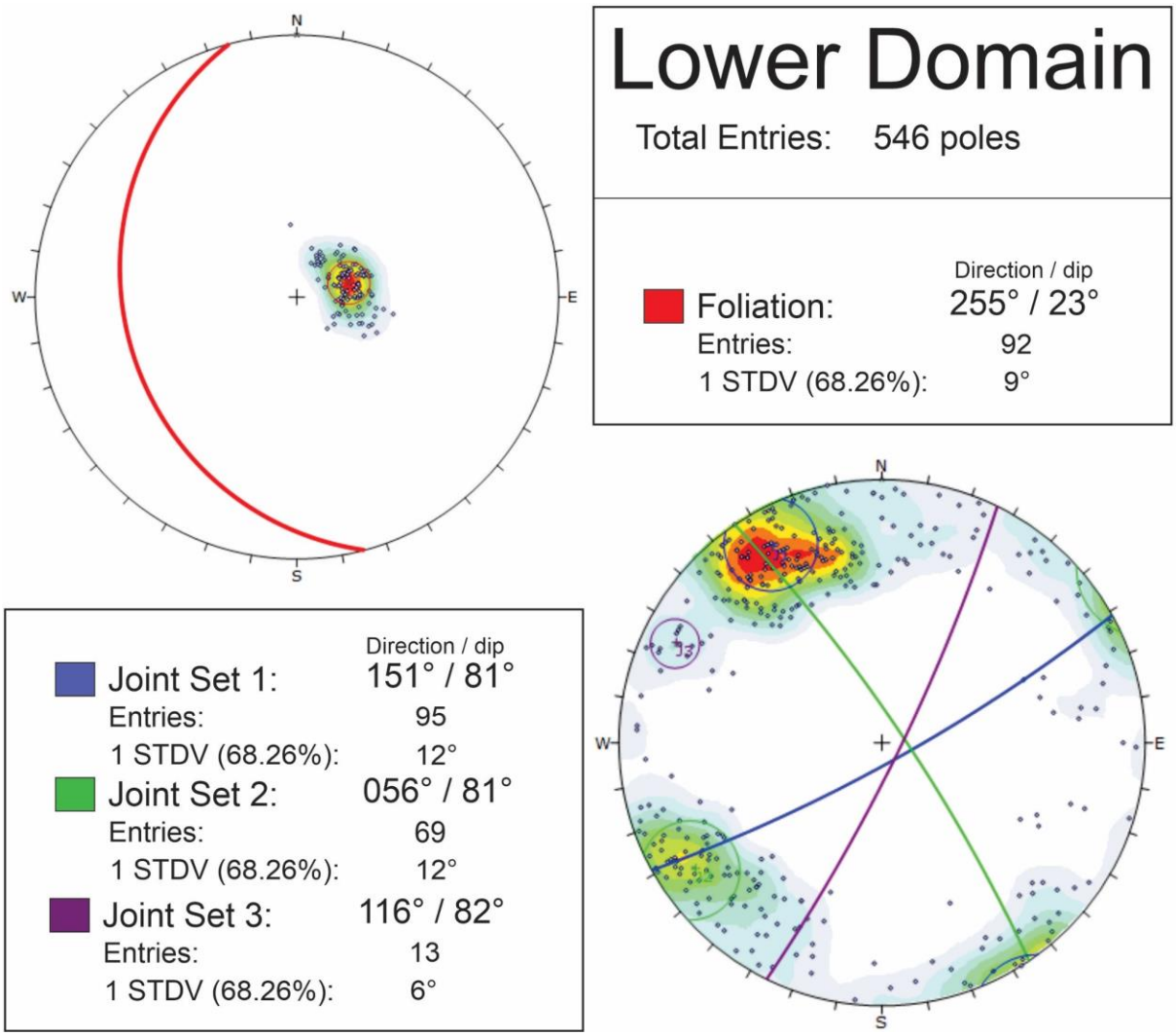

Figure 9: Averaged structural elements within the lower domain The averaged joint values are based of measurements with similar striking direction on opposite sides of the stereonet and gathered around the highest density areas.

5.1.2 The Upper Domain

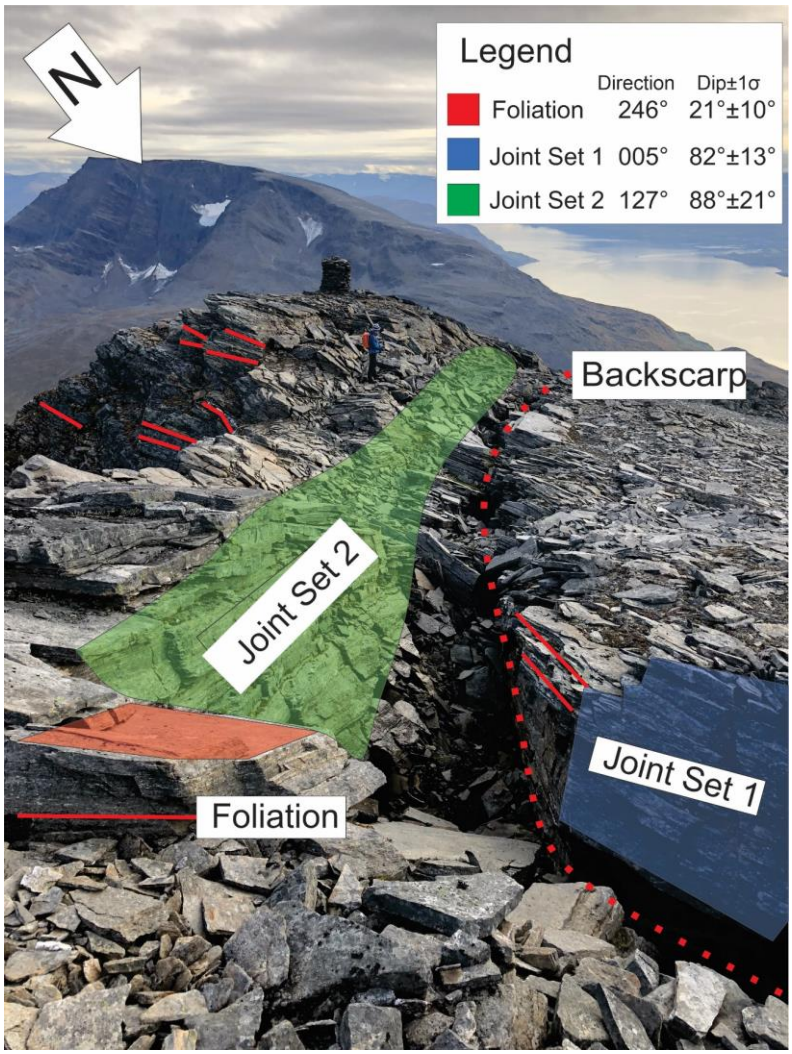

Figure 10: Example structural features in upper domain.

In the upper domain the structural sets vary slightly. Measurements were gathered from 800m.a.s.l to the peak. The total gathered measurements from the upper domain amounts to 793 pole entries, which has been averaged into foliation and three sets of joints.

The foliation plane has an averaged dip direction and dip of 246°/21° with deviation of 10°. The cluster is spread but has a clear concentration (Figure 10). The foliation plane is generally smoother than the lower domain and appear as very persistent planes. Spacing between the planes seem to be less as well compared to the lower domain.

Out of the three joint sets two of them appear as more dominant. Joint set 1 is a W-E striking with good clustering on both sides of the plot. The averaged pole has a dip direction and dip

of 005°/82°, with a deviation of 13° (Figure 10). Joint set 2 strikes NE-SW and has an averaged dip direction and dip of 127°/88°. The cluster is spread giving it a relatively high standard deviation of 21° (Figure 10). This large deviation reflects the changing orientation of the set along the ridge where measurements were taking. From the peak it shifts from NNE-SSW striking directions to NE-SW striking directions further downslope. Joint set 3 has less recognised poles and has a small cluster which gives a N-S striking plane. The averaged dip direction and dip is oriented 084°/73° with deviation of 10° (Figure 10).

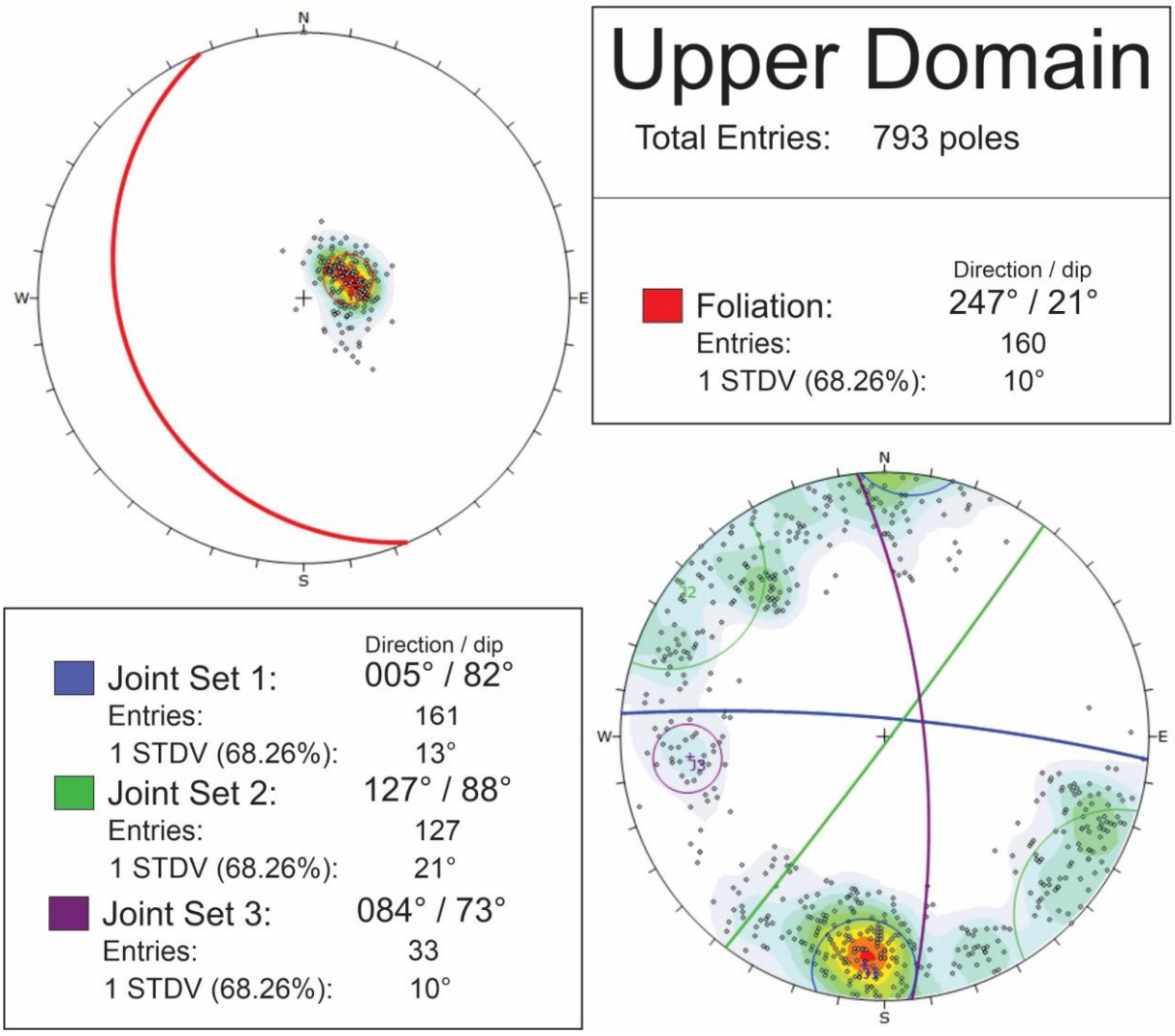

Figure 11: Structural measurements from the upper domain. The averaged joint set values are based of measurements with similar striking direction on opposite sides of the stereonet and gathered around the highest density areas.

5.1.3 Deformed Domain

The deformed domain has the most collected data, with 1384 pole entries. Similarly, as before foliation and three joint sets are defined as structural groups.

The foliation and joints within the deformed area are spread out in comparison to the first two domains but display a reliable clustering. The averaged pole dip direction and dip for foliation is 205° / 21° with a deviation of 9° (Figure 12). Joint set 1 has a NE-SW striking orientation with averaged dip direction and dip 302°/77° and deviation of 18° (Figure 12). Joint set 2 is W-E orientated with averaged dip direction and dip 356° / 79° and deviation of 14° (Figure 12). Joint set 3 has an averaged dip direction and dip of 042°/76° striking NW-SE, and deviation of 10° (Figure 12).

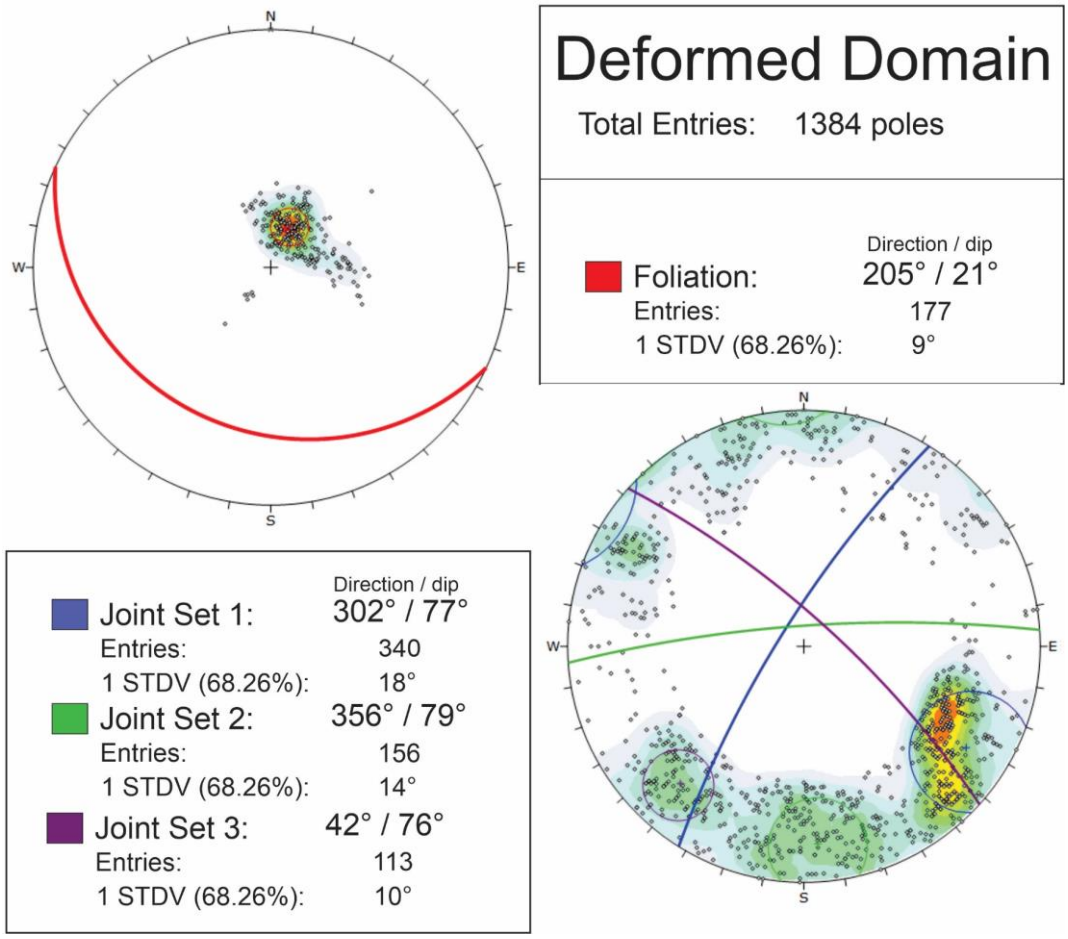

Figure 12: Structural measurements and elements within the deformed domain The averaged joint values are based of measurements with similar striking direction on opposite sides of the stereonet and gathered around the highest density areas.

5.2 Kinematic analysis

Kinematic analysis is applied to the domains illustrated on Figure 13. Slope dip and aspect of each of the domains is given respective ArcGIS Pro tool *zonal statistics*, which collect a mean value and its deviation over a given area (Figure 13).

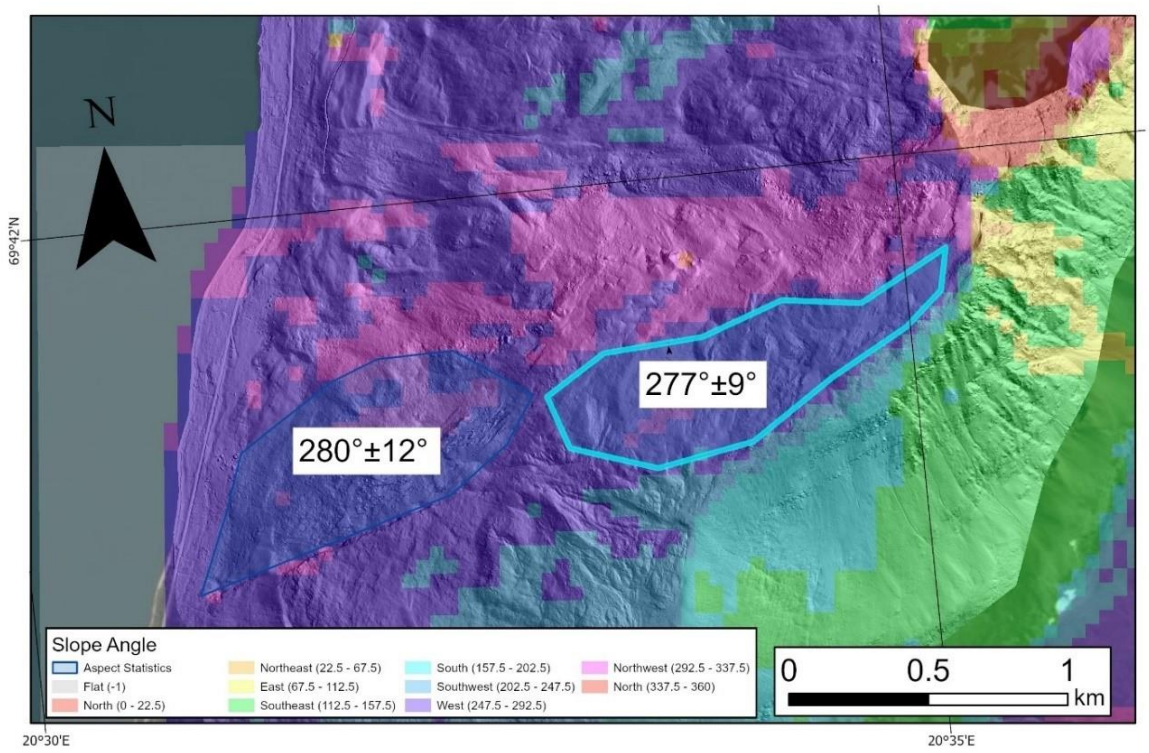

Figure 13: Overview map of slope aspect on Stáluvárri DEM has been resampled to 50m x 50m cells before creating the aspect raster. Aspect within the different parts of the mountain sides decided using the Zonal Statistics tool in ArcGIS Pro.

5.2.1 Lower domain Kinematics

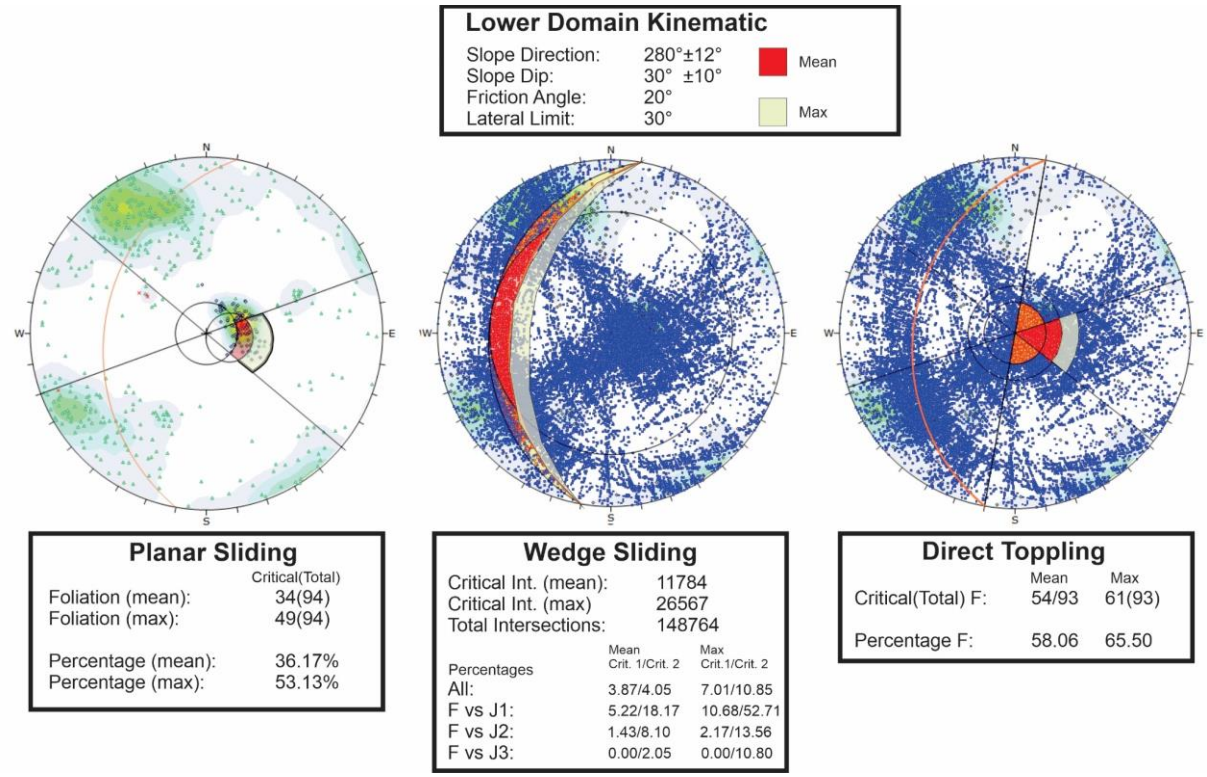

Figure 14: Kinematics analysis for the lower domain Mean and maximum values considered for planar sliding, wedge sliding and flexural toppling.

Within the lower domain the aspect is 280°±12° with a slope dip of 30°±10°. Planar sliding has a relatively high number of foliation poles within the critical zone with a percentage ranging between 36-52% (*Figure* 14).

Wedge sliding has a percentage of 8-18% of intersections within the critical zones when all intersections are considered. Intersections between foliation and joints has the only potential for sliding, where one plane sliding between foliation and joint 1 stand out with critical zone percentage ranging between 18-52% (*Figure* 14)

Direct toppling has considers mainly intersections between foliation and elements, and show to a high percentages 58-65% (*Figure* 14).

Out of the three considered failure types, planar sliding and direct toppling along foliation stands out as the scenario with the highest likelihood for initiation. Apart from this wedge sliding between foliation and joint set 1 has a relatively high potential as well, but similarly only when sliding happens along the foliation plane.

5.2.2 Upper Domain Kinematic analysis

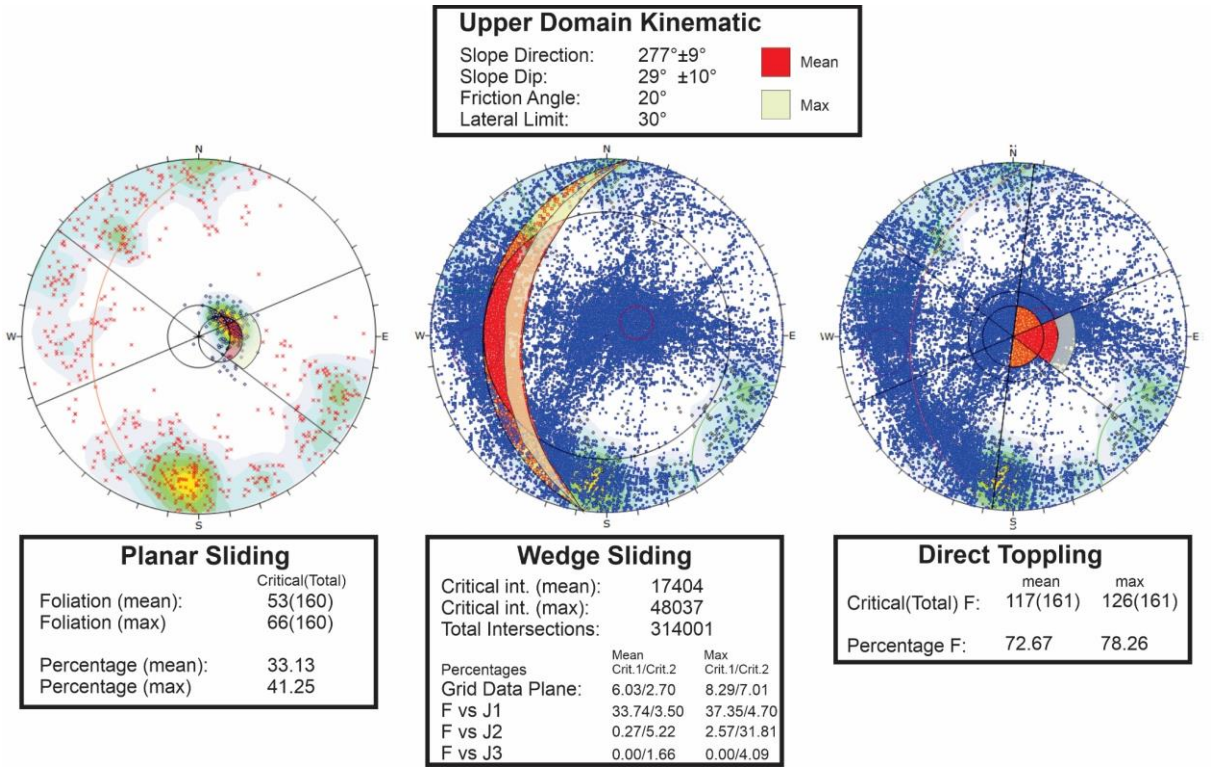

Figure 15: Kinematics analysis for the upper domain Mean and maximum values are considered for all planar sliding, wedge sliding and flexural toppling.

The Upper domain has slightly changed values for the slope properties, with an aspect of 277°±9° and slope dip of 29°±10°. Kinematics for planar sliding has high percentage of poles falling under the critical zone, between 33-41% (Figure 15).

Wedge sliding has a total percentage of intersections falling within the critical zones between 8.73-15.3%. When sliding happens along both planes, foliation and joint set 1 has a percentage of 34-37% falling within the critical zone. When sliding happens along one plane, foliation and joint set 2 has a percentage ranging between 6-32% within the critical zone (Figure 15).

Direct toppling between intersections of foliation and other planes show to very high around 72-78% likelihood (Figure 15).

Foliation and direct toppling show both to relatively high likelihoods for sliding

5.3 Morphological mapping

Morphological mapping along the slope is based on observations done through the desktop data, field observations, drone material and previously established Quaternary maps. Combining these observations a composite morphological map of the surficial ground cover is constructed as well as a morpho structural map of linear structures of deformational origin.

5.3.1 Surficial cover

Through orthophotos and field observations a few different categories for surficial ground cover have been defined, which includes varying amount of vegetation and quality of the rock cover. Figure 16 includes some examples of the surficial ground cover which are relevant for later assessments.

The vegetation is classified into two categories, *Dense Vegetation* and *Thin Vegetation* (Figure 16A and B). Dense vegetation on Stáluvárri is sections of the slope which is covered by densely packed forestation. There are some variations on how far up dense forestation reaches, as sections below displacement processes have an upper limit of 200 m.a.s.l. but with sparse patches above this. In the southern to southwestern side of the slope dense forestation reaches up to around 600 m.a.s.l (Figure 16B). From field observations the more densely vegetated areas are a mix of birch, spruce and pine trees which can stretch up to around 200 m.a.s.l. Above this point the vegetation is either densely packed birch or medium packed birch (Figure 16A). Beyond this the vegetation transitions into *thin vegetation,* where there is either only a few birch trees, some bushes, or sections where vegetated soil can be observed.

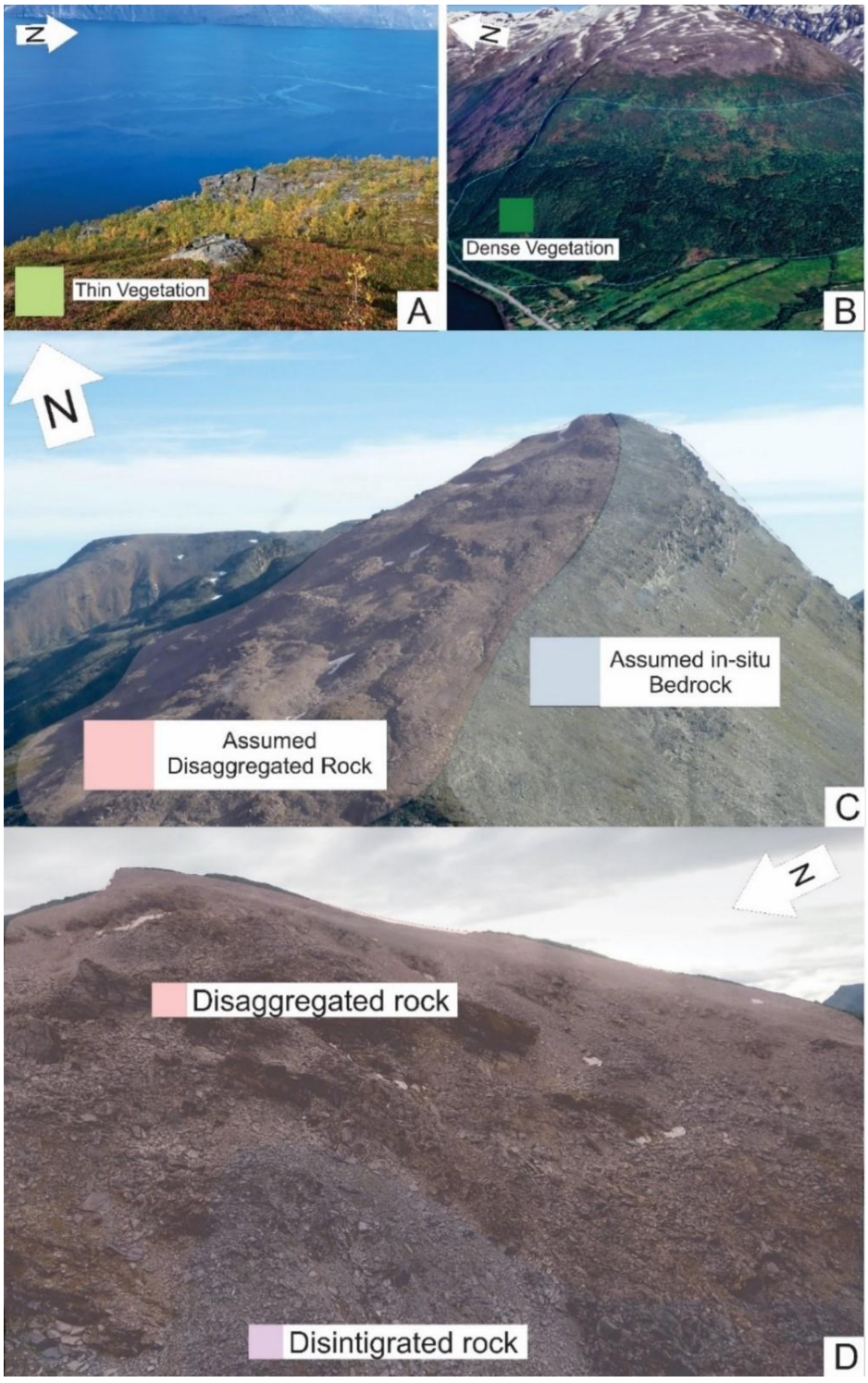

Figure 16: Classifications of the different surficial ground cover observedA) and B) illustrates the differences in vegetation types from thin vegetation to dense vegetation. B) gathered from Google Earth @2024 Airbus. C) shows the difference of the stable bedrock position and the disaggregated rock sections. Picture by Reginald Hermanns 2013. D) Transition between the disaggregated rock to the collection of disintegrated rock. Picture by Sindre Norheim 2018.

The development of the surficial rock cover is categorized based on what stage of rock slope deformation the section is within. Assumed stable and undeformed *bedrock* positions can be found along the southeastern ridge of Stáluvárri (Figure 16C). Towards the eastern to southeastern vertical side of the ridge toppling and rock fall occur as the mountain toe has multiple collections of talus deposit. The horizontal bedrock positions are often covered by deposits as results of weathering, with thin to thick cover of loose cobble to small boulder sized rocks.

The west facing side of the slope has surficial cover which are either *disaggregated rock* or *disintegrated rock* (Figure 16C and D). The disaggregated rock sections here is classified by areas where deformational structures can be observed, remote sensing detect movement and where outcrops of seemingly intact rock can be observed. Gravitational processes cause steeper areas of the disaggregated sections to be covered with talus, with cobble to boulder sized rocks (Figure 16C and D).

The disintegrated rock section seen in Figure 16D is at the edge of the disaggregated rock sections, seen in areas where the slope steepness suddenly increases. Rock material found within this section is very varied from larger boulders measuring 1-5m in size to collections of very disintegrated rocks.

Apart from the unstable rock slope classifications, quaternary features are also classified when relevant. *Rock glaciers* is relevant here as movement could be observed while using remote sensing dependent on if they are still active (Tolgensbak & Sollid, 1988). These can be characterized by lobe shaped deposits and occur in a few locations up the slope (Figure 17).

Around the 200m elevation on the slope there are large ridges traversing the contour line. Looking at them through elevation profiles they appear as either flat lying surfaces or slightly raised ridges of 10m. These are the *lateral moraines* from the quaternary glaciations (Figure 17). Within the disaggregated rock section, a small section of the lateral moraine has its ridge peak displaced downslope about 20m in elevation from the lateral moraine on the stable position.

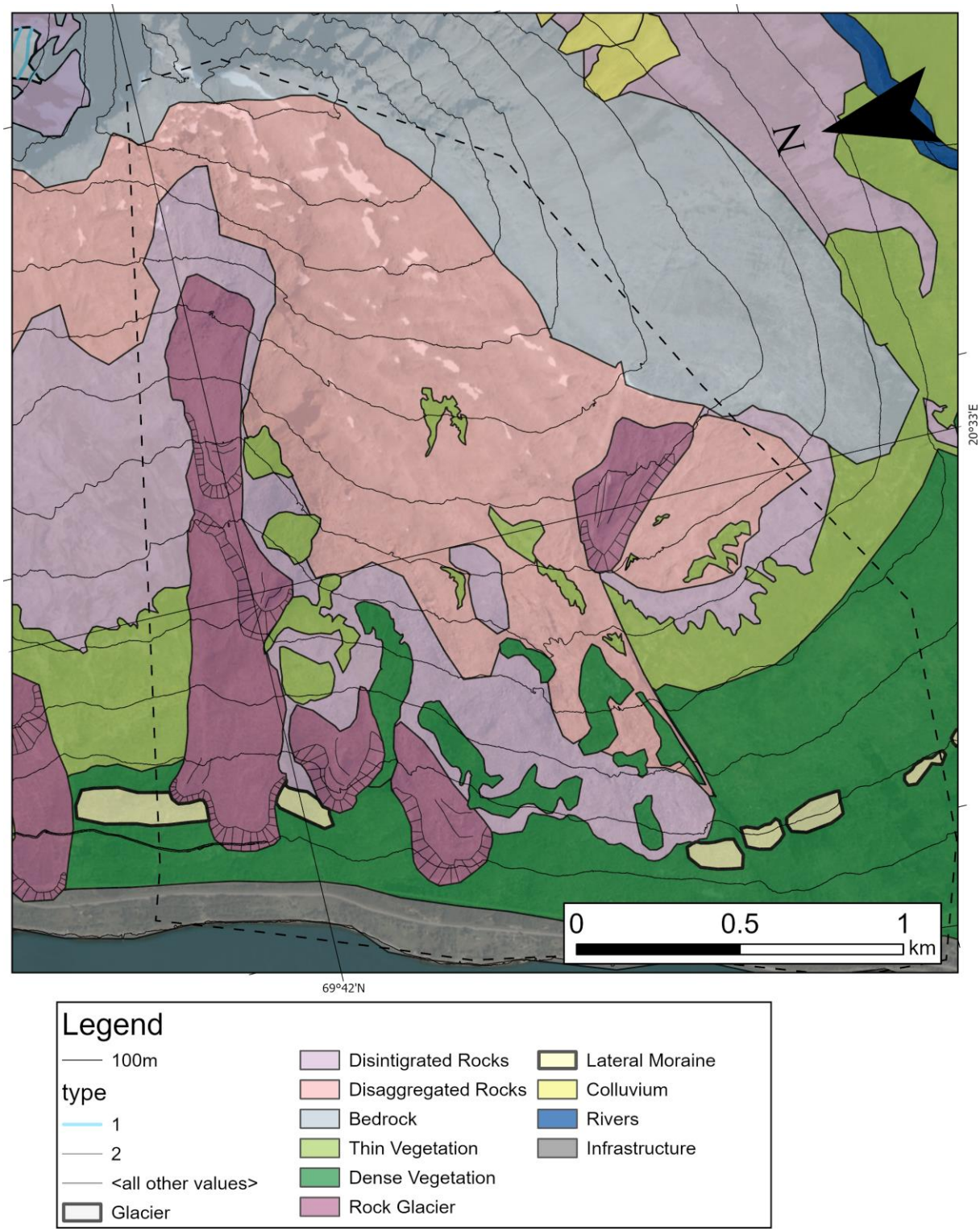

Figure 17: Morphological map of the surface cover on Stáluvárri Beyond the extent area the mapping is done with less detail in focus. The contour lines are separated at every 100m. Background map @Kartverket, Geovekst, kommuner – Geodata AS

5.3.2 Morphostructural Mapping

This section will address linear deformational features along the slope, using field observations, slope inclination map, DEM and orthophotos. Through the gathered field and desktop observations a morphostructural map of the area has been interpreted (Figure 19).

At the peak of Stáluvárri a significant westwards steeply down dipping slope surface can be traced from the north following from Figure 18B, to Figure 18A before it gradually flattens out in the south. The maximum height of the slope surface is about 20m, and it can be traced 500m before it flattens out in the south. For the upper section of Stáluvárri this is one of the clearer backscarp development and is rupture surface which can be seen cross cutting the foliation in Figure 18A and potentially more following the foliation in Figure 18B. However, viewing the slope from the south of Figure 18B it is cross cutting it, so it is likely matter of perspective caused by the planes oblique orientation to each other. Eastern side of the peak has westward dipping fractures crossing the in similar directions as the backscarp.

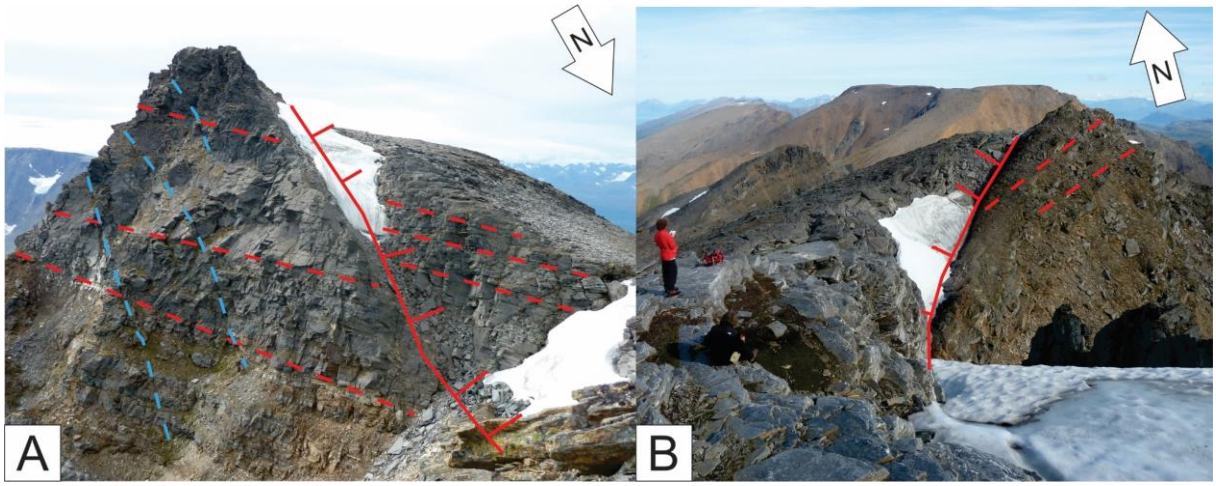

Figure 18: Scarp observed on the top of the mountain. This is the assumed backscarp along the peak with left side looking southwest and right side looking northeast. A) distinct declined rock surface can be seen here with fractures in the back following a similar orientation. Foliation is cross cut by the scarp. Pictures by Reginald Hermanns 2013.

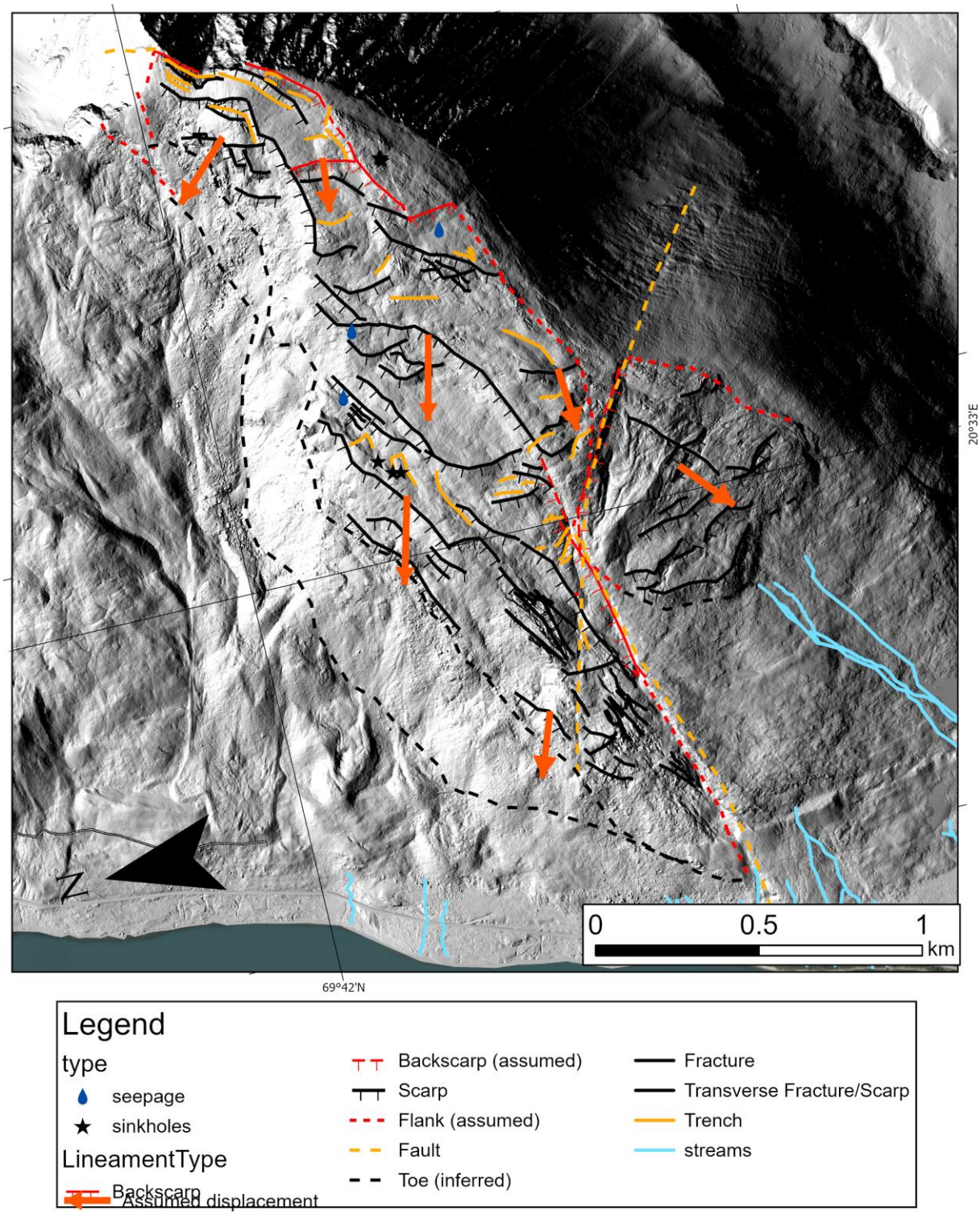

Figure 19: Morpho structural map of Stáluvárri Various separate domains have been defined based on amount of displacement in the rock mass, where some sections show to higher amount of displacement.

At the upper surface of the scarp, on a dislocated body fractures and trenches can be seen developing parallel to it towards the southwest. This can be seen as a structure developing from the peak as a semi open fracture which has separated around 2m (Figure 20D), continuing into another fracture downhill towards the southwest (Figure 20B) ending as a infilled trench which has a gap of 2m in the section where the scarps elevation is flattening out (Figure 20C). Straight west of the scarp in Figure 18, a section going downhill appear as a horst and graben system where the elevation fluctuates. These appear as scarps and counter scarps (Figure 20D)

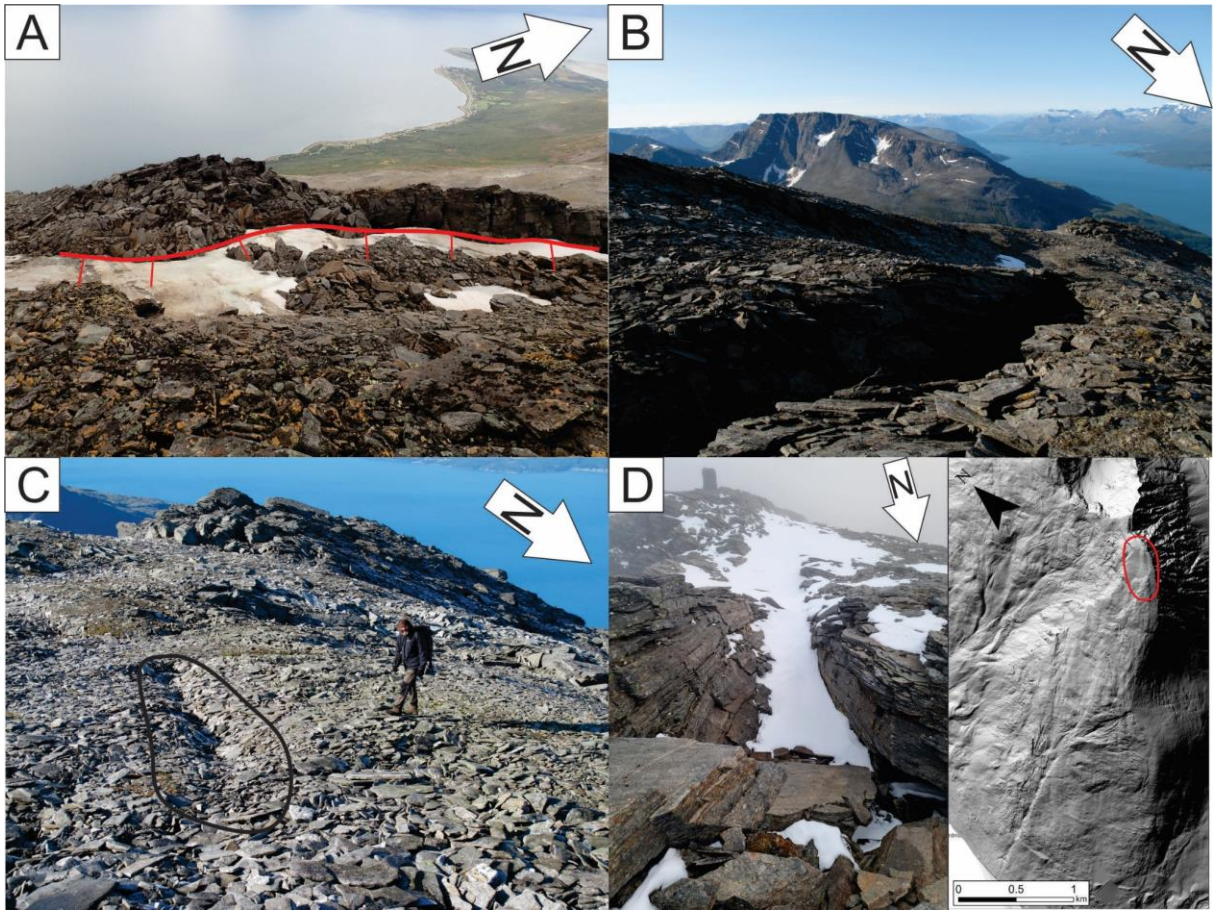

Figure 20: Structures which can be seen along the top ridge which indicate displacement processes. A) is looking down the slope at a horst and graben system, picture taken by Maria Bredal 2018. B) large fracture near the peak, picture taken by Halvor Bunktholt 2010. C) an infilled trench near the peak top, picture taken by Halvor Bunkholt 2010. D) a fracture at the peak of Stáluvárri

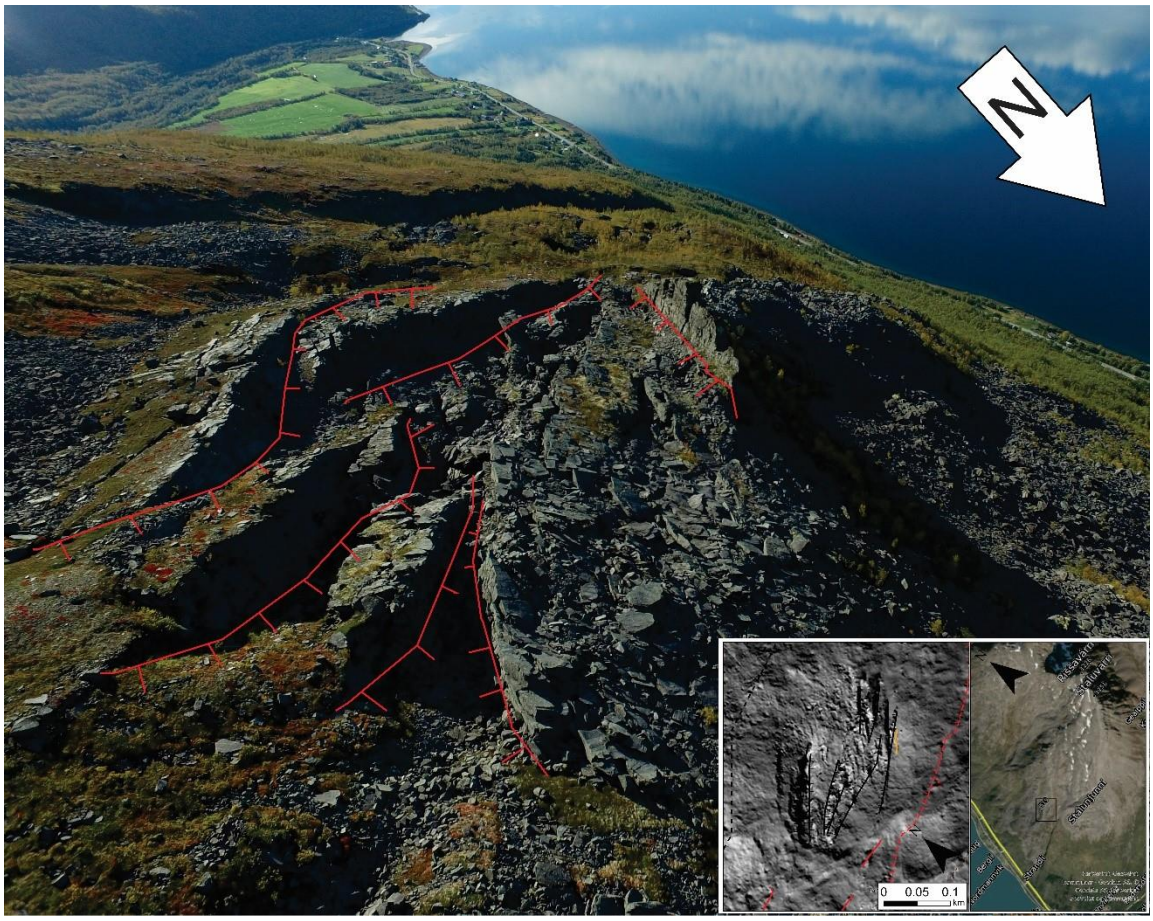

Figure 21: Large horst and graben system within the lower domain. which can be traced downslope towards the west as open fractures. Picture taken by Sindre Norheim 2018.

Within the lower sections of the slope (Figure 21) several horst and graben systems have developed along a NE-SW striking direction, creating a highly fractured area of disaggregated rock with depressions and elevation gains of 5-10m. These are developing scarps, trenches and fractures forming a very distinct section. Downslope from the outer edge of this system, the inclination increases rapidly, and the surface cover develops into disintegrated rock. Behind the large horst at the edge of the system dense vegetation has developed. The larger NW-SE arête following the southern edge of this system is potentially a larger fault. It can be traced further up as a scarp in the upper domain (Figure 22).

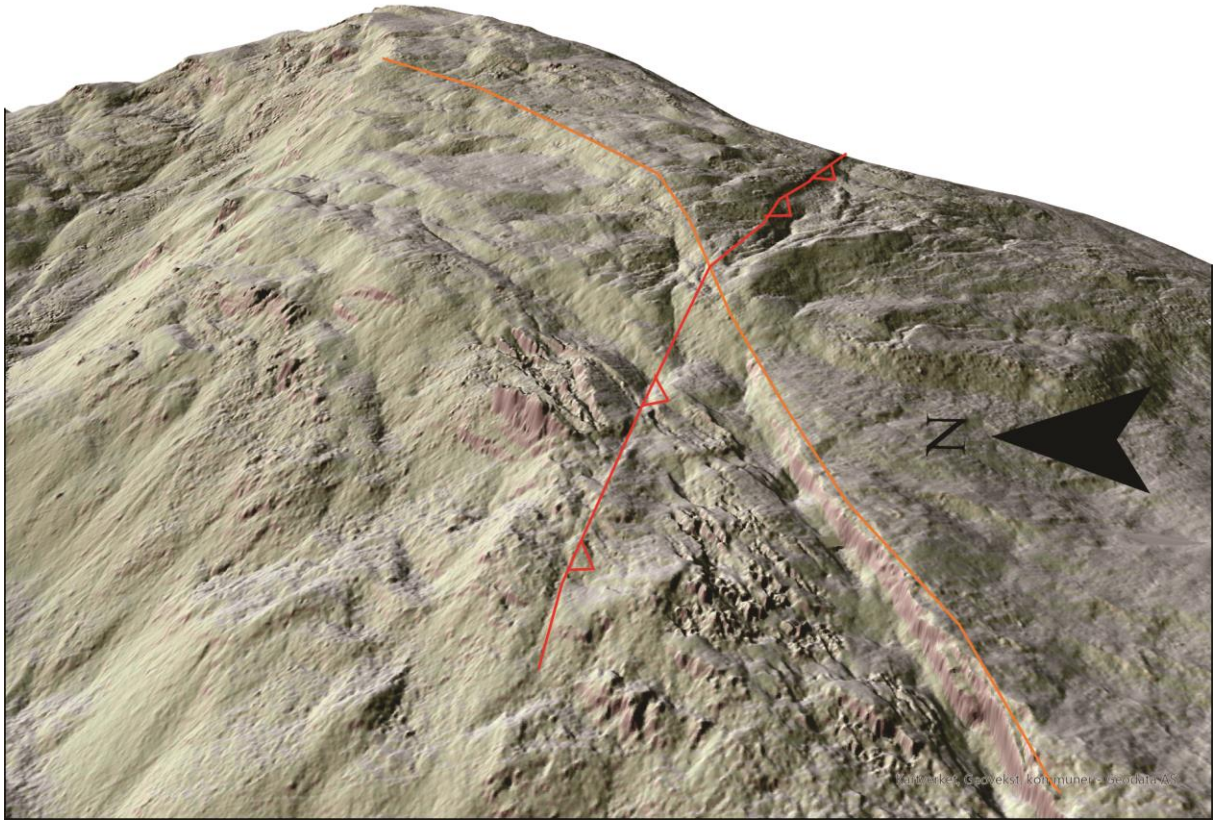

Figure 22: Large faults following the NW-SE (orange) and NE-SW (red). The NW-SE is not identified by the surface further up but seems to have a similar orientation in the upper section.

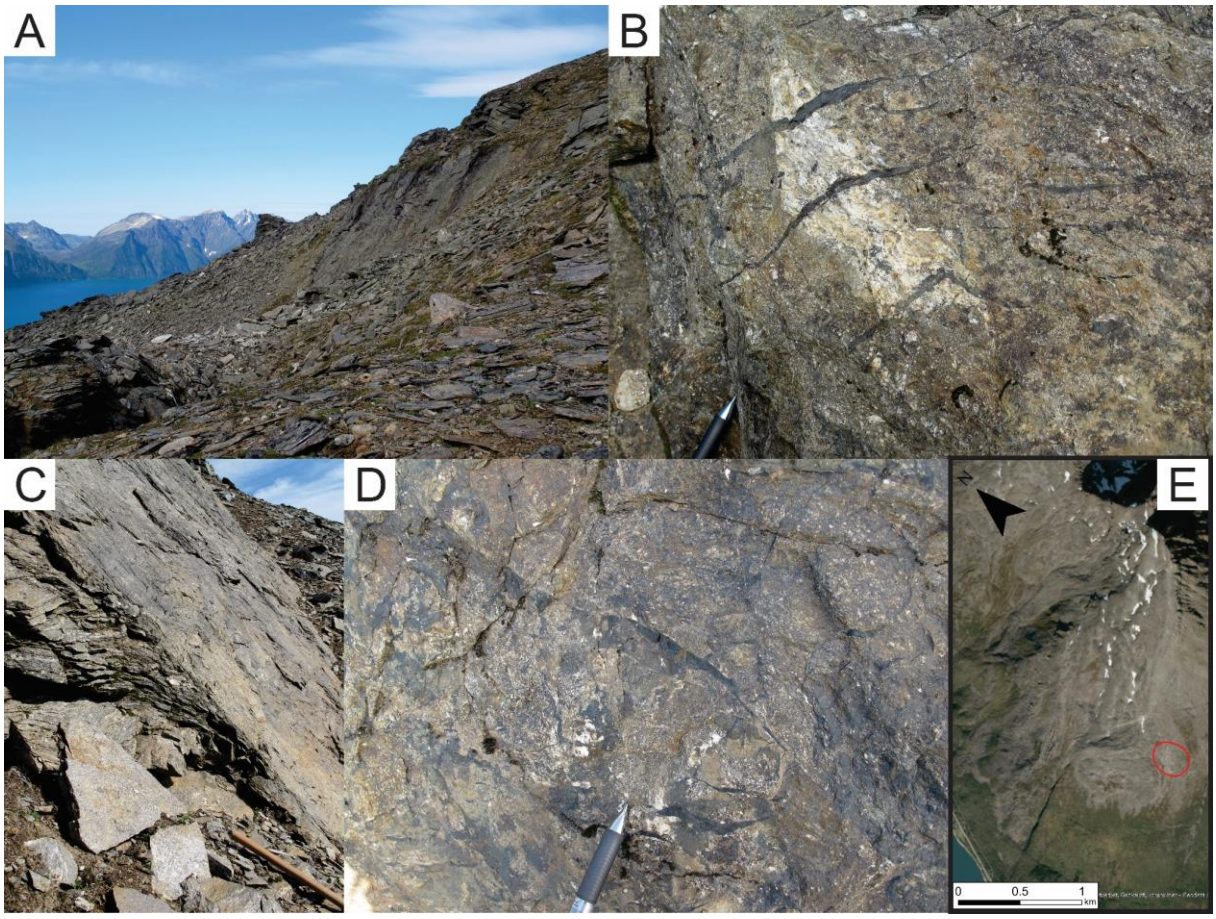

Figure 23: Fault plane evidence from lower domain soutwest facing section A) shows a section where some displacement process is visible in front of a wall face. B) is a close up pseudotachylyte forming on the surface of said plane. C) indicates a downslope deformation of the surface. D) shows another surface with pseudotachylyte. E) shows the approximated location of the pictures taken by Halvor Bunkholt 2010.

One major lineament on the map can be identified by surface alterations as a fault plane. Along a NW-SE striking lineament, seen crossing the slope relatively close red line on Figure 22, can be traced on the surface between 1.5-2km in length, a distinct shear sense and evidence of deformation is visible. Figure 23C shows a downward folding in the foliation and a smoothed outer sliding surface. In other sections of the face pseudotachylyte mineralisation is evident seen as darker strips of finely grained rock on Figure 23B and D), a result of frictional melting due to earthquakes or in some instances large landslides (Fossen, 2016). The steeply dipping shear sense and mineralisation indicate normal faulting happening at greater depths with higher temperatures where more ductile conditions are present.

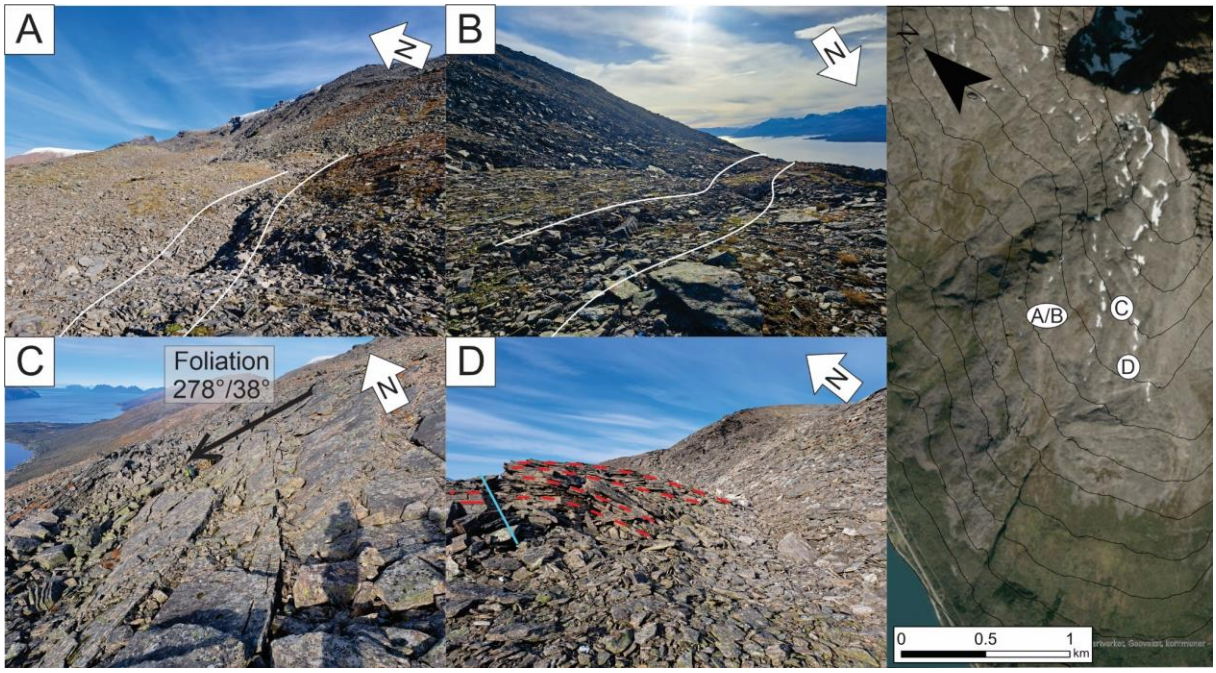

Figure 24: Morphstructural observations along a few more sections. A) and B) displays some infilled trenches in the middle of the deforming domain. C) Foliation rotated 20-30 degrees within the disaggregated rock body. D) downturned foliation in front of a large scarp section towards the southwest.

Within the lower sections of the upper deformed domain several infilled trenches appear as far down as 700m.a.s.l indicating continuing extensional deformation of the disaggregated body. Figure 24C shows foliation on disaggregated rock being slightly rotated towards the west, while D) shows foliation rotating from out of the slope into a more parallel position again. It is located very close to a scarp and is dip oriented towards west-southwest.

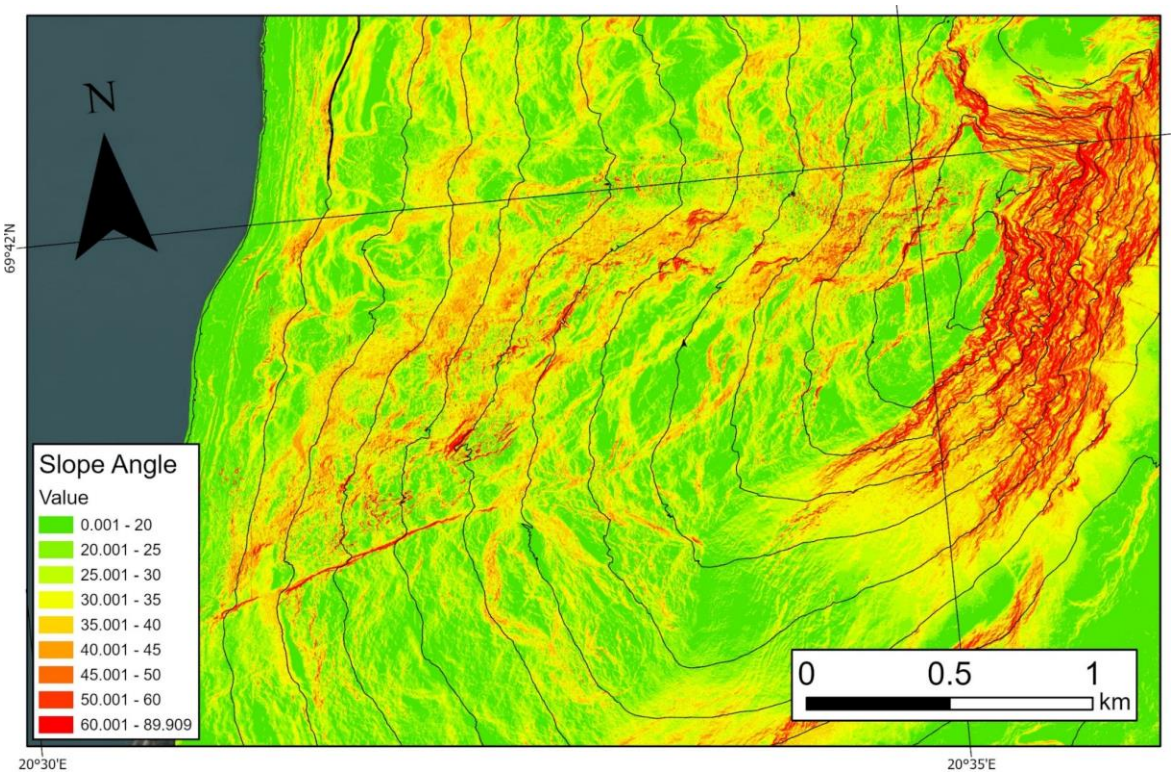

Figure 25: Map of Stáluvárri showing how the slope inclination develops up the mountain. Within the upper section a lot of developed sudden increases in elevation can be seen in, with an average raise of 20m.

For mapping scarps, trenches, and other surface visible lineaments, a slope angle map as well as the DEM has been used for finding rapid elevation changes (Figure 25). Within the upper domain of the slope sudden increase in inclination can be observed in multiple locations, but the surfaces are often masked by talus formations. Two main orientation directions for the scarps can be seen within the upper domain. One of them being an often more elongated system striking between NE-SW to ENE- WSW. The second orientation has striking direction NNE-SSW to N-S for sections following the western slope aspect closer to the lower domain southwest facing aspect these appear more often as NW-SE. The average elevation rise of these scarps are 20-30m. Flatter surfaces on the slope are often between 10-20°. Some locations along the upper domain have been observed to have running water which has been marked as seepage (Figure 19).

Within the lower domain most of the observed lineaments appear as large trenches and open cracks separating larger bodies of disaggregated rocks. There is a clear dominant development towards the of W-E and ENE-WSW striking lineaments. Smaller fractures can appear as either connecting these larger trenches or as independent, striking in a NW-SE direction.

5.4 Movement data

This section will cover available movement data from Stáluvárri, which includes gathered dGNSS data, InSAR data and extensometer data.

5.4.1 dGNSS

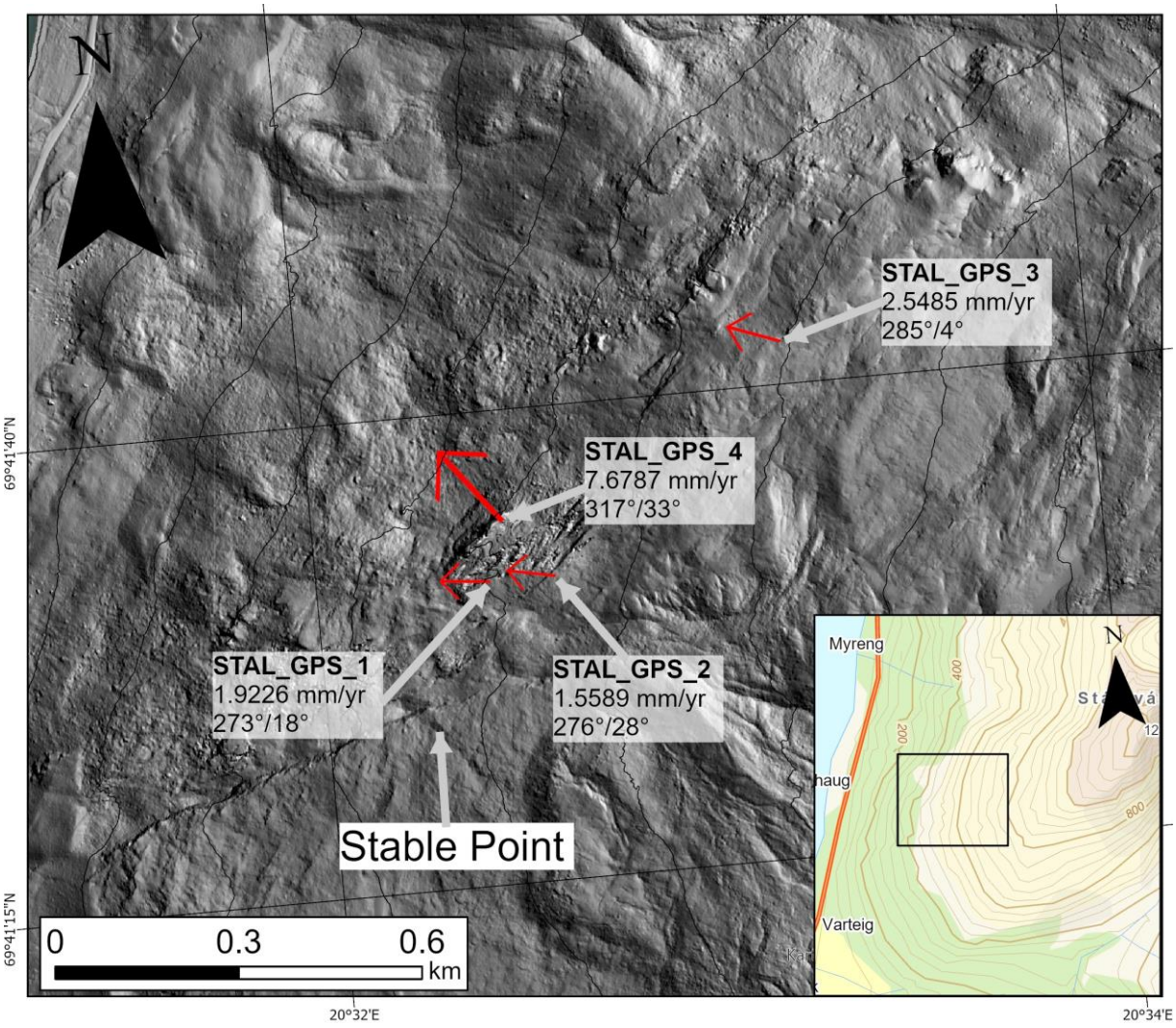

Figure 26: Points of dGNSS positions on Stáluvárri,collected by NGU. Horizontal displacement shown as vectors on the map and mm/yr represent the 3d displacement. All gathered values are the mean from least square regression.

Within the highly fractured area GPS 1 has a horizontal component of 270°±5° and a vertical component of 18°±8° (Fig. 18). Slope dip and displacement plunge is relatively parallel here. GPS 2 has a horizontal component towards 276°±5° with a vertical component of 28°±6° (Figure 27). Plunge of the displacement is slightly steeper than the slope. Both GPS positions have relatively low 3D displacement velocities below 2mm/yr. Within the lower domain GPS

4 stands out as the 3D displacement velocity is around 8mm/yr. It has a horizontal component towards 317°±3° and a vertical component plunging 33°±1° (Figure 27).
GPS 3 located some distance away has an annual 3D displacement velocity around 2.5mm/yr. The horizontal displacement direction is 285°±7°, while the vertical component has a plunge of 4°±4° (Figure 27). The slope dip here is around 20-30° towards 290°, meaning the displacement vector is going out of the slope.

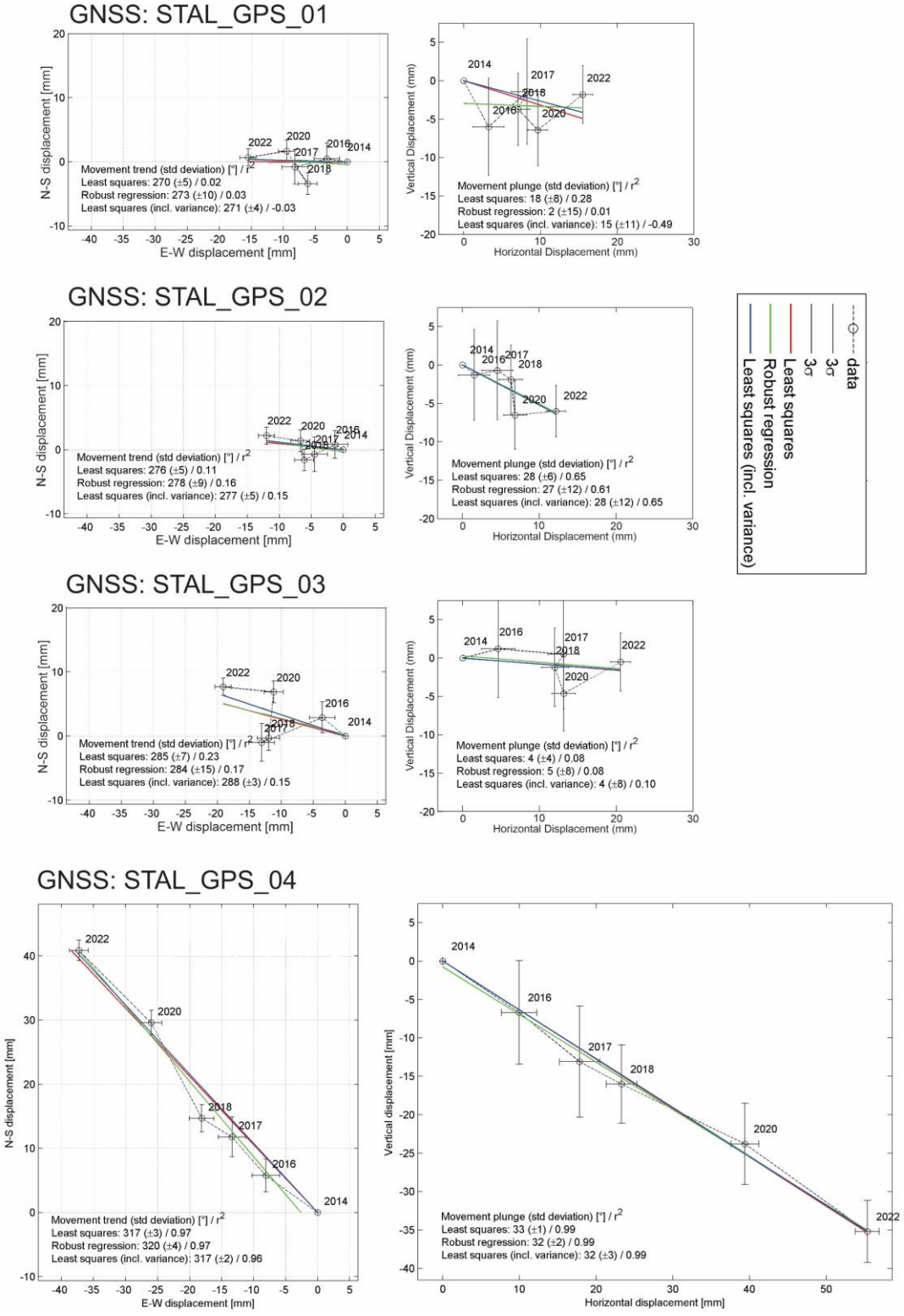

Figure 27: Displacement graphs based on the yearly data gathered. Left side displays the N-S and E-W displacement, while the right side displays the vertical and horizontal displacement. For each of them a three different regression are models used for illustrating the gathered movement.

5.4.2 Extensometers lower domain

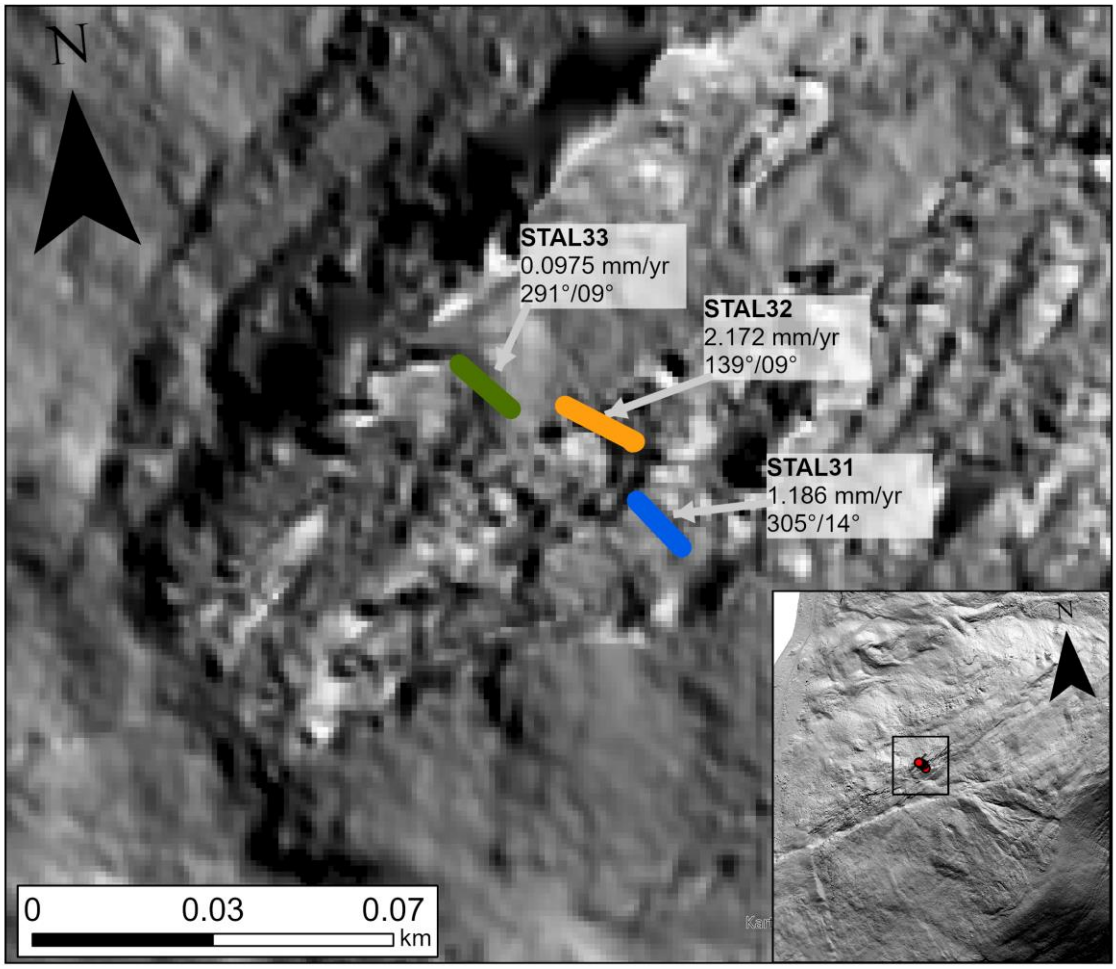

Figure 28: Locations of extensometer tape within the lower domain fractured area, with respective gathered velocities from linear regression for each of them. Dip direction and dip is the tapes orientation between the placed hooks. Location points for Stal32 might be misplaced as its overall direction is a bit wrong compared to the given orientation.

STAL31 and STAL32 have relatively consistent displacement rates along the tape directions with an annual velocity of 1.186 mm/yr and 2.172 mm/yr respectively (Figure 28, Figure 29). Stal33 has a very different observed displacement as it seems to be shrinking or staying relatively close to 0 mm/yr (Figure 28, Figure 29). Table 1 below show to the velocities for each point with their respective horizontal and vertical displacement. Aligning the horizontal components along one of the directions is used to gather the overall movement of the whole section. In this case STAL32 and STAL33 has been aligned with the horizontal component of STAL31. Between the two first crack measurements and their respective hook points an overall displacement velocity of 3.232 mm/yr is achieved towards 305°. Between the

STAL31-STAL32 aligned displacement and the displacement of STAL33 the total displacement velocity decreases slightly to 3.147 mm/yr, but since the displacement is so miniscule it's reasonable to assume that the STAL31-STAL32 and STAL33 is displaced at the same velocity.

Table 1: Displacement rates along the extensometer tape first between hook points, then divided into horizontal and vertical displacements. Lastly the horizontal displacement has been aligned along STAL31 axis.

	Direction and dip	Velocity between hooks	Horizontal velocity	Vertical velocity	Horizontal Aligned to STAL31
STAL31	305°/14°	1.186	1.151	0.287	1.151
STAL32	139 °/09°	2.172	2.145	0.3398	2.081
STAl33	291°/09°	-0.09755	-0.09635	-0.01526	-0.08507

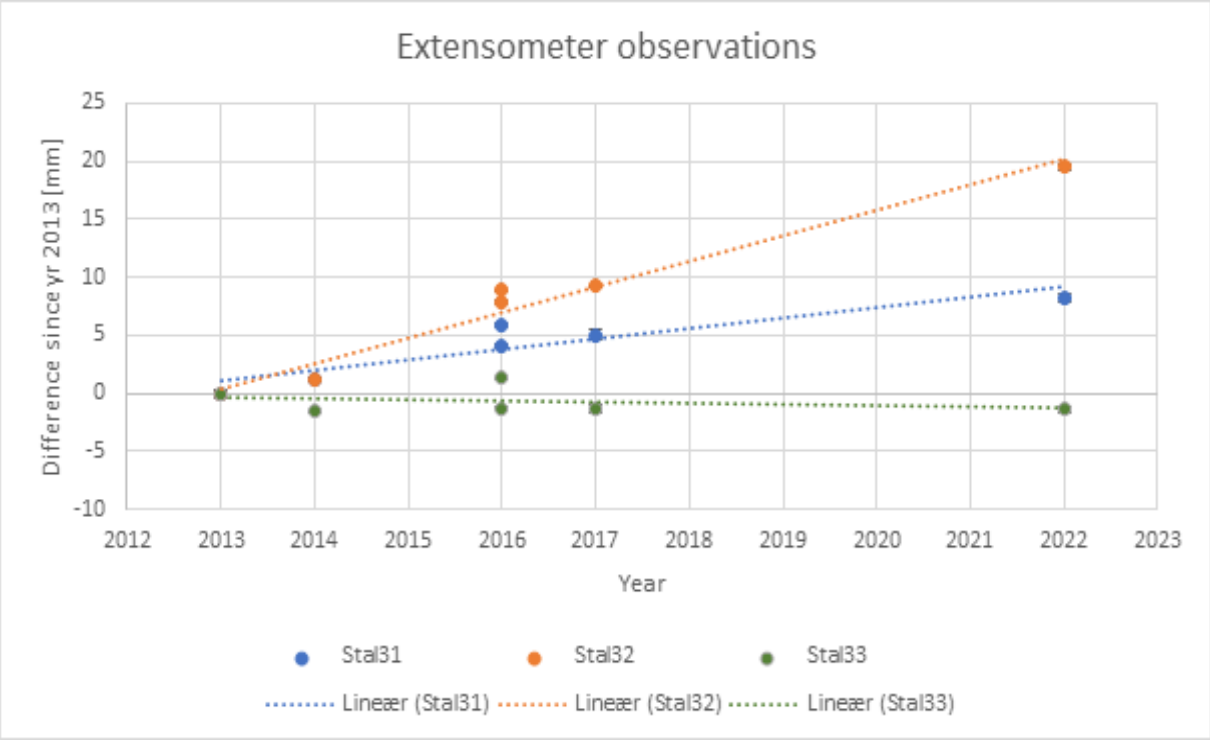

Figure 29: Extensometer data from fractured system within the lower domain Three different positions have been recorded over the years. Two points gathered in 2016 meant to correct for newer equipment used.

5.4.3 InSAR Movement

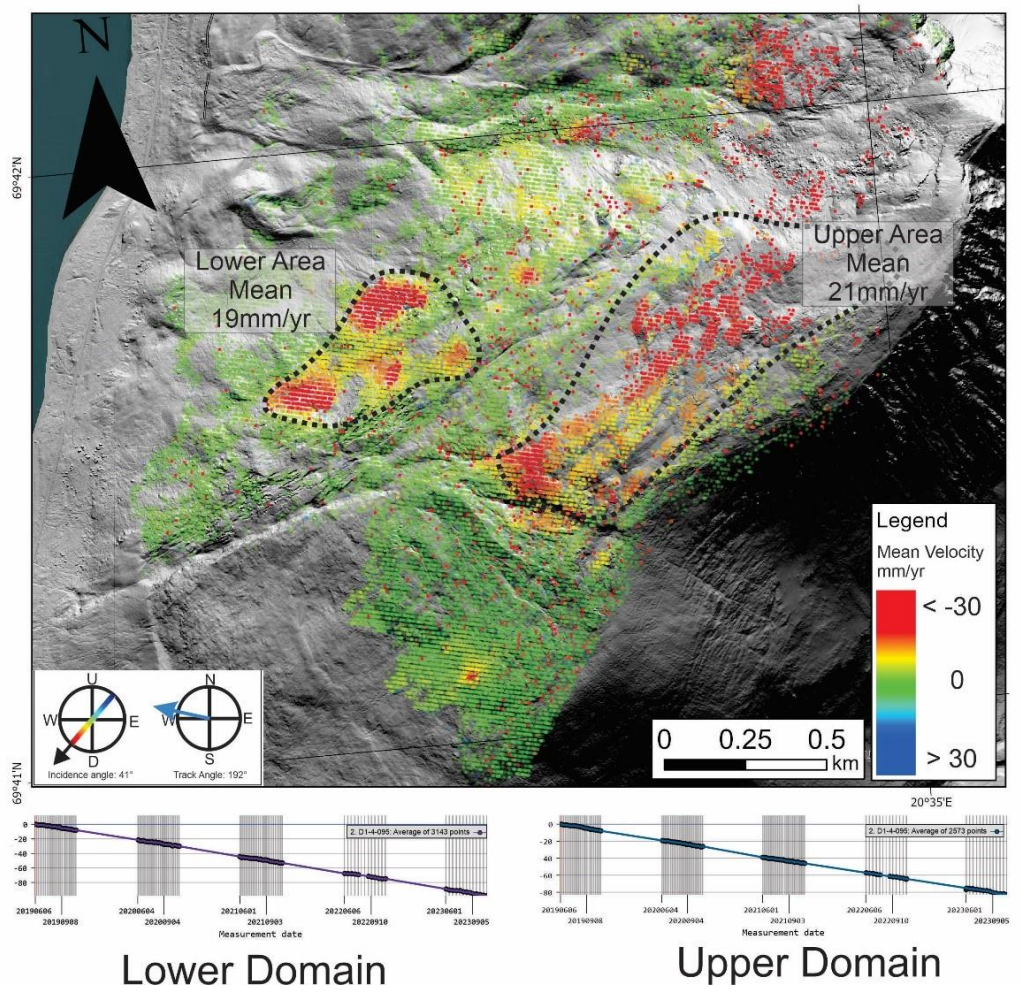

Figure 30: InSAR data with averaged movement for the two domains which stand out with the amount of yearly displacement.

InSAR dataset considered in here and in later chapters is *Descending1-4-095*. Within the lower deformed domain there is good coverage of movement data, while the deformed upper domain has good to semi-good within the descending dataset. Two clusters of data points has higher observed yearly displacement. The lower domain has an average displacement of 19mm/yr along the satellites LOS, and an upper area with an average of 21mm/yr along the LOS (Figure 30).

Some locations on the dataset appear as blind spots with missing data (Figure 30). These blind spots could appear as missing due to the LOS being blocked where the slope inclination is too high, especially relevant for the upper domain where cliffs often are equal or greater than the incidence angle of 41°. Two other reasons for blind spots are the sections where year-

round snow cover exists, and sections within the lower area with dense vegetation (Figure 30).

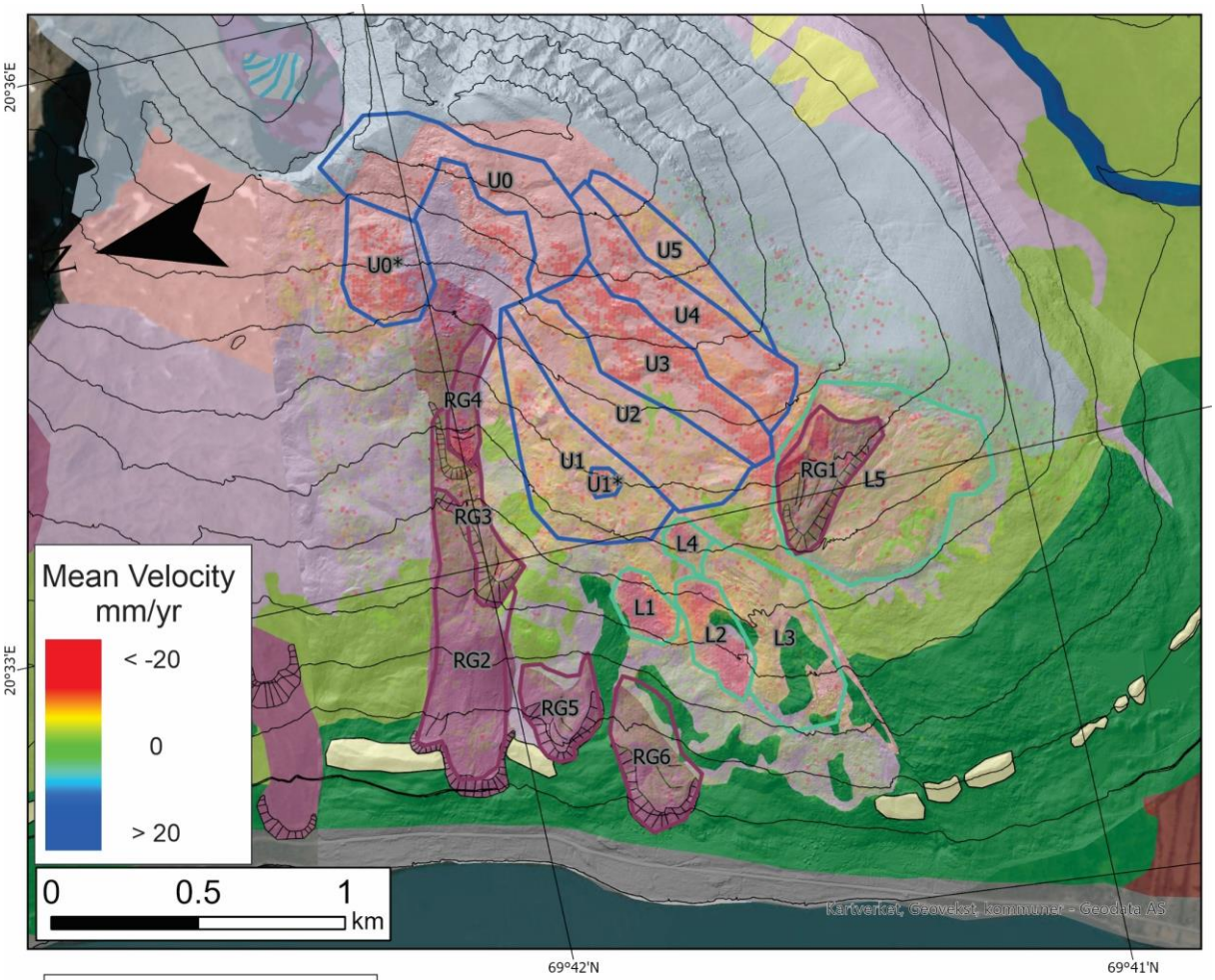

Mean Velocity (mm/yr)

Lower Area	U0	U0*	U1	U1*	U2	U3	U4	U5
Mean Velocity	-66	-40	-6	-14	-4	-27	-18	-7

Lower Area	L1	L2	L3	L4	L5
Mean Velocity	-32	-18	-3	-12	-2.5

Rock Glacier	RG1	RG2	RG3	RG4	RG5	RG6
Mean Velocity	-5	-1	-3	-10	0	-1

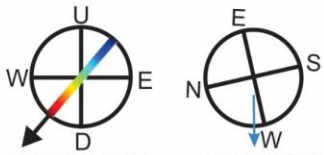

Figure 31: InSAR movement along the slope gathered from descending1-4-095 from 2019-2023.

To get a better understanding of how the displacement develop downslope, different sections and landforms has been defined. This includes an upper section, a lower section and rock glaciers (Figure 31).

The yearly rock glacier displacement has zero to considerably low recorded velocities within RG2, RG3, RG5 and RG 6, while RG1 and RG4 located further up the slope has yearly displacements of -5 mm/yr and -10mm/yr respectively (Figure 31).

Within the upper section along U5-U1 there is a gradual increase of recorded velocities downslope between U5 and U3 before it drops down to low velocities within U2 and U1 (Figure 31). Some locations within U1 have increased recorded velocities, for example within U1*. U0 close to the peak sporadic data points is collected and have relatively high velocities recorded, with an average of -66mm/yr (Figure 31). U0* shows high mean velocities but has not been focused on since no field observations have been collected in that area.

The lower Domain L1-L4 have spots with relatively great movement velocities, with an increase downslope. L1 and L2 have great mean velocities around -32 and -18mm/yr (Figure 31). Both are located in relatively steep sections with a lot of disintegrated rocks. Within the more fractured area observed velocity for L3 is relatively low with -3mm/yr (Figure 31). L4 located above the fractured area have relatively high velocities with a mean of -12mm/yr (Figure 31). This section is located within a rather steep hill with a talus deposit.

5.5 Lithology

Samples were collected from a few different positions on the slope to investigate the lithologies. Most of the samples were collected from in-situ positions of either bedrock or disaggregated blocks, but sample IN01 and IN07 are from loose rock material (Figure 32). From the various samples two main types of lithologies can be identified. The most abundant lithology gathered is mica schist (or biotite-rich mica schist) which includes IN01, IN02, IN05, IN06 and IN07. IN03 and IN04 have a more gneissic composition, while IN08 seems to be from a finer grained amphibolite lens.

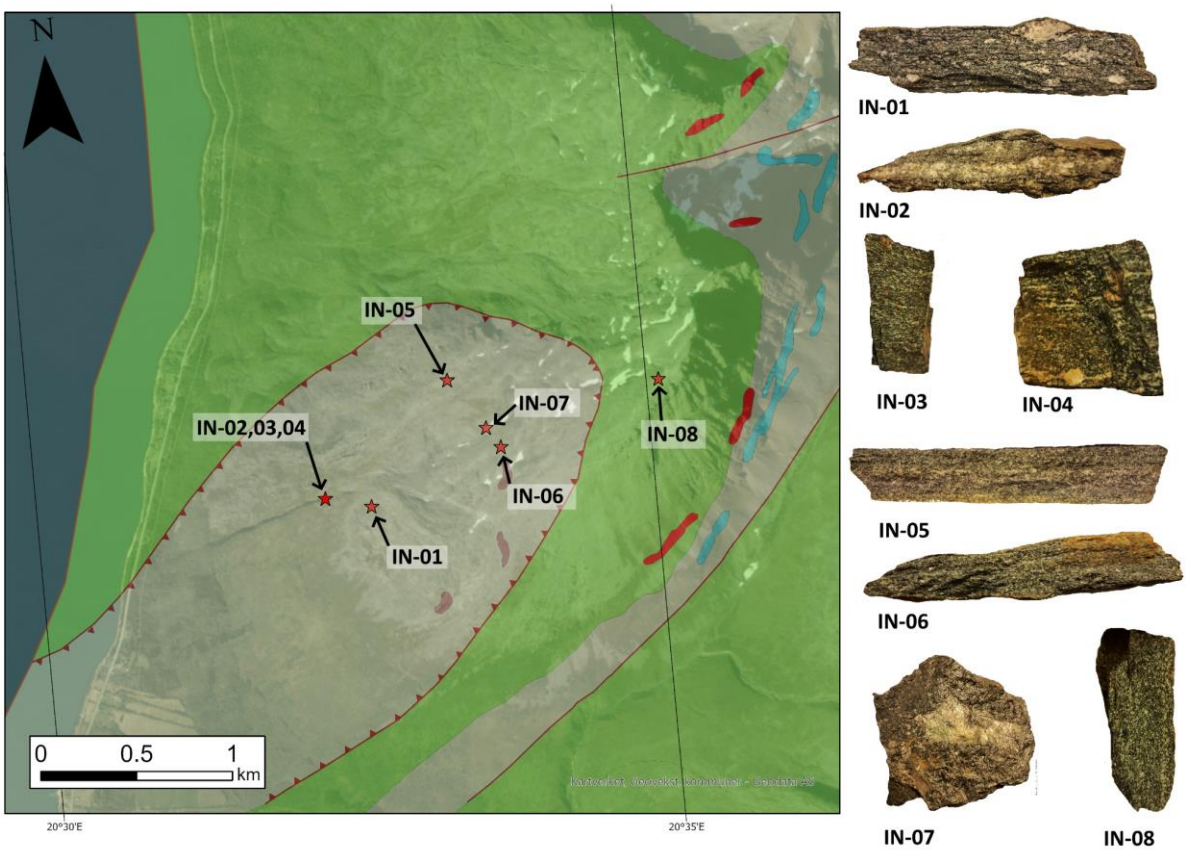

Figure 32: Localities of the various samples collected on Stáluvárri.

The mica schists are composed of dominantly quartz, feldspar, biotite, muscovite, and garnets, but sometimes includes either amphibole or chlorite. Since the felsic minerals quartz and feldspar have generally similar strength properties they are considered as one group. The same applies for the mica minerals biotite and muscovite as both are relatively similar. Other minerals mentioned will not be considered further as they don't amount to a specifically high percentage of the composition.

The mica schist sample have generally very similar compositions with variations mostly when considering the amount of felsic minerals compared to the mica minerals. There is a slight differentiation between the quartz and feldspar composition for the schists as they vary mostly between 40-65% (Figure 33). Since the mica minerals muscovite and biotite make up the other half of the composition these vary therefore similarly between 40-60% (Figure 33). Garnets within the thin sections has a variation between 0-5% (Figure 33).

Structural elements observed in the mica schists is either foliation or microfractures or the grains. Mica minerals observed in the thin sections has similar orientation throughout and can be followed as persistent planes crossing the whole section, with the felsic minerals and garnets causing some undulation along the planes (Figure 34). This is true for most of the thin sections, but IN07 stand out as mica minerals are the dominant percentage and cover the thin section to a greater extent. Microfractures observed are not very frequent within the schist samples but can appear as grain sized features following a similar direction throughout. IN01 has fracturing on the felsic grains perpendicular to the foliation. IN02 has a microfracture systems which is relatively persistent through the thin section, which can be observed crossing perpendicular to the foliation. The fractures seen on IN02 follows for the most part the felsic minerals but can affect the mica minerals in some locations (Figure 34). The rest of the samples did not have notable fracturing.

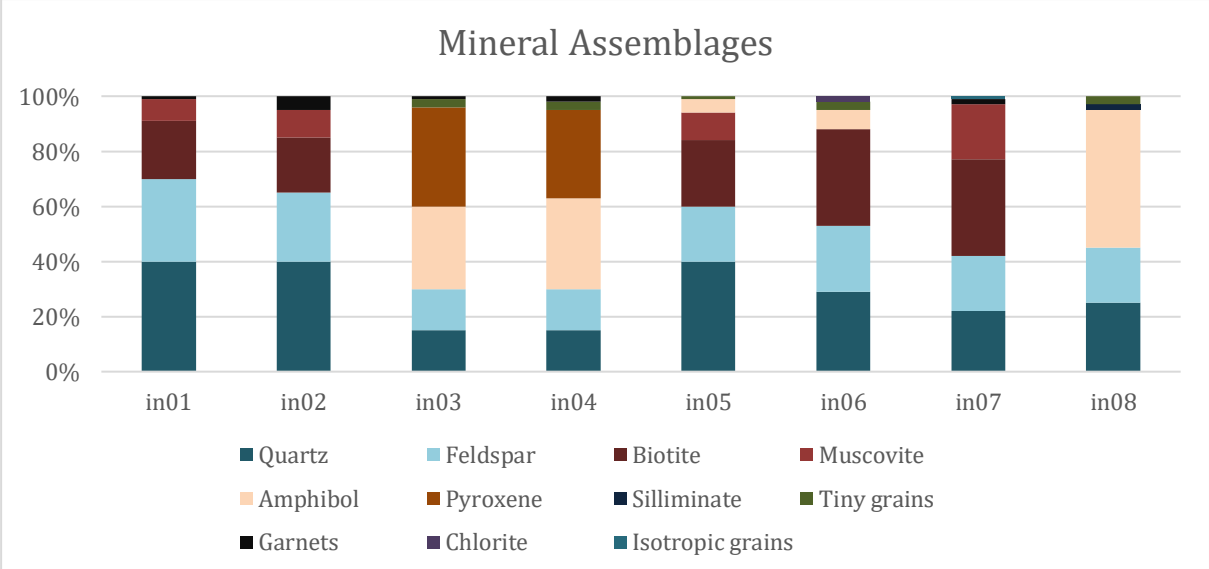

Figure 33: Approximated mineral assemblages from the various samples on, sorted into mainly quartz, feldspar, pyroxene and amphibole

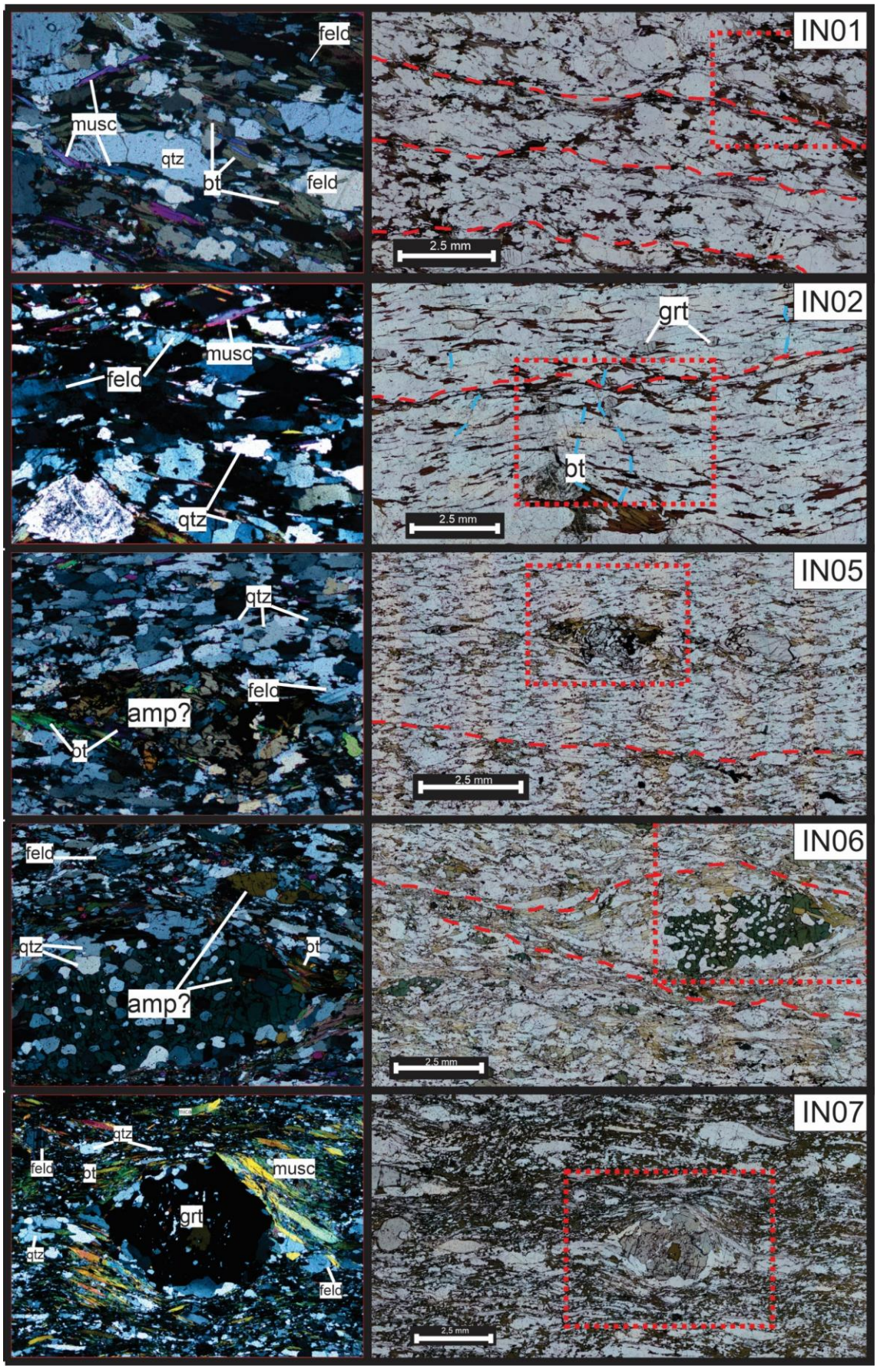
feld
musc
qtz
bt
feld
IN01
2.5 mm
musc
feld
qtz
grt
IN02
bt
2.5 mm
qtz
feld
amp?
bt
IN05
2.5 mm
feld
qtz
bt
amp?
IN06
2.5 mm
qtz
feld
bt
musc
grt
qtz
feld
IN07
2.5 mm

Figure 34: Mica schist thin sections , red dashed lines are meant to highlight some of the more persistent foliation planes. IN02 can be seen displaying some microfracture systems highlighted by blue dashed lines. Left side is cross polarized light and right side is plain polarized. qtz=quartz, feld=feldspar, bt=biotite, musc=muscovite, amp= amphibole, grt=garnet

The gneiss samples of IN03 and IN04, and amphibolite sample IN08, has mineralogical compositions dominated by quartz, feldspar, amphibole, and pyroxene. Lesser minerals include garnets and sillimanite. Similarly, quartz and feldspar are grouped together here as felsic minerals, and amphibole and pyroxene are grouped together as mafic minerals.
IN03 and IN04 has a felsic matrix composition of around 30%, where they form more equally sized grains. Most of the felsic minerals in these samples is covered with a matrix which makes it hard to identify exactly what is being observed, so they are given equal value. The mafic composition close to 70% of the sample and form elongated grains following similar uniaxial direction (Figure 33). IN08 has around 45% felsic minerals, and ca. 50% mafic minerals. There is also decreased elongation of the grains on IN08 (Figure 35).

Grain sized fractures on mafic minerals within all samples form in various directions, but the dominant directions are either along elongation or perpendicular to inclined on it. The Amphibole grains has the characteristic 60-120° cleavage. Where the felsic minerals are not influenced to much by matrix this grain sized fracture system can be observed in similar directions as well, though often more irregular.

Large microfracture systems crossing the entire thin section can be seen within IN03, where mainly two orientations can be seen. The most persistent and dominating one is oriented perpendicular to the elongation and has an undulating shape which splits both the mafic and felsic minerals (Figure 35). The less persistent fracture crosses parallel to the elongation, and can be seen splitting the mafic minerals, while leaving the felsic mostly untouched. Sample sized fractures along the perpendicular direction is not visible within IN04, but there are a few undulating parallel directed ones. Here as well they are not as persistent through the grains but develops dependent on if it’s a mafic or felsic mineral. IN08 has few fracture systems observable.

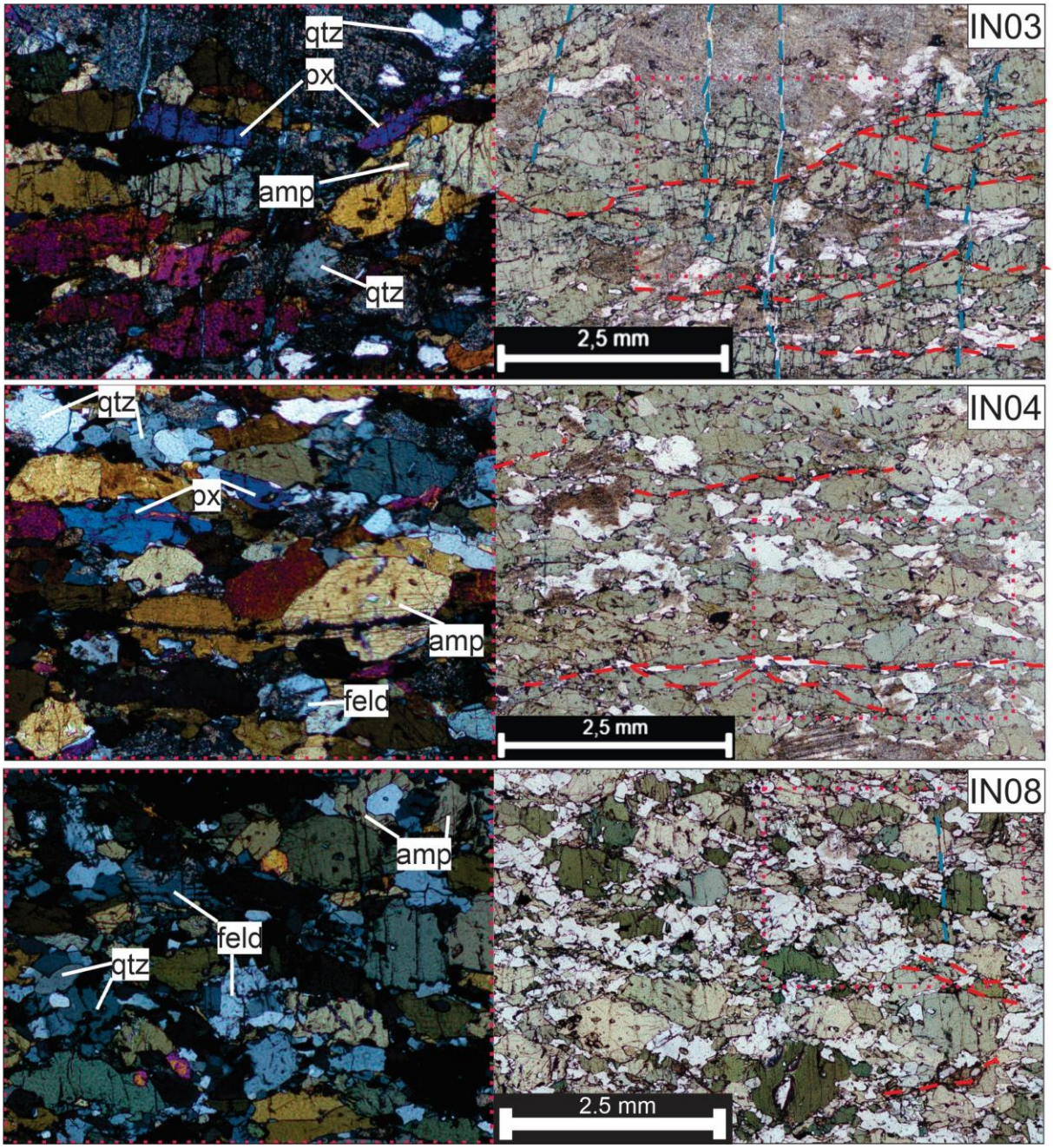

Figure 35: Overview pictures gneissic and amphibole-rich samples. Left side is cross polarized light (xpl) and right side is plane polarized light (ppl). Red lines represent fracture systems with a parallel orientation and blue lines are perpendicular oriented fractures qtz=quartz, feld=feldspar, amp= amphibole, px=pyroxene

Table 2: Mineral compositions and descriptions of the samples.

No.	Mineral assemblage	Grains	Fractures and foliation
IN01 Biotite Mica schist	Quartz 40 Feldspar 30 Biotite 21 Muscovite 8 Garnet 1	<1mm Some larger qtz, feldspar and garnet	Fracturing on quartz and feldspar grains, following either foliation or perpendicular to it. Peristant foliation along the mica minerals
IN02 Biotite Mica schist	Quartz 40 Feldspar 25 Biotite 20 Muscovite 10 Garnets 5	1-2.5 mm	Persistent fracturing through quartz, often interrupted by the mica. Mica dominated foliation
IN03 Gneiss	Quartz 15 Feldspar 15 Pyroxene 36 Amphibole 30 Garnet 1 Tiny grains 3	Up to 2.5mm grains. Finer matrix on top of felsic minerals	Persistent fractures through the whole sample, in two directions, parallel and perpendicular to the elongation.
IN04 Gneiss	Quartz 15 Feldspar 15 Pyroxene 32 Amphibole 33 Tiny grains 3 Garnets 2	Around 1mm grains	Fractures through mafic minerals along the foliation
IN05 Biotite Mica Schist	Quartz 40 Feldspar 20 Biotite 24 Muscovite 10 Pyroxene 5 Tiny grains 1	<250-500 microns	Not much fracturing, foliation planes along the mica minerals
In06 Biotite Schist	Quartz 29 Feldspar 24 Biotite 35 Chlorite 2 Amphibole 5 Pyroxene 2 Tiny grains 3	<1.0mm mostly but some larger grains	Persistent mica foliation through the thin section, no major fractures visible in the thin section
In07 Biotite Mica Schist	Quartz 22 Feldspar 20 Biotite 35 Muscovite 20 Isotropic 1 Garnet 2	<1 mm but some larger garnet	No visible, even on grains, good foliation connection on the mica minerals through the whole sample
In08 Amphibolite?	Quartz 25 Feldspar 20 Amphibole 50 Sillimanite 2 Tiny grains 3	<1 mm	No visible larger fractures in the thin section, but good cleavage and fracturing on pyroxene and amphibolite

6 Discussion

This discussion will try to establish the controlling factors of the rock slope deformation on Stáluvárri. This includes the lithological differences, assessing the subsurface section and trying to develop which type of slides are present. Potential scenarios are defined which will be given a risk assessment using a standardized spreadsheet developed by NGU.

6.1 Lithology

Lithological properties of a slope have some implications for the stability as certain composition can either strengthen or weaken the rock. Though the lithological sequence is a lot more complex than the geological bedrock map by Zwaan et al. (2006), mainly two rock types are assumed on Stáluvárri as thrust nappes. Metapelitic rocks such as mica schist has very anisotropic properties, where the mineral orientation of the mica causes the internal strength to be differentiated along two axes lowering the friction angle of foliation schistosity (Wylie & Mah, 2005). Mica schists are a very common lithology for RSDs in Troms County, especially around the eastern side of Lyngenfjorden (Bunkholt et al., 2012; Vick et al., 2020b). Banded Gneiss is comparably a lithology exhibiting more competent strength properties.

Within the lower domain three samples have been assessed, two of them represent the more competent banded gneiss and one of them of the anisotropic mica schist. The upper deformational domain is a lot more represented by mica schist, with the exception of IN08, which originated from an amphibolite lens. However, field observations suggests more mica schist being present at the peak as well.

The major difference in surficial cover and linear structures seen across these two positions could be associated with this difference Lower deformed domain are influenced by a more competent lithology which could one explanation for the larger abundance clear outcrops, less disintegrated material, and large pillar formations. The brittle properties of the mica schist are associated with the higher degree of disintegration within the upper domain.

Comparing the bedrock map and the collected samples it seems to be consistently a higher amount of mica schist on the slope, especially in sections further up. Without a more detailed investigation of the bedrock in the area it is hard to say exactly where the geological

boundaries are, but a crudely illustrated assumption of the contact can be seen in Figure 36 below.

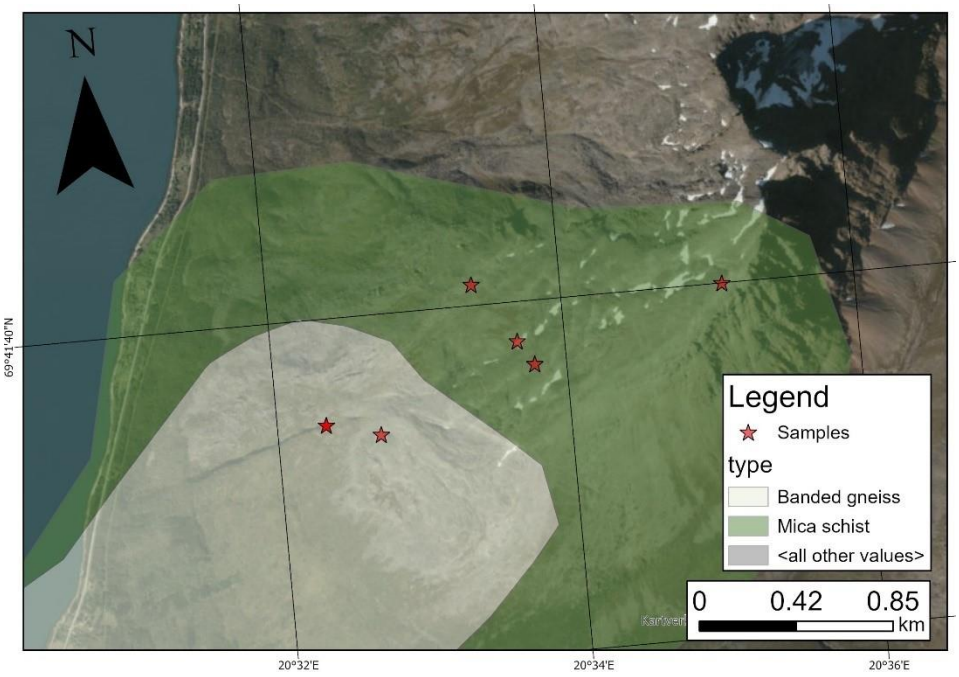

Figure 36: Proposed adjustment to the bedrock map. Based however on very limited observations from field and samples

6.2 Displacement data

As provided in Chapter 5.4 some displacement observations were gathered along the lower domain which can indicate some ideas about the displacement trends. Especially the gathered data from dGNSS and extensometer can help provided some insight into the displacement and directions of the lower disaggregated rock bodies.

GPS1 and GPS2 both have similar horizontal directions towards 270-275° and both points are placed along the middle to inner section of the horst and graben system (Figure 37). Comparably GPS4 which record larger amount of displacement towards 320° are located on the outermost dislocated pillar. Since GPS4 is located on one of the pillars which are exposed to a cliff (Figure 37), its displacement rate and direction could be a very local effect of toppling or a rotation of the block. As seen with the extensometer observations, further downslope on the dislocated pillar the displacement rate along the horizontal direction is around 3mm/yr less. Thus, the understanding on this is that the block does not move uniformly meaning that GPS4 can be considered a localized trend. As GPS1-3 generally has a similar trend they are assumed to be the more accurate for overall displacement vectors.

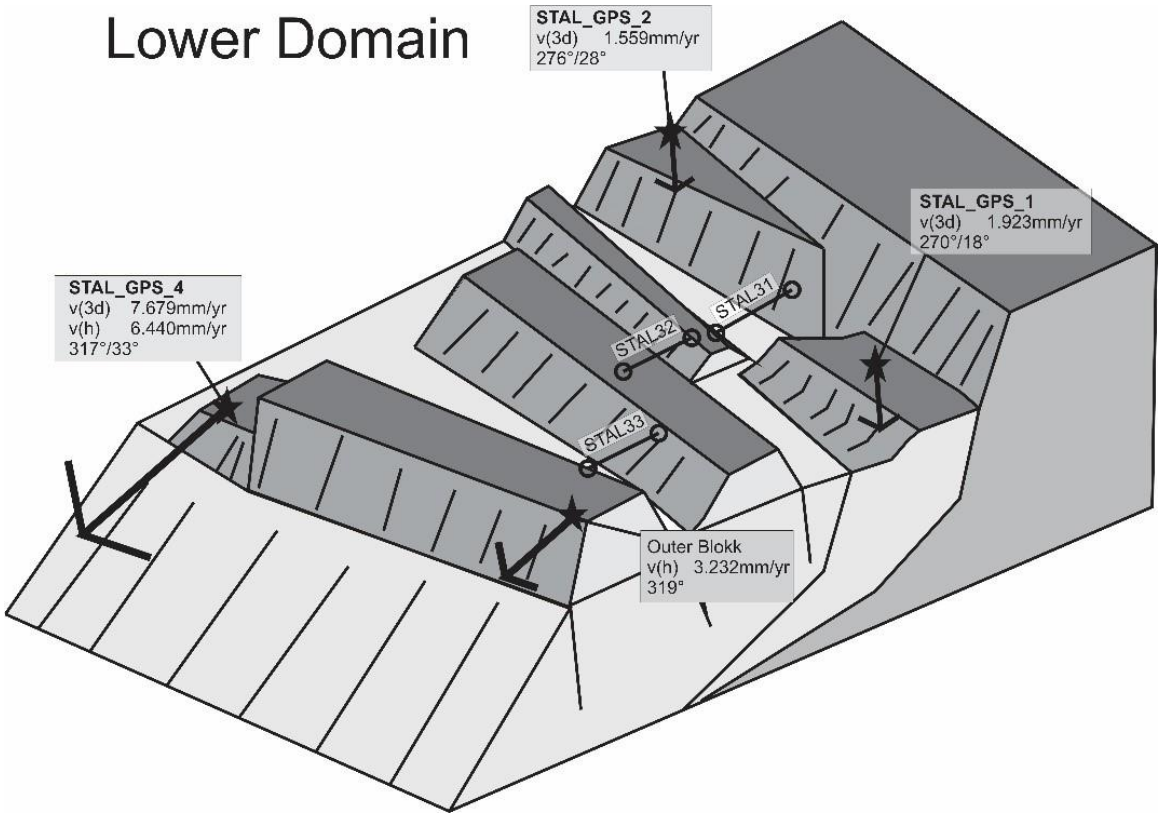

Figure 37: Conceptual model of the block movements within the lower domain, with hook points between the cracks and GPS points on the various dislocated blocks. Displacement rate for GPS4 is decomposed to the horizontal displacement v(h).

Another aspect of the movement data is the alignment of all the gathered observations. As presented above the main trend of the GNSS displacement is towards 270-285°. From the InSAR dataset presented in chapter 5.4.3 the satellite LOS is aimed toward 282° at a 40° incidence angle. Along both domains the GNSS displacement and InSAR displacement is around parallel to subparallel in orientation, meaning InSAR can give a good indication of the slope deformation, especially along the western direction. InSAR displacement rates will be used in the hazard assessment later, as the other observations are relatively few.

6.3 Defining scenarios

As Stáluvárri is a relatively large and complex field with considerable variations in slope properties, four different scenarios have been defined meant to adjust for this. Scenario 1 follows the lower deformational domain, and its upper extent can be traced along the NE-SW fault. Scenario 2 follows from the peak tracing its lower extent along the same fault. Scenario 3 will not be mentioned during this part of the discussion as it shares a lot of its deformational properties with scenario 2. It will however be used in the later hazard assessment. Scenario 4 defines the more southwestern facing deformation and has its upper extent along the NW-SE defined normal fault.

Each scenario is accompanied by cross sections of the defined area. The bearing of the cross-section A through D is oriented along the displacement direction towards 270-285° since as discussed in chapter 6.2 the general trend follows this bearing. Cross section E-E' follows perpendicular to the topography as both it and the lineaments indicate this direction. The foliation and joints for each cross section has been corrected to the apparent dip. Lithological boundaries on the cross sections are based on the bedrock map by Zwaan et al. (2006) where the subsurface position of the boundaries is approximated loosely on the two connecting points the profile.

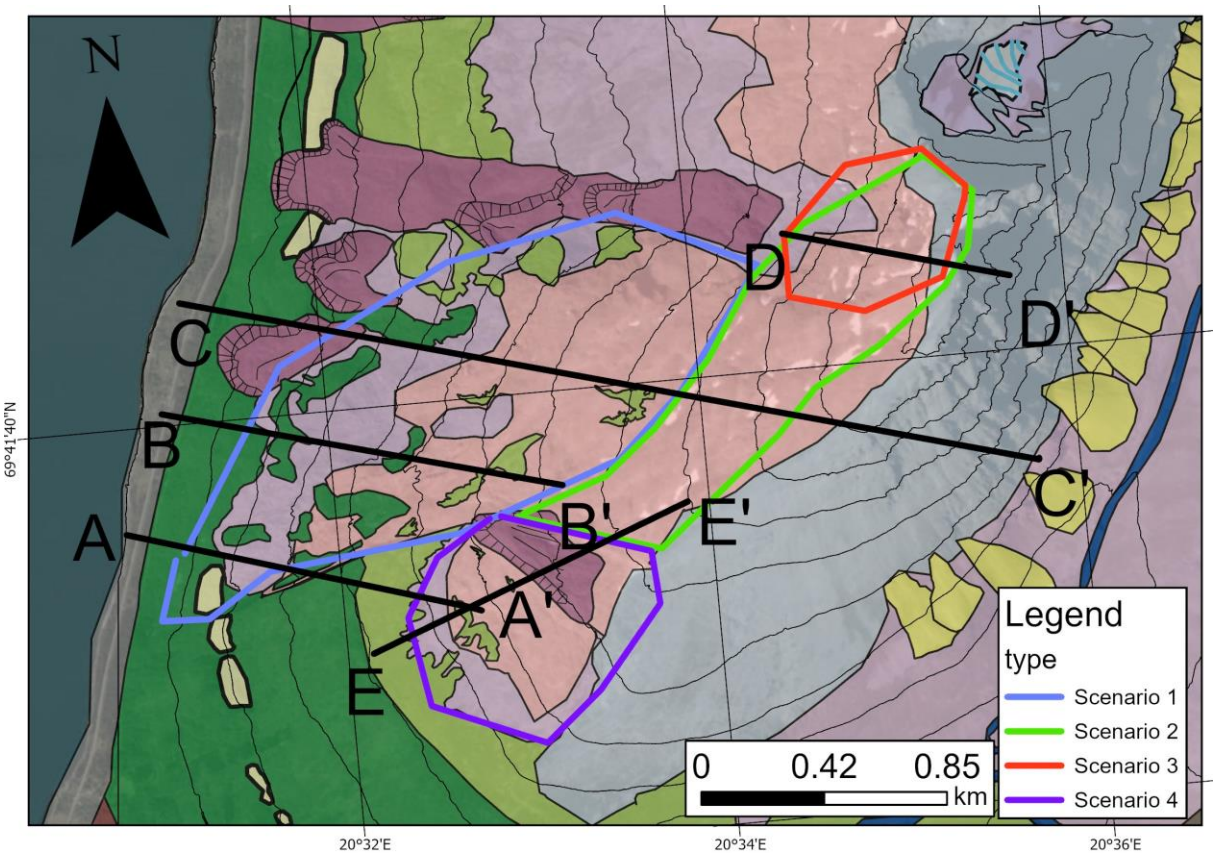

Figure 38: Cross sections and scenarios on Stáluvárri . A-A' and B-B' follows the lower domain, and C-C' and D-D' along the upper domain. E-E' shows the southwest facing slopes instability.

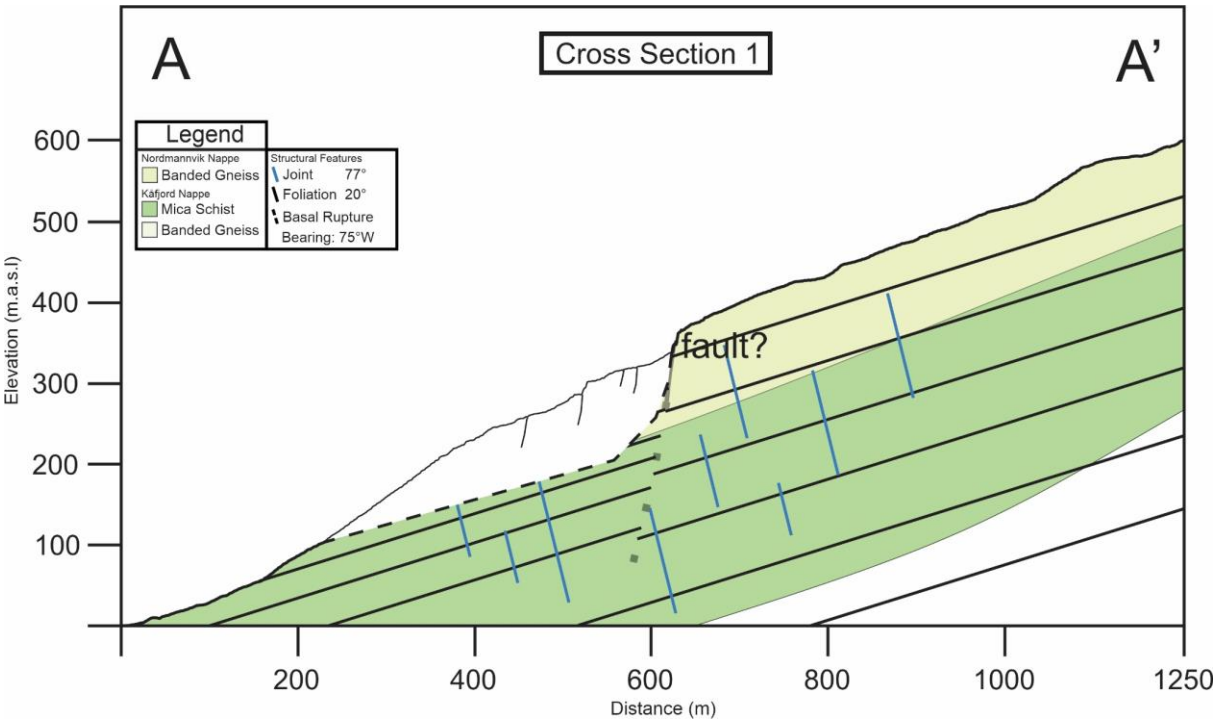

Figure 39: Cross section 1 from scenario 1 , where fractures and trenches are exposed on the surface and one major scarp.

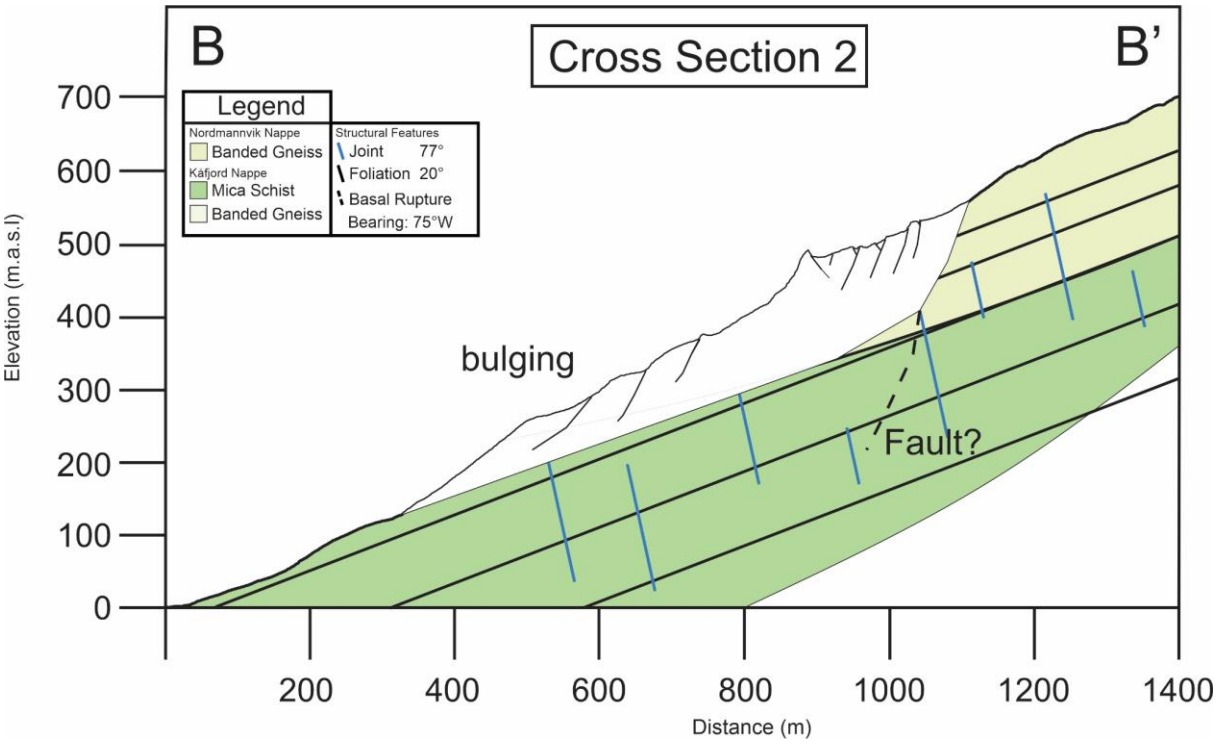

Figure 40: Cross section 2 from scenario 1 , where multiple horst and graben structures can be seen along the upper section of it and step surface along the lower segments.

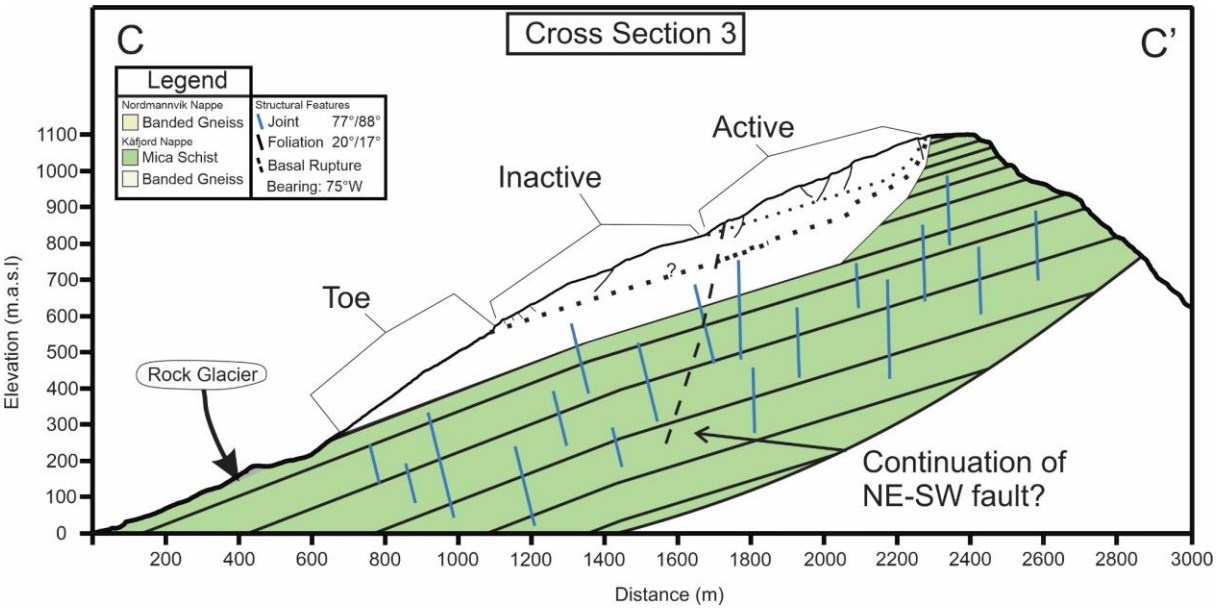

Figure 41: Cross section 3 along the upper domain of the slope. Differentiated between the slow-moving inactive section and the faster moving active section. Tracing the NE-SW fault from scenario 1 appear to be a continuation of it as evidence of fFigure 22.

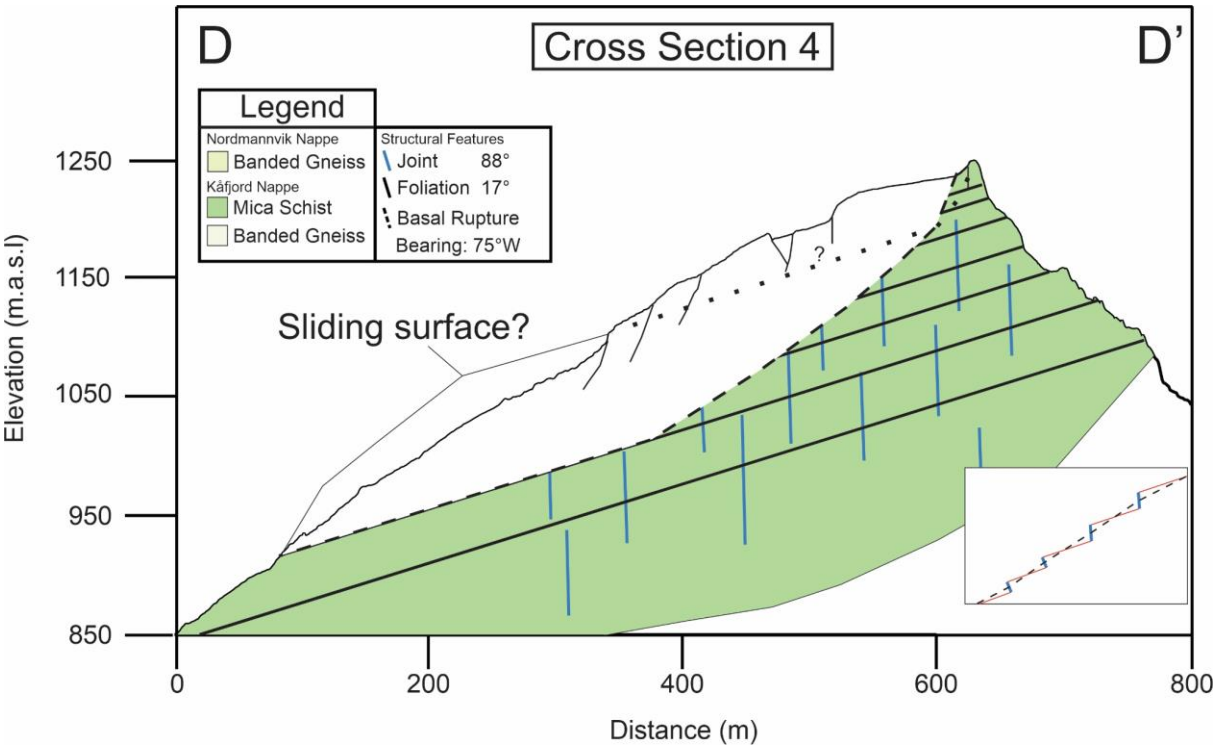

Figure 42: Cross section 4 of deformational structures on the peak. Relatively shallow dipping foliation, where horst and graben structures can be seen along the top.

6.3.1 Scenario 1

Scenario 1 is defined by the lower domains characteristic large and very fractured section of disaggregated rock with an area covering 1km^2 (Figure 38). In general, lower displacement rates are most apparent within this section and is normally below well below 0.5mm/yr at present day. Below on the steeper sections of the slope some displacement rates up to around 20 mm/yr can be seen. However, these are more often related to sections with large talus collections or disintegrated rock and most likely related to surficial displacement processes by downward creeping of the talus. Because of the relatively low displacement rate on the slope today but with a highly extensional surface lineaments, especially in sections like Figure 21 horst and graben system, it is interpretated as being a relic instability which has stabilized considerably.

6.3.1.1 Fracture system and rear rupture surface

The large block separated field within scenario 1 has as mentioned a NE-SW striking orientation (Figure 21). As shown to in chapter 1.5.2 this is one of the major strike directions for faults in Troms County. These fractures have oblique orientation to the slope dip and the gathered general trend of displacement.

The larger southern arête has not been identified with having clear surficial signs of being a fault field during fieldwork, but as shown to in the thin section work the lithologies close to this has a large abundance of microfractures, both crossing the whole section and on the grains. As per Anders et al. (2014) microfractures can be used to identify detachments which has a tectonically influenced origin and then can be used to distinguish them from structures originating as landslides. This supports the assumption that both the large fault and the fractured area are pre-dating the landslide and are therefore reactivations. This is assumed to be the rear rupture surface to lateral rupture in the lower sections of scenario 1. Towards the north of the fault the assumed continuation of it can be seen rotating towards the NNE-SSW

6.3.1.2 Basal Rupture Surface

The toe of the deformation in scenario 1 has not been accurately identified. An inferred toe segment has been assumed by cross section 1, cross section 2 and cross section 3 and is based on where the foliation could potentially daylight along the steeply dipping slope. Another reasoning for this position is how the quaternary deposits have been affected by the displacement. Several of the lower rock glaciers seems to be superposed by the disintegrated

rock material. The lateral moraine at the lower end of the fault has a downward displacement of 20m to the moraine on the stable position, potentially meaning this is the the lower section of the toe (Figure 17).

Apart from foliation the basal rupture surface is also possible to be associated with the thrust fault between the Nordmannvik Nappe and the Kåfjord Nappe. Thrust faults between the imbricated nappe stacks weaken the strength properties of the rock and enhance the anisotropic properties (Brideau et al., 2005; Vick et al., 2020a; Vick et al., 2020b). The underlying mica schist is another supporting factor for the contact between the nappes to be the basal rupture surface, as it would potentially also be the weaker lithology of the two. The apparent dip of the thrust fault on the cross sections are dipping around 26°, relatively close to foliation dip and well within the range for becoming a propagating discontinuity surface.

6.3.2 Scenario 2

Scenario 2 covers another large section of ca. 0.5km^2 and is located along the top section of the slope with a very varying topographic relief and an abundance of surficial talus material. In general displacement velocities within this scenario is somewhere between around 30mm/yr, but due to large amounts of surficial talus cover on steeply dipping scarps itis likely that some of this observed movement could originate from creeping movement of the disintegrated rock.

6.3.2.1 Scarps and Rear rupture

Scarps and Infilled trenches along the peak are abundant and has mainly two striking directions, where NNE-SSW is the most persistent scarp and ENE-WSW appear connecting these in conjugate manner. Downslope the ENE-WSW scarps are rotated to NE-SW striking directions. Depressions form often in front of the scarps and can be seen as small graben structures between a scarps and counter scarp.

The interpreted rear rupture of scenario 2 follows adjacent to joint set 2 from the upper domain. As seen in Figure 18 the foliation is cut by this surface supporting this as the rear rupture surface. The rear rupture surfaces appear to be similar to what is happening in scenario 1 with NE-SW striking surface which rotate towards NNE-SSW.

6.3.2.2 Basal rupture surface and lateral limit

The toe is hard to define but could be assumed to share the same lower and upper boundary as scenario 1. No real evidence of the toe is gathered but the basal rupture surface has a high kinematic feasibility for foliation sliding which can be traced as a gently dipping outgoing surfaces on cross sections. Another possible outgoing toe surface for foliation to emerge is just below the active zone seen in (Figure 41). Foliation could make a outgoing surface here, but again the whole section is covered by extensive talus.

6.3.3 Scenario 4

Scenario 4 is its own unit as it has displacement direction towards the southwest and is well defined by NW-SE normal fault in its rear. It is seemingly not as connected to the upper scenario 2 but there are evidence of scenario 2 having a displacement direction towards the southwest as well by rotated material in that direction and scarps (Figure 24D).Scenario 4 is another segment which there is very slowly deformation with mean velocities around 2.5mm/yr.

The rear rupture surface is associated with a large normal fault striking NW-SE. The foliation here is generally dipping to steeply on the slope to have any meaningful daylighting possibilities. But an inferred basal rupture is displayed where the outgoing surfaces crosses the foliation plane to daylight. The toe has some more concrete evidence compared to the other sections as there are streams seen along the bottom of it.

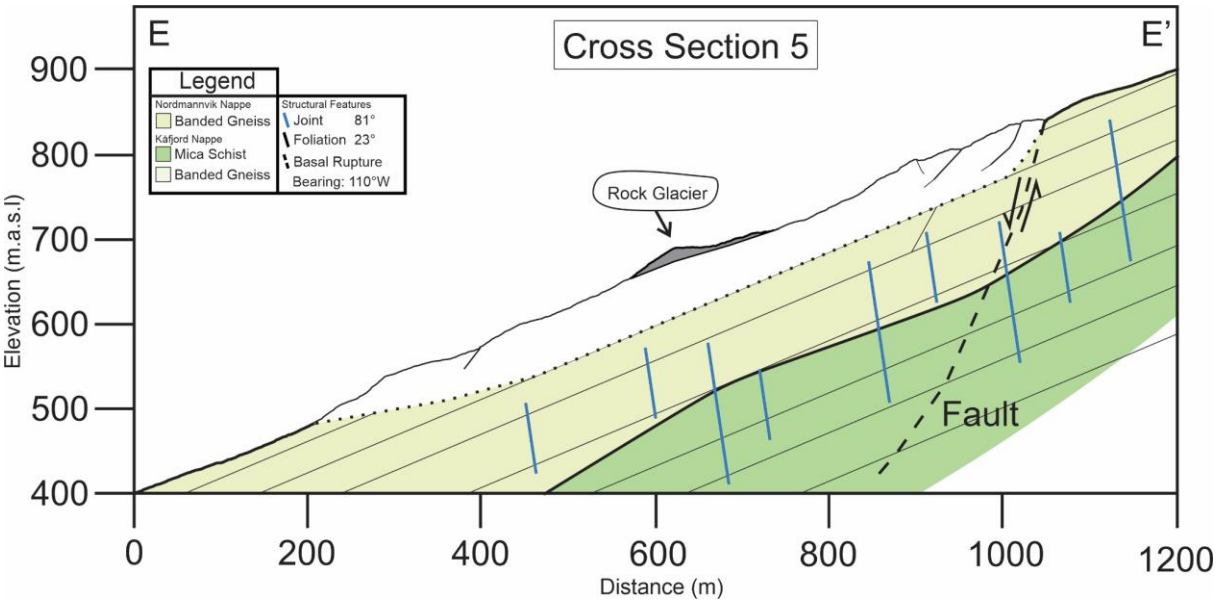

Figure 43: Cross section 5 on scenario 4 following the slope deformation along scenario 4. where normal faulting is present along the rear rupture surface.

6.4 Conceptual model

As shown to so far Ståluvárri is a slopeaffected by a lot of sections being displaced in different manners. A short interpretation of the development of the slope is displayed in Figure 44. Exactly when downslope deformation started can't be said for certain without cosmogenic dating of the exposed surfaces, but a potential maximum age can at least be associated with the deglaciation from Kåfjorden around 10 000 BP (Corner, 1980).

Most of the slope show evidence that the rear rupture of each scenario is connected to weakness zones related to a steeply dipping surface as reactivations of the post-Caledonian fault planes and the brittle properties of jointing. Scenario 4 is especially relevant in this as the normal fault has very similar orientations to other sites in northern kåfjord with similar aspect and displacement direction, such as Gillavarri, Gavtavarri and Nomedalstinden (Bunkholt et al., 2013; Vick et al., 2020b). The main sliding planes are most likely the foliation for all scenarios as it forms a relatively consistent outgoing surface on the slope, but possibly some more rotation in the lower sections of scenario 4. The processes has been generalized pretty much to the two main components of vertical rear rupture surface and planar basal rupture surface, but the subsurface section is likely a lot more complicated than that, as more the foliation and joints commonly arranges themself as rock bridges instead of being as direct as illustrated in the cross sections (Elmo et al., 2018; Vick et al., 2020b).

The general size and of the landslides on Ståluvárri are highly associative the concept of deep-seated gravitational slope deformation (DSGSD), especially for the western side of the slope. Ståluvárri has previously also been suggested by Bunkholt et al. (2013) as a slope inhibiting typical signs of being a DSGSD.

DSGSD are a landslides which are often are characterized by large volumes (>0.5km^2) and slow deformational rate (Agliardi et al., 2012). The toe of the deformation is often ill defined as they are located in steep relief areas with a lot of talus cover caused by secondary avalanche processes as the masses is displaced (Agliardi et al., 2012).
The western side of Ståluvárri can be seen correlating with these descriptions of the toe as there is large abundance of rockfall accumulation both on the slope and at its toe. Lateral limits are also often not easy to identify on the slope (Agliardi et al., 2012), which has been the case for Ståluvárri.

The rear region of DSGSDs ischaracterized by extensional elements such as scarps, graben and trenches where they are masked by gravitational driven talus material. (Agliardi et al., 2012; Crosta et al., 2013). These extensional elements can in some cases be associated with reactivations of inherited tectonic elements (Agliardi et al., 2012; Bunkholt et al., 2013). For Norway this would often be associated with elements originating from the post-Caledonian extension and rifting, and specifically for Stáluvárri related to NNE-SSW striking Jurassic - Cretaceous dextral oblique normal faults and NW-SE striking late Cretaceous - early Paleogene normal faults (Bergh et al., 2007).

Lithological correlation with metapelitic rock types with strong anisotropic properties has been made for DSGSD (Agliardi et al., 2012; Crosta et al., 2013), fitting for the lithological compositions present on Stáluvárri. DSGSDs also show to that they necessarily don't develop uniformly but can develop in multiple subareas of a slope, with either fluctuating boundaries or boundaries related to each other (Agliardi et al., 2012). The interpreted scenarios show to this as the indicated amount of displaced material of seemingly different stages, velocities and direction change in various sections of the slope.

Due to the generally slow displacement rate these types of landslides has, potential slowly progressing failures which can span thousands of years, slowly altering the whole topography of the mountain (Agliardi et al., 2012). Initiation DSGSDs shows strong correlation with deglaciations and seismic events. Deglaciations can affect the rock slope in various ways, this could be related to steepening of the relief, confining factors of the slope being released or related to seismic events related to isostatic uplift (Crosta et al., 2013). An maximum age on Stáluvárri related to this could be interpreted by the lower lateral moraine and its displaced ridge.

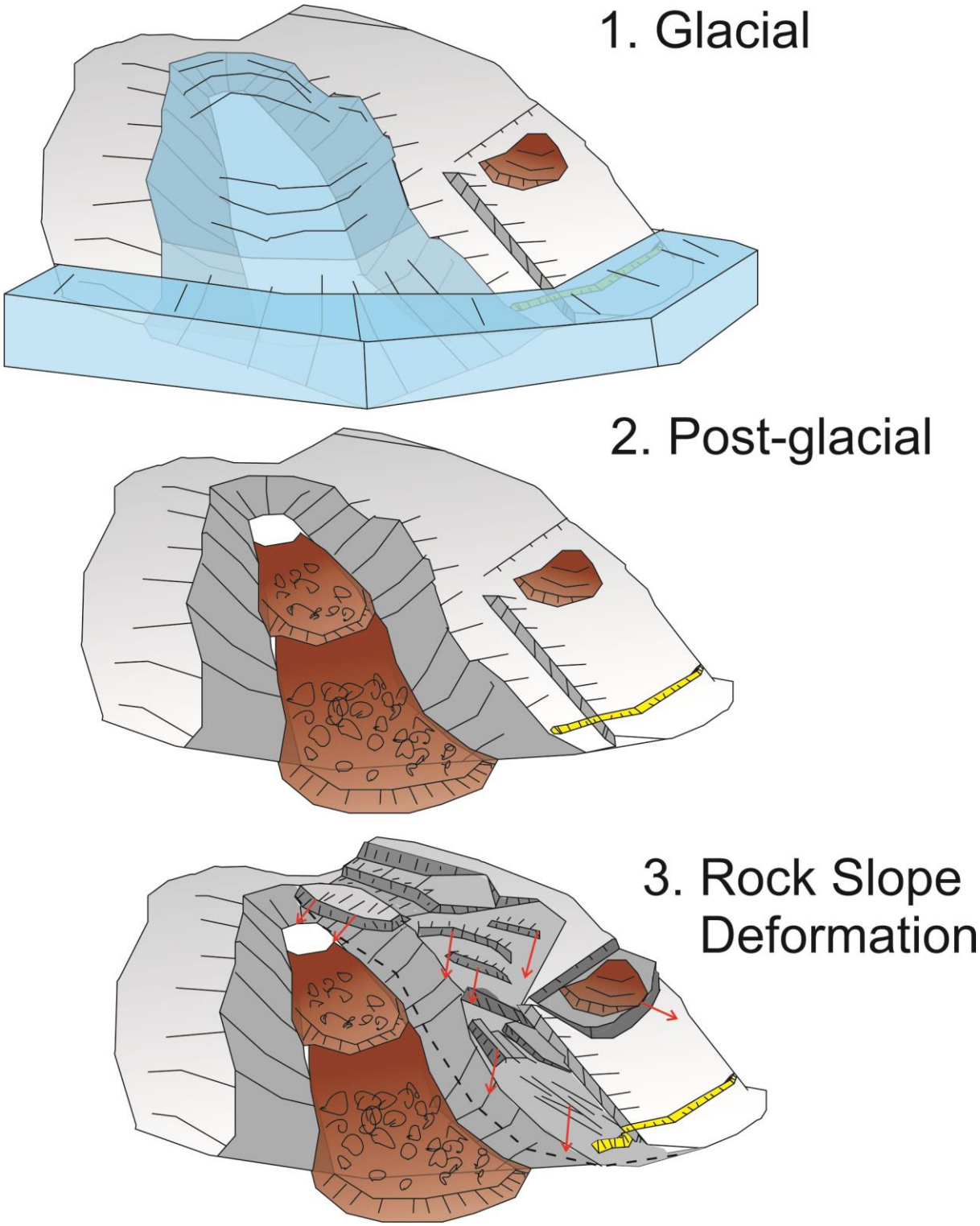

Figure 44: Simplified conceptual model of the development of the Stáluvárri , showing interpreted displacement directions in relation to each other. Stippled line indicate the maximum potential lower limit.

6.5 Hazard assessment

One goal of this project was to relate the observations of the hazard assessments to what scenarios could potentially release. The defined scenarios 1-3 will be given values dependent on the threat they pose individually. NGU assess RSD hazards based on nine basic criterions, which are given differential values depending on how they are perceived to increase instability. Three of the four scenarios have been assessed for how these elements are perceived. Each scenario is accompanied by reports showing the perceived values given to the criterions, which can be found in Appendix A. There was not done a consequence analysis of the slope, as there is not enough collected data on estimated volumes of the rock slope failures for doing simulated hazard zones of the potential displacement waves to support this. But from primary consequences of a release, it can be assumed to be within the lower consequence scenario as there is only 14 residencies at the toe of the west facing slope and no critical infrastructure. Table 3 shows the different classes for each scenario, while in Figure 45 the assessed hazard can be seen represented by solid black lines where the mean, 5% percentile and 95% could b traced.

Scenario 1 and 2 has relatively low hazards associated with them, while scenario 3 is within the lower sections of nominal annual likelihood class 1:5000. However, there is a good bit of spread on it. As seen in relation to its slope the surficial cover is affected by disintegrated material, which could be as a result of direct toppling of the displaced material here, as kinematic feasibility tests show to high likelihood for this (Figure 15, Figure 17). This could potentially lower the hazard of a direct sliding of the displaced material as it would be incrementally released.

Table 3: Scenario 1 through 3 with their hazard classification likely hoods and hazard points used hazard matriks.

Scenario 1	
Hazard Class	Likelyhood
Very Low	1.2 %
Low	61.9 %
Medium	36.9 %
High	0.0 %
Very High	0.0 %

Scenario 2	
Hazard Class	Likelyhood
Very Low	0
Low	48.25%
Medium	48.75%
High	3.00%
Very High	0

Scenario 3	
Hazard Class	Likelyhood
Very Low	0
Low	6.33%
Medium	79.00%
High	14.67%
Very High	0

Hazard Points	
Minimum	2.00
Maximum	6.75
Mode	4.00
Mean	4.29
5% persentile	2.59
95% persentile	5.73

Hazard Points	
Minimum	2.50
Maximum	7.50
Mode	5.00
Mean	4.80
5% persentile	2.89
95% persentile	6.50

Hazard Points	
Minimum	4.00
Maximum	7.50
Mode	6.00
Mean	5.85
5% persentile	4.40
95% persentile	7.00

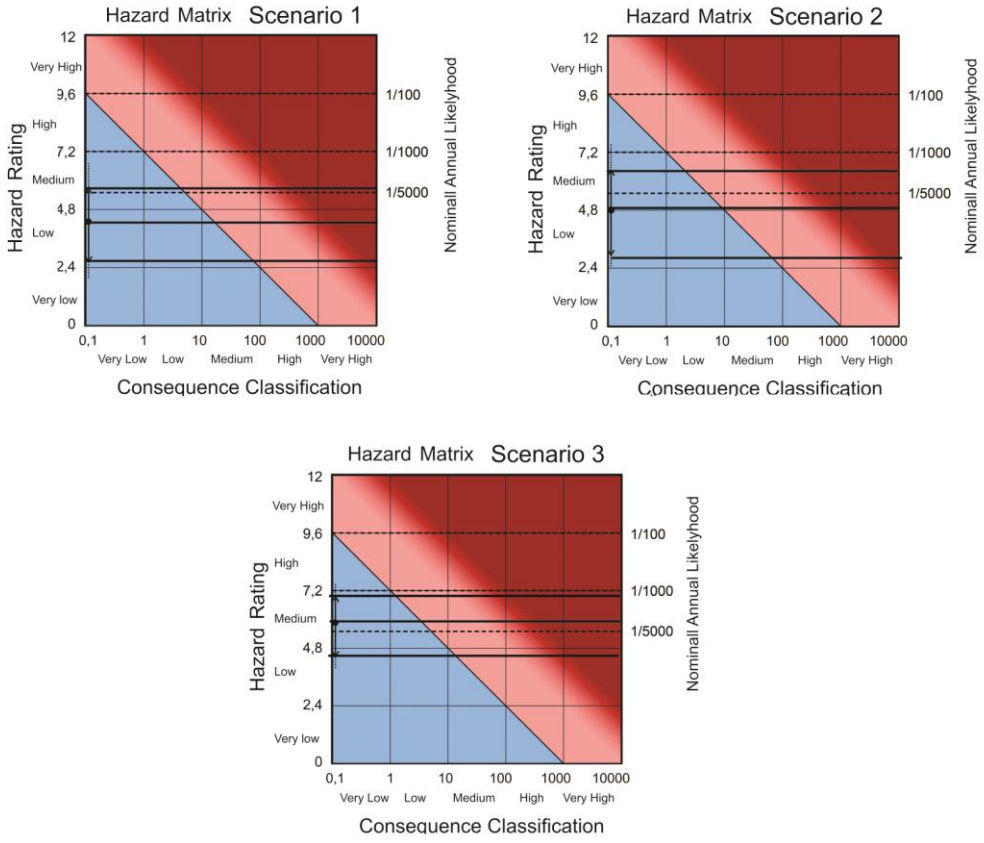

Figure 45: Risk matrix of the hazard assessment , interpreted as hazard matrix instead as consequence classification has not been done. Black solid lines are meant to represent the range where it could fall under when a consequence analysis is done.

7 Conclusion

During this geomorphological mapping and study of rock slope deformational processes on Stáluvárri it is shown to a that the field is a large and complex assortment of multiple rock slope deformational scenarios. The west facing slope in particular show to a huge section which is being displaced downslope and is visible affecting the whole mountainside. While the southwest facing slope can be seen inhibiting its own more confined displaced slope. In general, the slope shows clear signs of undergoing deep seated gravitational slope processes controlled by inherited extensional structures, reactivations of these and creeping displacement rates.

The basal sliding surface for all the assumed scenarios are likely related to foliation control. It generally has a 20° WSW dipping surface with potential to appear as outgoing planes on steeply dipping slopes, giving good correlation in kinematic tests. As Nordmannvik- and Kåfjord nappe has a thrust fault on the slope the boundary between the two could also form a potential basal rupture surface. However, due to the size of the deformed slope this can't be interpreted accurately without a more extensive subsurface analysis of the slope.

Post Caledonian extensional faulting is persistent throughout the slope and can be seen in mainly two directions related to NNE-SSW striking Jurassic - Cretaceous dextral oblique normal faults and NW-SE striking late Cretaceous - early Paleogene normal faults. This can be seen especially affecting the lower section of the slope in scenario 1 where a huge NE-SW lineament show clear signs of faulting and fracturing on thin sections and morphostructural surfaces.

What could have initiated the displacement processes has not been identified, but historically from other DSGSD the main initiation processes is either as result of deglaciation of a valley or as a result of larger earthquakes. The maximum age can be traced to lateral moraines which has been displaced downslope.

Possibilities for release of a larger landslide in present day seem low without a major tectonic event initiating major displacements again, but upper sections within scenario 3 show to slightly higher probabilities for release.

References

Agliardi, F., Crosta, G. B., & Frattini, P. (2012). 18 - Slow rock-slope deformation. In J. J. Claque & D. Stead (Eds.), *Landslides: Types, Mechanisms and Modeling* (pp. 207-221). Cambridge University Press.

Agliardi, F., Crosta, G. B., & Zanchi, A. (2001). Structural constraints on deep-seated slope deformation kinematics. *Engineering geology*, *59*, 83-102.

Anders, M. H., Laubech, S. E., & Schols, C. H. (2014). Microfractures: A review. *Journal of Structural Geology*, *69*, 377-394. https://doi.org/https://doi.org/10.1016/j.jsg.2014.05.011

Augland, L., Andresen, A., Gasser, D., & Steltenpohl, M. (2014). Early Ordovician to Silurian evolution of exotic terranes in the Scandinavian Caledonides of the Ofoten–Troms area – terrane characterization and correlation based on new U–Pb zircon ages and Lu–Hf isotopic data. *Geological Society, London, Special Publications*, *390*(1), 655-678. https://doi.org/10.1144/SP390.19

Bergh, S. G., Eig, K., Kløvjan, O. S., Henningsen, T., Olesen, O., & Hansen, J. (2007). The Lofoten-Vesterålen continental margin: A multiphase Mesozoic-Palaeogene rifted shelf as shown by offshore-onshore brittle fault-fracture analysis. *Norsk Geologisk Tidsskrift*, *87*, 29-58.

Bøe, R., Longva, O., Lepland, A., Blikra, L. H., Sønstegaard, E., Haflidason, H., Bryn, P., & Lien, R. (2004). Postglacial mass movements and their causes in fjords and lakes in western Norway. *Norwegian Journal of Geology*, *84*, 35-55.

Brideau, M., Stead, D., Kinain, D., & Fecova, K. (2005). Influence of tectonic structures on the Hope Slide, British Columbia, Canada. *Engineering geology*, *80*, 242-259.

Bunkholt, H. S. S., Redfield, T. F., Osmundsen, P. T., Oppikofer, T., Hermanns, R. L., & Dehls, J. (2012). Landslide processes in hard rock in Troms, Norway. In E. Eberhardt, C. Froese, K. Turner, & S. Leroueil (Eds.), *Landslides and Enginereed slopes* (pp. 855-861). CRC.

Bunkholt, H. S. S., Redfield, T. F., Osmundsen, P. T., Oppikofer, T., Hermanns, R. L., & Dehls, J. (2013). The Role of Inherited Structures in Deep Seated Slope Failures in Kåfjorden, Norway. In C. Margottini, P. Canuti, & K. Sassa (Eds.), *Landslide Science and Practice* (pp. 265-271). Springer, Heidelberg. https://doi.org/https://doi.org/10.1007/978-3-642-31325-7_35

Copernicus. (n.d.). *Sentinel-1*. Retrieved 21.02.2024 from https://sentinels.copernicus.eu/web/sentinel/missions/sentinel-1

Corner, G. D. (1980). Preboreal deglaciation chronology and marine limits of the Lyngen-Storfjord area, Troms, North Norway. *Boreas*, *9*, 239-249. https://doi.org/https://doi.org/10.1111/j.1502-3885.1980.tb00700.x

Crosta, G. B., Frattini, P., & Agliardi, F. (2013). Deep seated gravitational slope deformations in the European Alps. *Tectonophysics*, *605*, 13-33. https://doi.org/https://doi.org/10.1016/j.tecto.2013.04.028

Elmo, D., Donati, D., & Stead, D. (2018). Challenges in the characterisation of intact rock bridges in rock slopes. *Engineering geology*, *245*, 81-96.

ESA. (n.d.). *Introducing Sentinel-1*. Retrieved 21.02.2024 from https://www.esa.int/Applications/Observing_the_Earth/Copernicus/Sentinel-1/Introducing_Sentinel-1

Faber, C., Stünitz, H., Gasser, D., Jeřábek, P., Kraus, K., Corfu, F., Ravna, E. K., & Konopásek, J. (2019). Anticlockwise metamorphic pressure–temperature paths and nappe stacking in the Reisa Nappe Complex in the Scandinavian Caledonides, northern Norway: evidence for weakening of lower continental crust before and during continental collision. *Solid Earth*, *10*(1), 117-148. https://doi.org/10.5194/se-10-117-2019

Fossen, H. (2016). *Structural Geology* (2 ed.). Cambridge University Press.

Furseth, A. (2006). *Skredulykker i Norge*. Turn Forlag.

Gabrielsen, R., Braathen, A., Dehls, J., & Roberts, D. (2002). Tectonic lineaments of Norway. *Norwegian Journal of Geology*, *82*, 153-174.

Gisnås, K., Etzelmüller, B., Lussana, C., Hjort, J., Sannel, B., Isaksen, K., Westermann, S., Kuhry, P., Christiansen, H., Frampton, A., & Åkerman, J. (2016). Permafrost Map for Norway, Sweden and Finland. *PERMAFROST AND PERIGLACIAL PROCESSES*, *28*, 359–378.

Goodman, R. E. (1980). *Introduction to Rock Mechanics (Chapter 8)*. John Wiley.

Hermanns, R. L., Hansen, L., Sletten, K., Böhme, M., Bunkholt, H. S. S., Dehls, J., Eilertsen, R., Fischer, L., L'Heureux, J., Høgaas, F., Nordahl, B., Oppikofer, T., Rubensdotter, L., Solberg, I., Stalsberg, K., & Molina, F. X. Y. (2012a). Systematic geological mapping for landslide understanding in the Norwegian context. *Taylor & Francis Group, London*, 265-271.

Hermanns, R. L., Oppikofer, T., Anda, E., Blikra, L. H., Martina, B., Bunkholt, H. S. S., Crosta, G. B., Dahle, H., Devoli, G., Fischer, L., Jaboyedoff, M., Leow, S., Sætre, S., & Molina, F. X. Y. (2012b). *Recomended hazard and risk classification system for large unstable rock slopes in Norway*. NGU Rapport - 2012.029.

Hermanns, R. L., Oppikofer, T., Molina, F. X. Y., Dehls, J., & Böhme, M. (2014). Approach for Systematic Rockslide Mapping of Unstable Rock Slopes in Norway. In K. Sassa (Ed.), *Landslide Science for a Safer Geoenvironment* (Vol. 3). Springer.

Kuhn, D., J. Torizin, J., Fuchs, M., Hermanns, R. L., Redfield, R. F., & Balzer, D. (2021). Back analysis of a coastal cliff failure along the Forkastningsfjellet coastline, Svalbard: Implications for controlling and triggering factors. *Geomorphology*, *389*.

Leigh, J. R., Evans, D. J. A., Stokes, C. R., Andreassen, L. M., & Carr, R. J. (2021). Glacial and periglacial geomorphology of central Troms and Finnmark county, Arctic Norway. *Journal of Maps*, *17*(2), 348-366.

Mamen, J. (2023). *Troms (klima)*. Store Norske Leksikon.

Mangerud, J. (2004). Ice sheet limits in Norway and on the Norwegian continental shelf. *Development in Quaternary Sciences*, *2*, 271-294. https://doi.org/https://doi.org/10.1016/S1571-0866(04)80078-2

Mangerud, J., Gyllencreutz, R., Lohne, Ø., & Svendsen, J. I. (2011). Chapter 22 - Glacial History of Norway. In J. Ehlers, P. L. Gibbard, & P. D. Hughes (Eds.), *Developments in Quaternary Sciences* (Vol. 15, pp. 279-298). Elsevier. https://doi.org/https://doi.org/10.1016/B978-0-444-53447-7.00022-2

MET. (2023a). *Observasjoner og Værstatistikk*. https://seklima.met.no/years/sum(precipitation_amount%20P1Y)/last_5_years/SN91150,SN91500,SN91080,SN91180,SN91380,SN91551,SN91522/nb/

MET. (2023b). Observasjoner og værstatstikk https://seklima.met.no/seasons/mean(air_temperature%20P3M),min(air_temperature%20P6M),max(air_temperature%20P6M)/last_5_years/SN91551,SN91522,SN91502,SN91500,SN91380/nb/

NGU. (n.d.). *Hva er InSAR?* https://www.ngu.no/geologisk-kartlegging/hva-er-insar
NVE. (2019, 28.02.2023). *Differensiell satellittnavigasjonssystemer (dGNSS)*. https://www.nve.no/naturfare/overvaking-og-varsling/fjellskredovervaaking/instrumentering/differensiell-satellittnavigasjonssystemer-dgnss/
NVE. (2021, 26.09.2023). *Fjellskredovervåkning*. NVE. https://www.nve.no/naturfare/overvaking-og-varsling/fjellskredovervaaking/
NVE. (2023a, 05.02.2024). *Kontinuerlig overvåkede fjellpartier*. NVE. https://www.nve.no/naturfare/overvaking-og-varsling/fjellskredovervaaking/kontinuerlig-overvaakede-fjellpartier/
NVE. (2023b, 23.11.2023). *NVE Faresoner for store fjellskred*. NVE. https://temakart.nve.no/tema/fjellskred
Oppikofer, T., Nordahl, B., Bunkholt, H. S. S., Nicolaisen, M., Jarna, A., Iversen, S., Hermanns, R. L., Böhme, M., & Molina, F. X. Y. (2015). Database and online map service on unstable rock slopes in Norway — From data perpetuation to public information. *Geomorphology, 259*, 68-81. https://doi.org/http://dx.doi.org/10.1016/j.geomorph.2015.08.005
Oppikofer, T., Saintot, A., Otterå, S., Hermanns, R. L., Anda, E., Dahle, H., & Eiken, T. (2013). *Investigations on unstable rock slopes in Møre og Romsdal – status and plans after field surveys in 2012*.
Osmundsen, P. T., Redfield, T. F., & Henderson, I. H. C. (2009). ROS Fjellskred i Troms: status og planer.
Ramberg, I. B., Bryhni, I., Nøttvedt, A., & Rangnes, K. (2013). *Landet blir til - Norges geologi* (2 ed.). Norges Geologisk Forening.
Rocscience. (n.d). *Display Daylight Envelope*. rocscience.com. Retrieved 11.05 from https://www.rocscience.com/help/dips/documentation/planes-and-intersections/planes/display-daylight-envelope
Soil INSTRUMENTS. (2014). *Digital Tape Extensometer: User manual*. https://www.soilinstruments.com/products/extensometers/digital-tape-extensometer/
SSB. (2023, 12.12.2023). *Tettsteders befolkning og areal*. , Statistisk Sentralbyrå. https://www.ssb.no/befolkning/folketall/statistikk/tettsteders-befolkning-og-areal
Stead, D., & Wolter, A. (2015). A critical review of rock slope failure mechanisms: The importance of structural geology. *Journal of Structural Geology, 74*, 1-23. https://doi.org/https://doi.org/10.1016/j.jsg.2015.02.002
Thorsnes, G. (2024). *Troms*. Store Norske Leksikon. https://snl.no/Troms
Tolgensbak, J., & Sollid, J. L. (1988). *Kåfjord, Kvartærgeologi og Geomorfologi 1:50 000, 1634 II. Geografisk Institutt, Universitet i Oslo*. Geografisk Institutt, Universitet i Oslo, Geografisk Institutt, Universitet i Oslo.
Vick, L. M., Bergh, S. G., Höpfl, S., Percival, J., & Daines, E. (2020a). *The role of lithological weakness zones in rockslides in northern Norway*
Vick, L. M., Böhme, M., Rouyet, L., Bergh, S. G., Corner, G. D., & Lauknes, T. R. (2020b). Structurally controlled rock slope deformation in northern Norway. *Landslides, 17*(8), 1745-1776. https://doi.org/10.1007/s10346-020-01421-7
Wylie, D. C., & Mah, C. W. (2005). *Rock Slope Engineering: Civil and Mining 4th ed*. Taylor & Francis Group.
Zwaan, K. B., Dangla, P., & Quenardel, J. M. (2006). *Berggrunnskart KÅFJORD 1634 II, M 1:50.000. Norges geologiske undersøkelse*. Norges geologiske undersøkelse.

Appendix Material

Designated use	Name of tool/software

Phones for pictures and data collection	Samsung Galaxy A536B/DS (Android version 14)
Digital Field notebook	FieldMove Clino Pro v2.5.19
Structural data processing	Rocscience Dips 8.022
Rock cutting	MK Diamond 101XL (Brick Saw, Concrete Saw, Tile Saw)
GIS software	ArcGis Pro 3.0.0

Appendix A

Farevurdering av ustabile fjellpartier i Norge

Lokalitetens navn: Staluvarri **Scenario:** 1 **Utført av:** Iver **Dato:** 15/05/2024

Fareklasser	Sannsynlighet	Kumul. sannsyn.
Meget lav	1.2 %	1.2 %
Lav	61.9 %	63.1 %
Middels	36.9 %	100.0 %
Høy	0.0 %	100.0 %
Meget høy	0.0 %	100.0 %

Farepoeng	
Minimum	2.0
Maksimum	6.8
Modus	4.0
Gjennomsnitt	4.3
5% persentil	2.6
95% persentil	5.7

Tilpasset normalfordeling	
Gjennomsnitt μ	4.2
Standardavvik σ	1.0
μ - 2σ	2.2
μ + 2σ	6.1
Korrelasjonskoeff.	1.0000
K-S-test	1.4 %

1. Bakskrent	**Poeng**	**Norm. sannsyn.**
Ikke utviklet	0	33.3 %
Delvis åpen over bredden av det ustabile fjellpartiet (få cm til m)	0.5	0.0 %
Fullstendig åpen over bredden av det ustabile fjellpartiet (få cm til m)	1	66.7 %
Kommentar: fullt developed backscarp along the NE-SW fault plane		

2. Potensielle glidestrukturer	**Poeng**	**Norm. sannsyn.**
Ingen gjennomsettende strukturer er utgående i fjellsiden	0	0.0 %
Gjennomsettende strukturer faller gjennomsnittlig <20 grader eller er brattere enn fjellsiden	0.5	0.0 %
Gjennomsettende strukturer faller gjennomsnittlig >20 grader og er utgående i fjellsiden	1	100.0 %
Kommentar: the foliation is penetrative and dips slightly steeper than 20 degrees and is generally outgoing on the on the slope.		

3. Flanker	**Poeng**	**Norm. sannsyn.**
Ikke utviklet	0	0.0 %
Delvis utviklet på 1 side	0.25	100.0 %
Fullstendig utviklet eller åpen skråning på 1 side eller delvis utviklet på 2 sider	0.5	0.0 %
Fullstendig utviklet eller åpen skråning på 1 side og delvis utviklet på 1 sider	0.75	0.0 %
Fullstendig utviklet eller åpen skråning på 2 sider	1	0.0 %
Kommentar: fault seems to be the best estimation of a clearly defined flank		

4. Kinematisk analyse	**Poeng**	**Norm. sannsyn.**
Kinematisk mulighetstest tillater ikke planutglidning, kileutglidning eller utvelting	0	0.0 %
Brudd er delvis kinematisk mulig (bevegelsesretning er > ±30° i forhold til skråningsorientering)	0.5	0.0 %
Brudd er kinematisk mulig (bevegelsesretning er <= ±30° i forhold til skråningsorientering)	0.75	50.0 %
Brudd er delvis kinematisk mulig på utholdende svakhetsplan (bevegelsesretning er > ±30° i forhold til skråningsorientering)	0.75	0.0 %
Brudd er kinematisk mulig på utholdende svakhetsplan (bevegelsesretning er <= ±30° i forhold til til skråningsorientering)	1	50.0 %
Kommentar: Possible along the foliation, and the movement is less than 30 degree on slopes aspect, 50 given to each as the gneissic composition possibly could		

5. Morfologisk tegn på bruddflaten	**Poeng**	**Norm. sannsyn.**
Ingen indikasjon i morfologien	0	60.0 %
Morfologi av skråningen tyder på utviklingen av en bruddflate (utbulning, konkavitet-konveksitet, vannkilder)	0.5	40.0 %
Sammenhengende bruddflate er antydet i skråningens morfologi og kan kartlegges	1	0.0 %
Kommentar: Some streams in the lower section, but to much talus material to decide if they are related		

6. Bevegelseshastighet	**Poeng**	**Norm. sannsyn.**
Ingen signifikant bevegelse	0	70.0 %
>0 - 0.5 cm/år	1	30.0 %
0.5 - 1 cm/år	2	0.0 %
1 - 4 cm/år	3	0.0 %
4 - 10 cm/år	4	0.0 %
> 10 cm/år	5	0.0 %
Kommentar: The displacement rate is mostly very low (<3-4mm/yr), but increased in the disintigrated segment		

7. Akselerasjon (hvis bevegelsen er >0.5 cm/år og <10 cm/år)	**Poeng**	**Norm. sannsyn.**
Ingen akselerasjon eller endring i bevegelseshastigheten	0	100.0 %
Økning i bevegelseshastigheten	1	0.0 %
Kommentar: from the averaged displacement, it does not seem to be any sign of acceleration from insar data.		

8. Økning av steinsprangsaktivitet	**Poeng**	**Norm. sannsyn.**
Ingen økning av steinsprangsaktivitet	0	50.0 %
Økt steinsprangsaktivitet	1	50.0 %
Kommentar: Not enough observations, not enough observation, equal value		

9. Tidligere hendelser	**Poeng**	**Norm. sannsyn.**
Ingen postglasiale hendelser av liknende størrelse	0	33.3 %
En eller flere hendelser av lignende størrelse eldre enn 5000 år	0.5	33.3 %
En eller flere hendelser av lignende størrelse yngre enn 5000 år	1	33.3 %
Kommentar: Not enough observations,equale value		

Farevurdering av ustabile fjellpartier i Norge

Lokalitetens navn: Staluvarri **Scenario:** 2 **Utført av:** Iver **Dato:** 14/05/2024

Fareklasser	Sannsynlighet	Kumul. sannsyn.
Meget lav	0.0 %	0.0 %
Lav	48.3 %	48.3 %
Middels	48.8 %	97.0 %
Høy	3.0 %	100.0 %
Meget høy	0.0 %	100.0 %

Farepoeng	
Minimum	2.5
Maksimum	7.5
Modus	5.0
Gjennomsnitt	4.8
5% persentil	2.9
95% persentil	6.5

Tilpasset normalfordeling	
Gjennomsnitt μ	4.7
Standardavvik σ	1.1
μ - 2σ	2.5
μ + 2σ	6.9
Korrelasjonskoeff.	0.9991
K-S-test	4.6 %

1. Bakskrent	**Poeng**	**Norm. sannsyn.**
Ikke utviklet	0	0.0 %
Delvis åpen over bredden av det ustabile fjellpartiet (få cm til m)	0.5	50.0 %
Fullstendig åpen over bredden av det ustabile fjellpartiet (få cm til m)	1	50.0 %
Kommentar: partially to fully developed back scarp in the back, generally high amount of fluctation of it on the slope		

2. Potensielle glidestrukturer	**Poeng**	**Norm. sannsyn.**
Ingen gjennomsettende strukturer er utgående i fjellsiden	0	0.0 %
Gjennomsettende strukturer faller gjennomsnittlig <20 grader eller er brattere enn fjellsiden	0.5	0.0 %
Gjennomsettende strukturer faller gjennomsnittlig >20 grader og er utgående i fjellsiden	1	100.0 %
Kommentar: the foliation is penetrative and dips slightly steeper than 20 degrees and is generally outgoing on the on the slope.		

3. Flanker	**Poeng**	**Norm. sannsyn.**
Ikke utviklet	0	100.0 %
Delvis utviklet på 1 side	0.25	0.0 %
Fullstendig utviklet eller åpen skråning på 1 side eller delvis utviklet på 2 sider	0.5	0.0 %
Fullstendig utviklet eller åpen skråning på 1 side og delvis utviklet på 1 sider	0.75	0.0 %
Fullstendig utviklet eller åpen skråning på 2 sider	1	0.0 %
Kommentar: hard to decide concretely where the flanks are		

4. Kinematisk analyse	**Poeng**	**Norm. sannsyn.**
Kinematisk mulighetstest tillater ikke planutglidning, kileutglidning eller utvelting	0	0.0 %
Brudd er delvis kinematisk mulig (bevegelsesretning er > ±30° i forhold til skråningsorientering)	0.5	0.0 %
Brudd er kinematisk mulig (bevegelsesretning er <= ±30° i forhold til skråningsorientering)	0.75	0.0 %
Brudd er delvis kinematisk mulig på utholdende svakhetsplan (bevegelsesretning er > ±30° i forhold til skråningsorientering)	0.75	0.0 %
Brudd er kinematisk mulig på utholdende svakhetsplan (bevegelsesretning er <= ±30° i forhold til til skråningsorientering)	1	100.0 %
Kommentar: Possible along the foliation, and the movement is less than 30 degree on slopes aspect		

5. Morfologisk tegn på bruddflaten	**Poeng**	**Norm. sannsyn.**
Ingen indikasjon i morfologien	0	90.0 %
Morfologi av skråningen tyder på utviklingen av en bruddflate (utbulning, konkavitet-konveksitet, vannkilder)	0.5	10.0 %
Sammenhengende bruddflate er antydet i skråningens morfologi og kan kartlegges	1	0.0 %
Kommentar: Some streams in the lower section, but to much talus material to decide if they are related		

6. Bevegelseshastighet	**Poeng**	**Norm. sannsyn.**
Ingen signifikant bevegelse	0	30.0 %
>0 - 0.5 cm/år	1	40.0 %
0.5 - 1 cm/år	2	30.0 %
1 - 4 cm/år	3	0.0 %
4 - 10 cm/år	4	0.0 %
> 10 cm/år	5	0.0 %
Kommentar: The speed is mostly very low, but increased in the disintigrated segment		

7. Akselerasjon (hvis bevegelsen er >0.5 cm/år og <10 cm/år)	**Poeng**	**Norm. sannsyn.**
Ingen akselerasjon eller endring i bevegelseshastigheten	0	100.0 %
Økning i bevegelseshastigheten	1	0.0 %
Kommentar: from the averaged displacement, it does not seem to be any sign of acceleration from insar data.		

8. Økning av steinsprangsaktivitet	**Poeng**	**Norm. sannsyn.**
Ingen økning av steinsprangsaktivitet	0	50.0 %
Økt steinsprangsaktivitet	1	50.0 %
Kommentar: Not enough observations		

9. Tidligere hendelser	**Poeng**	**Norm. sannsyn.**
Ingen postglasiale hendelser av liknende størrelse	0	33.3 %
En eller flere hendelser av lignende størrelse eldre enn 5000 år	0.5	33.3 %
En eller flere hendelser av lignende størrelse yngre enn 5000 år	1	33.3 %
Kommentar: Not enough observations		

Farevurdering av ustabile fjellpartier i Norge

Lokalitetens navn: Staluvarri **Scenario:** 2 **Utført av:** Iver **Dato:** 14/05/2024

Fareklasser	Sannsynlighet	Kumul. sannsyn.
Meget lav	0.0 %	0.0 %
Lav	48.3 %	48.3 %
Middels	48.8 %	97.0 %
Høy	3.0 %	100.0 %
Meget høy	0.0 %	100.0 %

Farepoeng	
Minimum	2.5
Maksimum	7.5
Modus	5.0
Gjennomsnitt	4.8
5% persentil	2.9
95% persentil	6.5

Tilpasset normalfordeling	
Gjennomsnitt μ	4.7
Standardavvik σ	1.1
μ - 2σ	2.5
μ + 2σ	6.9
Korrelasjonskoeff.	0.9991
K-S-test	4.6 %

1. Bakskrent	**Poeng**	**Norm. sannsyn.**
Ikke utviklet	0	0.0 %
Delvis åpen over bredden av det ustabile fjellpartiet (få cm til m)	0.5	50.0 %
Fullstendig åpen over bredden av det ustabile fjellpartiet (få cm til m)	1	50.0 %
Kommentar: partially to fully developed back scarp in the back, generally high amount of fluctation of it on the slope		

2. Potensielle glidestrukturer	**Poeng**	**Norm. sannsyn.**
Ingen gjennomsettende strukturer er utgående i fjellsiden	0	0.0 %
Gjennomsettende strukturer faller gjennomsnittlig <20 grader eller er brattere enn fjellsiden	0.5	0.0 %
Gjennomsettende strukturer faller gjennomsnittlig >20 grader og er utgående i fjellsiden	1	100.0 %
Kommentar: the foliation is penetrative and dips slightly steeper than 20 degrees and is generally outgoing on the on the slope.		

3. Flanker	**Poeng**	**Norm. sannsyn.**
Ikke utviklet	0	100.0 %
Delvis utviklet på 1 side	0.25	0.0 %
Fullstendig utviklet eller åpen skråning på 1 side eller delvis utviklet på 2 sider	0.5	0.0 %
Fullstendig utviklet eller åpen skråning på 1 side og delvis utviklet på 1 sider	0.75	0.0 %
Fullstendig utviklet eller åpen skråning på 2 sider	1	0.0 %
Kommentar: hard to decide concretely where the flanks are		

4. Kinematisk analyse	**Poeng**	**Norm. sannsyn.**
Kinematisk mulighetstest tillater ikke planutglidning, kileutglidning eller utvelting	0	0.0 %
Brudd er delvis kinematisk mulig (bevegelsesretning er > ±30° i forhold til skråningsorientering)	0.5	0.0 %
Brudd er kinematisk mulig (bevegelsesretning er <= ±30° i forhold til skråningsorientering)	0.75	0.0 %
Brudd er delvis kinematisk mulig på utholdende svakhetsplan (bevegelsesretning er > ±30° i forhold til skråningsorientering)	0.75	0.0 %
Brudd er kinematisk mulig på utholdende svakhetsplan (bevegelsesretning er <= ±30° i forhold til til skråningsorientering)	1	100.0 %
Kommentar: Possible along the foliation, and the movement is less than 30 degree on slopes aspect		

5. Morfologisk tegn på bruddflaten	**Poeng**	**Norm. sannsyn.**
Ingen indikasjon i morfologien	0	90.0 %
Morfologi av skråningen tyder på utviklingen av en bruddflate (utbulning, konkavitet-konveksitet, vannkilder)	0.5	10.0 %
Sammenhengende bruddflate er antydet i skråningens morfologi og kan kartlegges	1	0.0 %
Kommentar: Some streams in the lower section, but to much talus material to decide if they are related		

6. Bevegelseshastighet	**Poeng**	**Norm. sannsyn.**
Ingen signifikant bevegelse	0	30.0 %
>0 - 0.5 cm/år	1	40.0 %
0.5 - 1 cm/år	2	30.0 %
1 - 4 cm/år	3	0.0 %
4 - 10 cm/år	4	0.0 %
> 10 cm/år	5	0.0 %
Kommentar: The speed is mostly very low, but increased in the disintigrated segment		

7. Akselerasjon (hvis bevegelsen er >0.5 cm/år og <10 cm/år)	**Poeng**	**Norm. sannsyn.**
Ingen akselerasjon eller endring i bevegelseshastigheten	0	100.0 %
Økning i bevegelseshastigheten	1	0.0 %
Kommentar: from the averaged displacement, it does not seem to be any sign of acceleration from insar data.		

8. Økning av steinsprangsaktivitet	**Poeng**	**Norm. sannsyn.**
Ingen økning av steinsprangsaktivitet	0	50.0 %
Økt steinsprangsaktivitet	1	50.0 %
Kommentar: Not enough observations		

9. Tidligere hendelser	**Poeng**	**Norm. sannsyn.**
Ingen postglasiale hendelser av liknende størrelse	0	33.3 %
En eller flere hendelser av lignende størrelse eldre enn 5000 år	0.5	33.3 %
En eller flere hendelser av lignende størrelse yngre enn 5000 år	1	33.3 %
Kommentar: Not enough observations